AD-A185 059 COMPUTER SIMULATION OF CW HF CHEMICAL LASER UNSTABLE RESONATOR PERFORMANCE(U) ILLINOIS UNIV AT URBANA DEPT OF AERONAUTICAL AND ASTRONAUTICA.. L H SENTMAN ET AL. 1/2

UNCLASSIFIED AUG 87 AAE-87-5 N00014-85-K-0326 F/G 9/3 NL

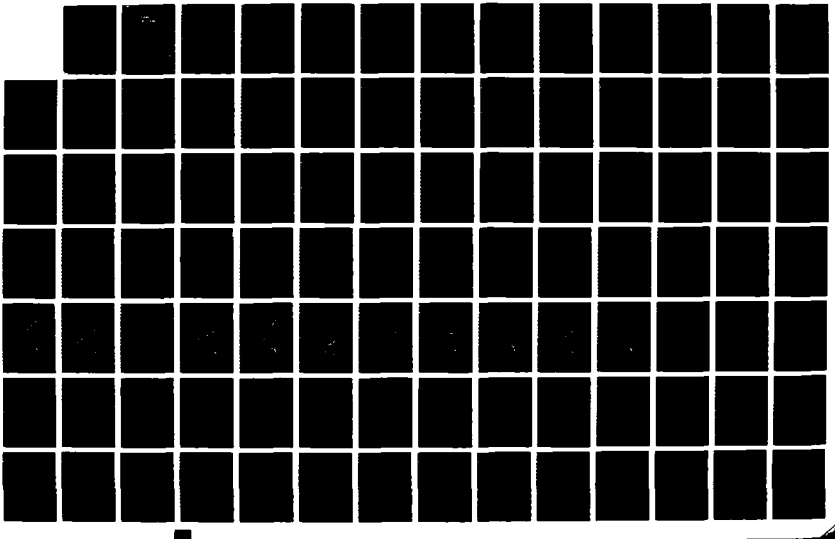

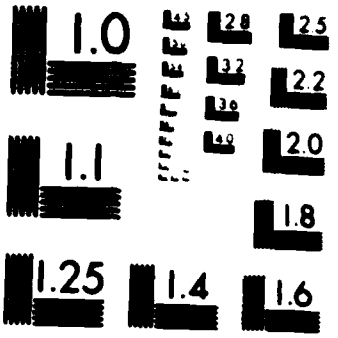

(12)

AAE

AERONAUTICAL AND ASTRONAUTICAL ENGINEERING DEPARTMENT

COMPUTER SIMULATION OF CW HF CHEMICAL LASER UNSTABLE RESONATOR PERFORMANCE

L. H. Sentman and J. O. Gilmore

ENGINEERING EXPERIMENT STATION, COLLEGE OF ENGINEERING, UNIVERSITY OF ILLINOIS, URBANA

Aeronautical and Astronautical Engineering Department

University of Illinois at Urbana-Champaign

Urbana, Illinois

Technical Report AAE TR 87-5

UILU Eng 87-0505

COMPUTER SIMULATION OF CW HF CHEMICAL LASER UNSTABLE RESONATOR PERFORMANCE

L. H. Sentman and J. O. Gilmore

Prepared for

Defense Advanced Research Projects Agency

1400 Wilson Blvd.

Arlington, VA 22209

August, 1987

SECURITY CLASSIFICATION OF THIS PAGE (When Data Entered)

REPORT DOCUMENTATION PAGE

READ INSTRUCTIONS BEFORE COMPLETING FORM

1. REPORT NUMBER: AAE 87-5 UILU ENG 87-0505	2. GOVT ACCESSION NO.: AD-A185 059
3. RECIPIENT'S CATALOG NUMBER:	
4. TITLE (and Subtitle): Computer Simulation of cw HF Chemical Laser Unstable Resonator Performance	5. TYPE OF REPORT & PERIOD COVERED: Technical Report
	6. PERFORMING ORG. REPORT NUMBER:
7. AUTHOR(s): L. H. Sentman and J. O. Gilmore	8. CONTRACT OR GRANT NUMBER(s): N00014-85-K-0326
9. PERFORMING ORGANIZATION NAME AND ADDRESS: Aeronautical and Astronautical Engineering University of Illinois at Urbana-Champaign Urbana, IL 61801	10. PROGRAM ELEMENT, PROJECT, TASK AREA & WORK UNIT NUMBERS:
11. CONTROLLING OFFICE NAME AND ADDRESS: Defense Advanced Research Projects Agency 1400 Wilson Boulevard Arlington, VA 22209	12. REPORT DATE: August 1987 13. NUMBER OF PAGES:
14. MONITORING AGENCY NAME & ADDRESS (if different from Controlling Office): Office of Naval Research Resident Representative Room 286, 536 South Clark Street Chicago, IL 60605	15. SECURITY CLASS. (of this report): UNCLASSIFIED 15a. DECLASSIFICATION DOWNGRADING SCHEDULE:

16. DISTRIBUTION STATEMENT (of this Report)

UNLIMITED

17. DISTRIBUTION STATEMENT (of the abstract entered in Block 20, if different from Report)

18. SUPPLEMENTARY NOTES

19. KEY WORDS (Continue on reverse side if necessary and identify by block number)

Chemical laser
Time-dependent oscillations
Unstable resonator performance

20. ABSTRACT (Continue on reverse side if necessary and identify by block number)

Inadequacies in the treatment of the fluid dynamic mixing that were not apparent in Fabry-Perot or stable resonator models were revealed with a wave optics unstable resonator model. The unstable resonator data as a function of resonator size and size of the laser were shown to provide a severe test of a coupled, wave optics, chemical kinetic, fluid dynamic model of a chemical laser. A mechanism for the observed time-depdendent oscillations that occur on lines whose saturated gain does not fill the unstable resonator was proposed. According

over

DD FORM 1 JAN 73 1473 EDITION OF 1 NOV 65 IS OBSOLETE

SECURITY CLASSIFICATION OF THIS PAGE (When Data Entered)

20. ABSTRACT

to the proposed mechanism, the time-dependent oscillations are the result of a competition between chemical pumping and radiative deactivation of upper laser levels of HF. The oscillations occur only if the media is not strongly coupled to the optical fields diffractively or geometrically. Computer calculations supported the proposed mechanism and new unstable resonator experiments were suggested.

TABLE OF CONTENTS

Page

I. INTRODUCTION.....1

II. COMPUTER SIMULATION OF CHEMICAL LASER UNSTABLE RESONATOR PERFORMANCE.....4

2.1 THE UNSTABLE RESONATOR MODEL.....8
2.2 PREVIOUS UNSTABLE RESONATOR CALCULATIONS.....14
2.3 UNSTABLE RESONATOR DATA.....14
2.3.1 RUN 34, LOW PRESSURE DATA.....19
2.3.2 RUN 36, LOW PRESSURE DATA.....21
2.3.3 COMPARISON OF CL II AND CL I UNSTABLE RESONATOR DATA.....26
2.4 COMPARISON OF THE A PRIORI UNSTABLE RESONATOR CALCULATIONS TO THE CL II DATA.....26
2.5 UNSTABLE RESONATOR BASELINING CALCULATIONS.....31
2.5.1 CL I CALCULATIONS.....66
2.6 SUMMARY OF UNSTABLE RESONATOR MODELING RESULTS.....67

III. UNSTABLE RESONATOR TIME-DEPENDENT OSCILLATIONS.....70
3.1 PROPOSED MECHANISM FOR THE TIME-DEPENDENT OSCILLATIONS IN AN UNSTABLE RESONATOR.....70
3.2 NUMERICAL INVESTIGATIONS OF THE PROPOSED MECHANISM.....74
3.3 RELATIONSHIP OF THE PROPOSED MECHANISM TO OTHER MODELS.....88
3.4 SUGGESTED EXPERIMENTS.....89
3.5 SUMMARY.....90

IV. CONCLUDING REMARKS.....92

REFERENCES.....94

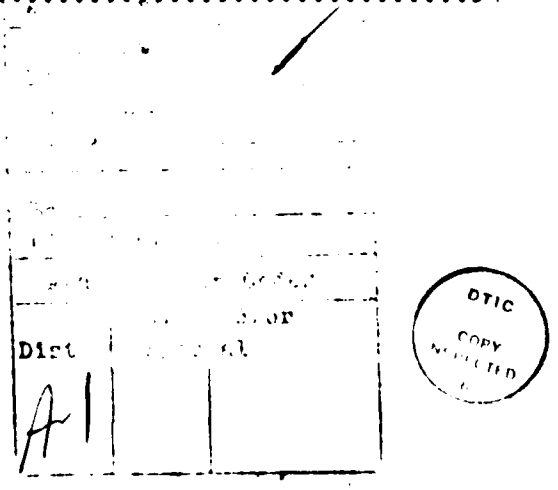

I. INTRODUCTION

The present study examines the computer simulation of cw HF chemical laser unstable resonator performance. Previous modeling[1,2] of the Fabry-Perot and stable resonator performance of the Helios CL II, arc driven, subsonic, continuous wave HF chemical laser demonstrated that the Fabry-Perot and stable resonator models needed to be separately baselined to Fabry-Perot and stable resonator data, respectively. The separate baselining appeared to be accounting for some aspect of the resonator modes which is not included in the resonator models. Based on the results from the Fabry-Perot and stable resonator modeling, unstable resonator modeling was examined with the goal of determining whether a different set of baseline parameters is required to model the unstable resonator data even though the wave optics unstable resonator model includes mode structure.

The results of the unstable resonator baselining process indicated that one set of baseline parameters that allow the model to predict unstable resonator data as the size of the resonator and size of the laser varied could not be found. It was, however, possible to obtain different sets of baseline parameters for individual resonator sizes. The best fit parameter set for the 2 mm slit case accurately predicated the total power, but also predicted a 20 nsec small amplitude oscillation that was not seen experimentally. The best fit parameter set for the 4 mm slit case accurately predicted the total power and period of the time-dependent oscillations, but underpredicted the

amplitude modulation. The best fit parameter set for the 5 mm slit case was a set of parameters obtained from baselining the Fabry-Perot model to stable resonator data[3,4]. This parameter set, used in previous unstable resonator modeling, accurately predicted the period and amplitude of the time-dependent oscillations, but overpredicted the total power. Neither the 2 mm slit nor the 4 mm slit baseline parameters predicted scale effects as the size of the laser was reduced by a factor of two.

The inability to obtain one set of baseline parameters for the unstable resonator model demonstrated that the model is inadequate. The limitations arise mainly from the treatment of the fluid dynamic mixing. The limitations imposed by the mixing model did not prevent the Fabry-Perot and stable resonator models from being baselined to the data. This suggested two possible explanations. Since the actual fluid dynamics is independent of the resonator and the unstable resonator model is a more exact treatment of the optics, the wave optics model of the unstable resonator may have brought out inadequacies in the mixing model that were not apparent with geometric optics models. Another possible explanation is that the way in which the optical fields sample the media in an unstable resonator has brought out the inadequacies in the mixing model. Fabry-Perot and stable resonators have no upstream/downstream coupling and full upstream/downstream coupling of the media and optical fields, respectively. The unstable resonator couples upstream of the optical axis and downstream of the optical axis, but not across the optical axis. Both possible explanations demonstrate that unstable resonator data as a function of resonator size and size of the

laser provide a severe test of a coupled, wave optics, chemical kinetic, fluid dynamic model of a chemical laser.

The unstable resonator model was used with the best fit parameter sets to study the time-dependent oscillations in an unstable resonator. Computer calculations indicated a correlation between the number of passes for a wave to exit the resonator after leaving the central Fresnel zone and the oscillation period. This correlation suggested that the time-dependent oscillations are the result of a competition between chemical pumping and radiative deactivation of the upper laser levels; the oscillations occur only if the media is not strongly coupled to the optical fields diffractively or geometrically. Computer calculations with the unstable resonator model supported the proposed mechanism. The calculations showed that the oscillations were damped by increasing the rate of the chemical pumping reactions, and the period was increased by increasing the degree of coupling between the media and the optical fields.

In Section II, unstable resonator computer modeling is examined and baseline parameters are determined for different resonator sizes. In Section III, a mechanism for the time-dependent oscillations is proposed. In Section IV, several concluding remarks and suggestions for future studies are presented.

II. COMPUTER SIMULATION OF CHEMICAL LASER UNSTABLE RESONATOR PERFORMANCE

Computer simulation of chemical laser performance must adequately model three coupled elements of chemical laser physics. These elements are the fluid dynamics of the flow field, including the fluid dynamic mixing of the fuel and oxidizer streams, the chemical kinetics occurring in the fluid media, and the optical resonator. The computer simulation of the Helios CL II and CL I, arc driven, subsonic, continuous wave HF chemical lasers is accomplished with the computer codes BLAZE II[5,6], MNORO3[7], MNORO3SR[1,8] and MNORO3UR[8]. The MNORO3, MNORO3SR, and MNORO3UR codes are rotational nonequilibrium models with Fabry-Perot, stable resonator geometric optics, and unstable resonator wave optics models, respectively. The BLAZE II code is a rotational equilibrium, Fabry-Perot model which calculates all fluid dynamic properties from input initial conditions. The BLAZE II code is well suited for the simulation of laser performance in terms of total outcoupled power, power contained in each vibrational band, and the length of the lasing zone. However, since BLAZE II employs rotational equilibrium kinetics, it cannot compute realistic power spectral distributions.

Because BLAZE II is a very inexpensive code to run when simulating chemical laser performance, BLAZE II calculations are always performed first. After suitable agreement between BLAZE II calculations and the data is obtained, the rotational nonequilibrium codes (MNORO3, MNORO3SR, MNORO3UR) are used. In the rotational nonequilibrium codes, profiles for the velocity, temperature, and pressure of the flow, the mass flow remaining in the primary stream, the mass flow remaining in the

secondary stream, and the ratio of the thickness of the mixed stream to the geometrical thickness of the flow are input data. These profiles are obtained from a rotational equilibrium model such as BLAZE II.

The flow field in the Helios CL II and CL I laser bodies is a complex three-dimensional flow[3], Fig. 1. A sketch of the appearance of the H_2 jets is shown on the left side of Fig. 1. These jets are well defined with the chemical reaction occurring at the interface of the primary (oxidizer) stream and the H_2 jets. The appearance of these jets as seen looking upstream is shown as Section AA in Fig. 1. To treat this complicated three-dimensional mixing, the flow was idealized as a series of alternating primary and secondary (fuel) slit nozzles[3] as shown on the right side of Fig. 1. The mixing calculation with BLAZE II was performed utilizing a linear scheduled mixing option[5,6].

The BLAZE II code integrates the governing ordinary differential equations describing the chemical kinetics and fluid dynamics. The integration is performed in the flow direction, starting at the nozzle exit plane. For the Helios CL II and CL I lasers, the nozzle exit plane coincides with the point of H_2 injection[3]. The integration requires the specification of all of the dependent variables in the equation set at the nozzle exit plane. For the fluid dynamic equations, the dependent variables that must be specified consist of the static temperature and pressure at the nozzle exit plane, the cross sectional area of the flow channel, the mass flow rates of the primary and secondary streams, and the chemical composition of the primary and secondary streams. To obtain values for these starting conditions, the static pressure is measured 5 mm downstream of the H_2 injectors and the static pressure at

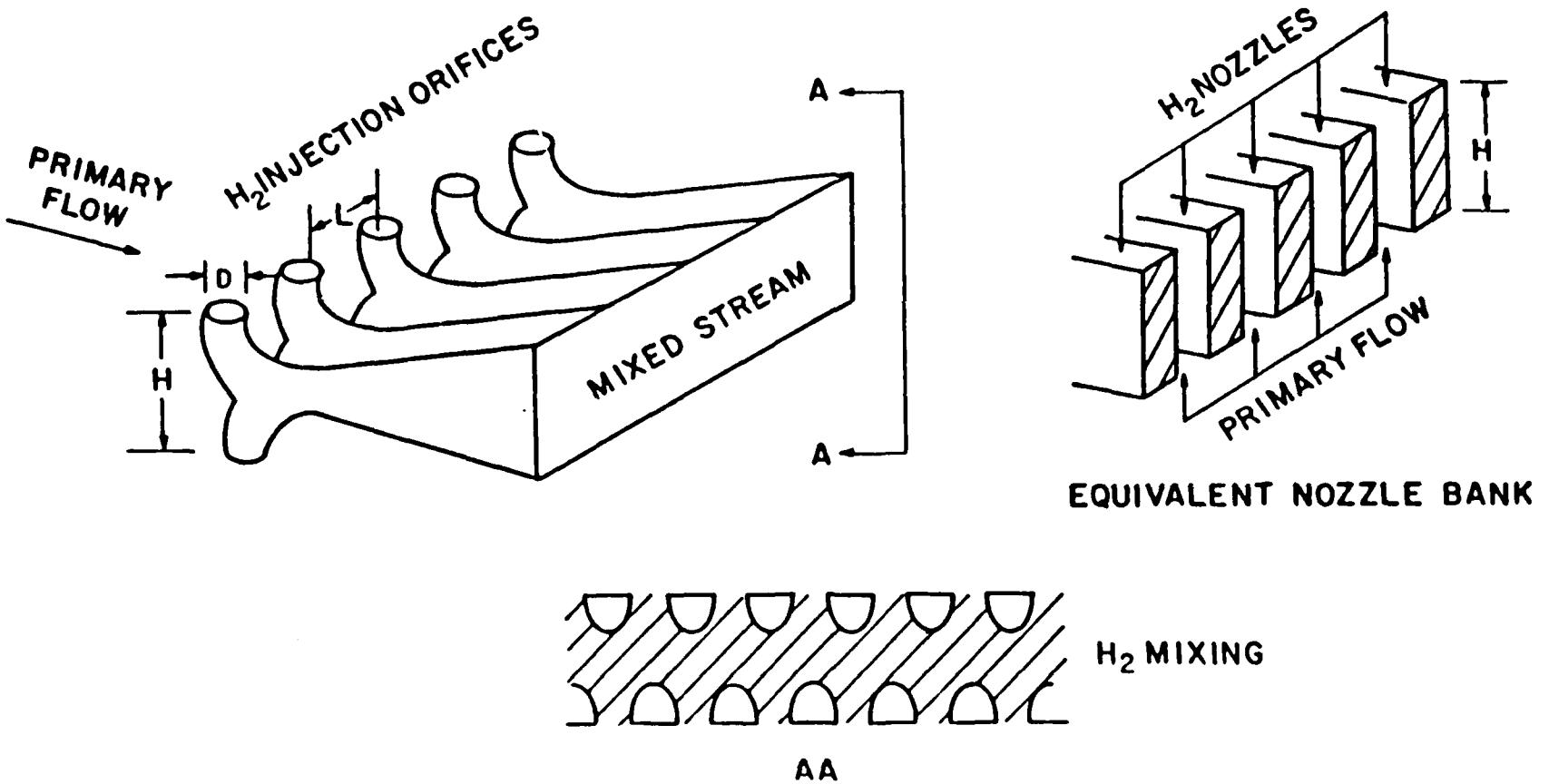

Figure 1 Illustration of the actual mixing geometry and the equivalent nozzle geometry.

the nozzle exit plane (H_2 injectors) is varied until the pressure at 5 mm downstream agrees with the measured value. The cross sectional area of the flow channel and the mass flow rates are measured. The static temperature of the flow at the nozzle exit plane (H_2 injectors) and the mass fractions of F, O_2, SF_6, SF_x (x = 1-5), and SO_2 are unknown. The mass fractions are unknown because the degree to which SF_6 is dissociated in the arc is unknown. In addition to these quantities, the lengths after which the primary and secondary streams are completely mixed must be specified as input data since a scheduled mixing model is used. Thus, to model the Helios CL II and CL I lasers, there are four a priori undetermined quantities that must be specified. The four quantities are the percent SF_6 dissociation in the arc, the static temperature of the flow at the H_2 injectors, the primary mixing length, and the secondary mixing length. A set of these four quantities, called baseline parameters, must be chosen so that the model will accurately predict laser performance. The process of determining the values of these parameters is called baselining.

An objective of this study was to examine unstable resonator modeling in light of Fabry-Perot and stable resonator modeling results which showed that both the Fabry-Perot and stable resonator models needed to be separately baselined to Fabry-Perot and stable resonator data, respectively[1,2]. The Fabry-Perot model was baselined to Fabry-Perot data because the model did not accurately predict the data when a set of parameters obtained from baselining the Fabry-Perot model to stable resonator data was used. When the baseline parameters determined from baselining Fabry-Perot model to Fabry-Perot data were used in the

stable resonator model, the model did not accurately predict stable resonator data. Thus the stable resonator model was baselined to stable resonator data. The separate baselining of the Fabry-Perot and stable resonator models appears to be accounting for some aspect of the resonator modes which is not included in the resonator models[1,2]. The goal in this study was to determine whether a different set of the four baseline parameters is required to model the unstable resonator data even though the wave optics unstable resonator model includes mode structure. To serve as an aid in discussing the unstable resonator modeling, brief summaries of the unstable resonator model, previous unstable resonator calculations, and the unstable resonator data are given.

2.1 THE UNSTABLE RESONATOR MODEL

The efficient, rotational nonequilibrium, chemical kinetic, fluid dynamic model denoted MNORO3[7] was coupled to the Air Force Weapons Laboratory physical optics strip resonator model[9]. The resulting code is denoted MNORO3UR. The geometry of the confocal unstable resonator is shown in Fig. 2. The MNORO3 model assumes that the flow and chemistry are independent of the transverse coordinate z. The optical cavity is modeled as a strip, confocal unstable resonator. The beam is diffractively propagated through the cavity using a solution of the Huygens-Fresnel integral which is obtained by a fast Fourier transform technique. The optics model is coupled to the chemical kinetics model through the thin skin gain approximation in which the active medium is assumed to be a thin sheet in front of the large mirror. The solution

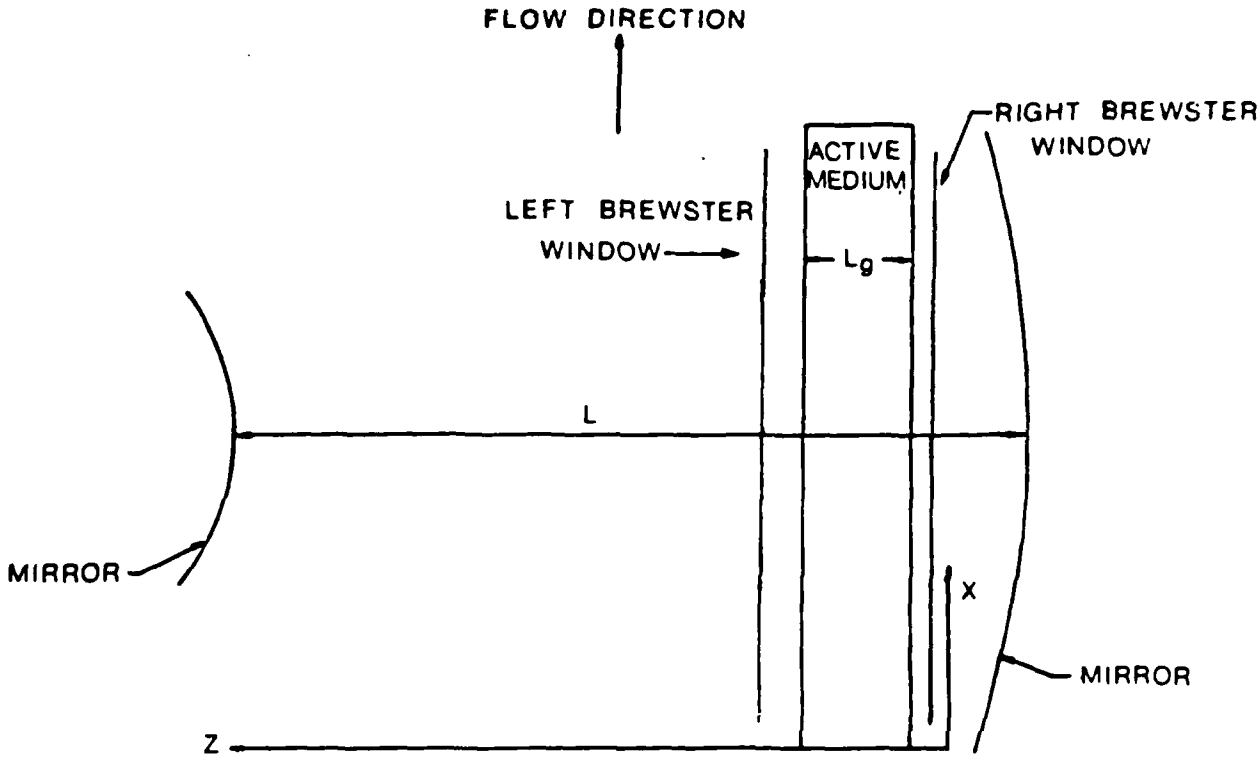

Figure 2 Confocal unstable resonator geometry.

is an iterative one. The calculation starts by passing a plane wave of about the expected intensity (obtained from a rotational nonequilibrium Fabry-Perot model such as MNORO3) through the empty cavity. The resulting intensity distribution is sent to the chemistry. The species equations are then solved with the given intensity distribution and the thickness of the mixed flow, L_e, and the gains on each spectral line are calculated and sent to the optics. The stored wave from the preceding optics calculation is then propagated through the cavity and incremented by the gain distribution from the chemistry. This process is repeated until the difference between successive iterates is less than some prescribed amount. Because each iterate in the solution of the steady state equations corresponds to one round trip of the radiation through the cavity, each iterate may be regarded as a time step in the development of the steady state solution[10,11,12]. Thus, fluctuations in the power from iterate to iterate may be regarded as time-dependent oscillations.

The period of the time-dependent oscillations is calculated by multiplying the number of iterates in one period by the photon round trip transit time. For a mirror spacing of 100 cm, the round trip transit time for a photon is 6.67 nsec. The oscillation period, then, is the number of iterates for one period multiplied by 6.67 nsec. The percent amplitude modulation is calculated by dividing the peak-to-valley power difference by the average power.

All of the Helios CL II and CL I unstable resonator data to which the MNORO3UR model was compared were taken with Brewster windows attached to the laser. There were no vacuum mirror mount data. To

improve the comparisons between the external mirror mount data and the predictions of MNORO3UR, Brewster window losses were added to the unstable resonator model.

Cavity losses introduced by the Brewster windows were modeled in a previous stable resonator study[1]. The Brewster window losses were determined for the stable resonator model after the model had been baselined to vacuum mirror mount data. In the stable resonator model, each time the intensity distribution was passed through a Brewster window, it was multiplied by an effective transmissivity,

$$I_{\text{after B.W.}}(x) = t_w \, I_{\text{incident}}(x) \qquad (2.1\text{-}1)$$

where $I(x)$ is the intensity distribution and t_w is the effective transmissivity of the Brewster window. By varying the value of t_w and comparing the calculated total powers to stable resonator external mirror mount data, a value of the effective transmissivity of the Brewster windows was determined. For both the left and right Brewster windows, t_w was set at 0.97.[1]

Unlike the stable resonator model, the unstable resonator model is a wave optics model. Thus, the unstable resonator model performs calculations in terms of the electric field, with intensities calculated from the electric field as needed. Since intensity is proportional to the square of the electric field strength,

$$I \propto E^2 = \vec{E} \cdot \vec{E} \qquad (2.1\text{-}2)$$

the incident electric field must be multiplied by the square root of the effective transmissivity used in the stable resonator model,

$$\vec{E}_{\text{after B.W.}} = \sqrt{t_w}\,\vec{E}_{\text{incident}} \qquad (2.1\text{-}3)$$

With this modification, Brewster window losses were included in the unstable resonator model. The placement of the Brewster windows in the optical cavity is shown in Fig. 2.

The value of t_w used in the unstable resonator model could not be determined as in the stable resonator case since there were no unstable resonator vacuum mirror mount data available. Instead, unstable resonator calculations were performed to evaluate the use of the stable resonator value of t_w in the unstable resonator model. The calculations were performed with $t_w = 1.0$ (no losses) and $t_w = 0.97$ for both the left and right Brewster windows for the low pressure Run 34 flow rates. The calculations used a set of baseline parameters determined by baselining the Fabry-Perot model, MNORO3, to stable resonator data[3,4]. These parameters, denoted the FPSR parameters, were used because they had been employed in the past unstable resonator calculations[8,10,11]. The unstable resonator calculations are compared to corresponding stable resonator calculations in Table 1. Since the value of t_w from the stable resonator model resulted in total power reductions that were comparable for both the unstable and stable resonator models, the value of $t_w = 0.97$ for both the left and right Brewster windows determined for the stable resonator model could be used with the unstable resonator model.

Resonator	Total Power (Watts)	Δ%
Stable resonator data, EMM[1]	28.2	
MNORO3SR[1] (t_w = 1.0)	35.23	
		27%
MNORO3SR[1] (t_w = 0.97)	25.55	
Unstable resonator 5 mm slit data, EMM[10,11]	2.25	
MNORO3UR, 5 mm slit (t_w = 1.0)[10,11]	11.00	
		35%
MNORO3UR, 5 mm slit (t_w = 0.97)	7.11	

Table 1 Comparison of the effect of Brewster window losses on stable and unstable resonator calculations for the low pressure Run 34 flow rates. The stable resonator baseline parameters were used in the MNORO3SR calculations and the FPSR parameters were used in the MNORO3UR calculations.

2.2 PREVIOUS UNSTABLE RESONATOR CALCULATIONS

An a priori calculation with the unstable resonator model, MNOR03UR, predicted the existence of time-dependent oscillations on lines whose saturated gain did not fill the unstable resonator[8,10,11]. The results of this calculation for a 50% geometric outcoupled, confocal unstable resonator with a large mirror diameter of 1.0 cm are presented in Figs. 3 through 5 and Table 2. The calculation was performed for the low SF_6 and low H_2 flow rates, Run 34, at a laser cavity pressure of 5.4 Torr. The FPSR baseline parameters were used in the calculation. There were no Brewster window losses included and thus the total power was overpredicted. As shown in Figs. 3 through 5 and Table 2, the calculation predicted a 40 nsec oscillation of the total power with an amplitude modulation of 36%. These oscillations occurred on lines whose saturated gain did not fill the resonator. On the individual lines, the period of the oscillations was approximately 40 nsec and the amplitude modulation varied from 18% to 100%. Since these oscillations were not a numerical instability[12] and are undesirable in a laser device, a laboratory experiment was devised to determine whether the oscillations occurred as predicted.

2.3 UNSTABLE RESONATOR DATA

The Helios CL II and CL I lasers were fully characterized in previous studies[2,3,4,10,11,13]. For completeness, the CL II and CL I unstable resonator data are summarized below.

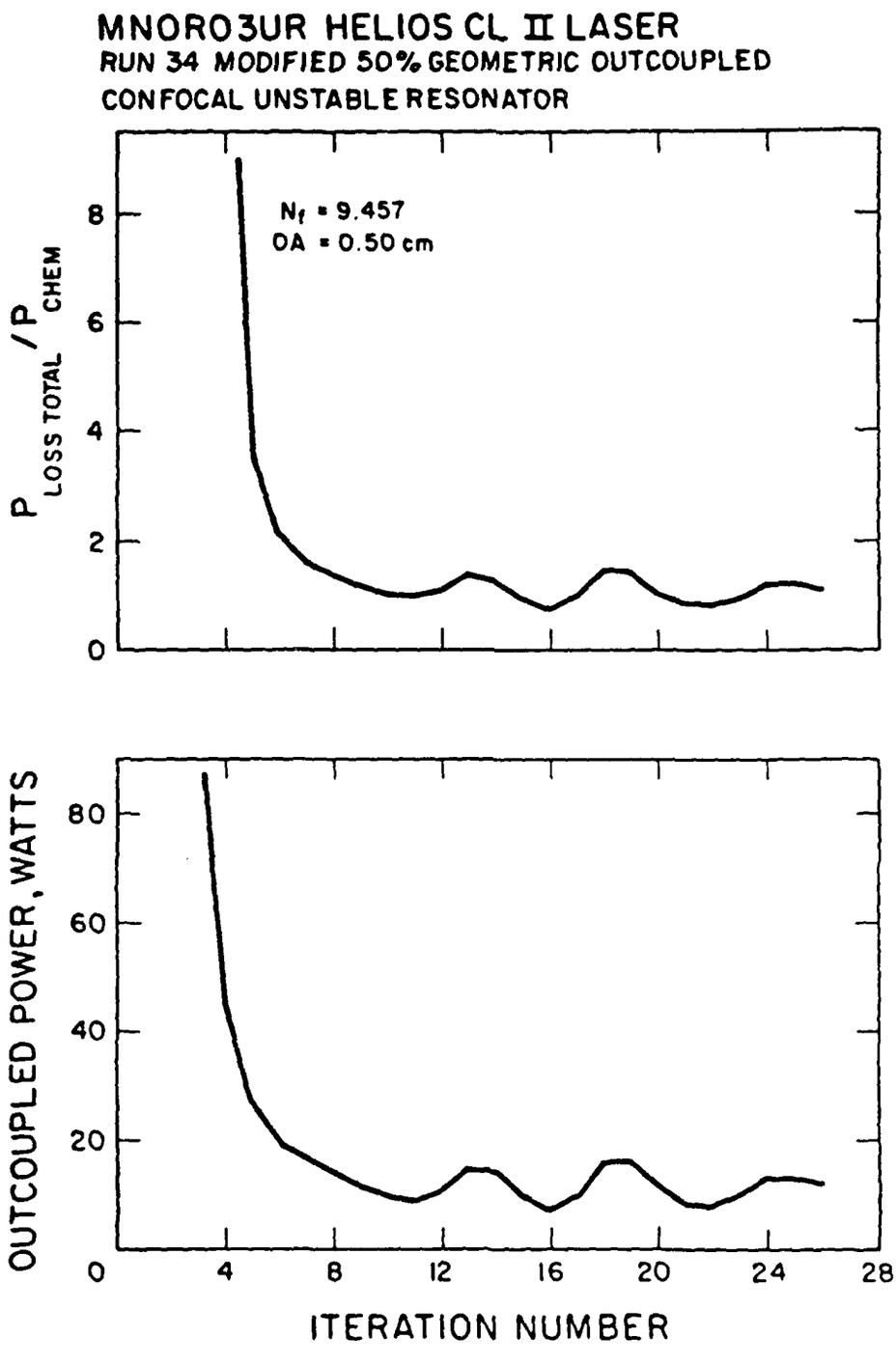

Figure 3 MNORO3UR convergence parameter $P_{loss\ total}/P_{chem}$ and the multiline outcoupled power calculated in the optics[8], P_{out}, versus iteration number for rotational nonequilibrium for a 50% geometric outcoupled, confocal, unstable strip resonator with a large mirror diameter of 1.0 cm for the Helios CL II laser for Run 34 at 5.4 Torr[10,11]. The FPSR baseline parameters were used.

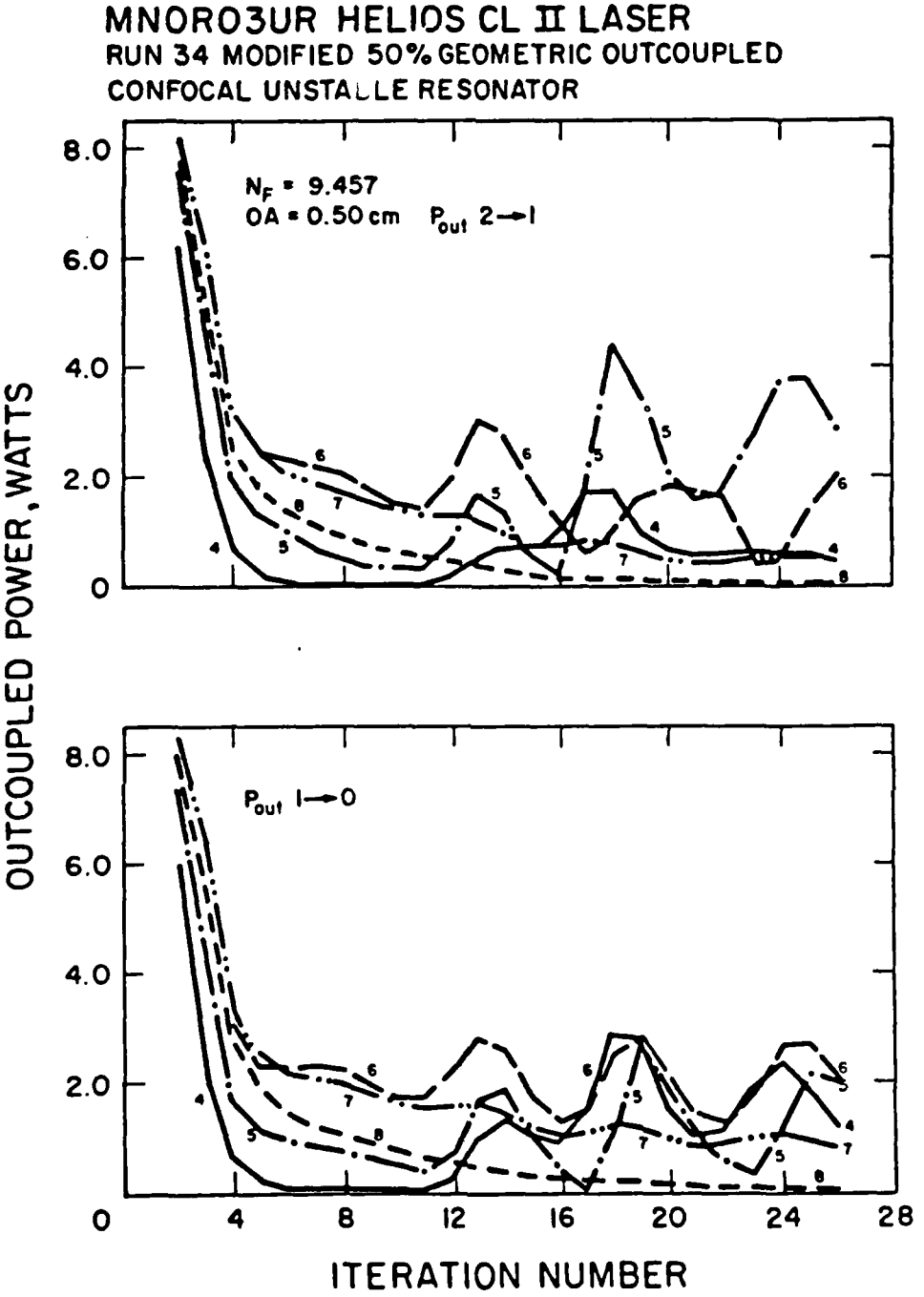

Figure 4 MNORO3UR outcoupled power[8], P_{out}, for individual lines versus iteration number for a 50% geometric outcoupled, confocal, unstable strip resonator with a large mirror diameter of 1.0 cm for the Helios CL II laser for Run 34 at 5.4 Torr[10,11]. The FPSR baseline parameters were used.

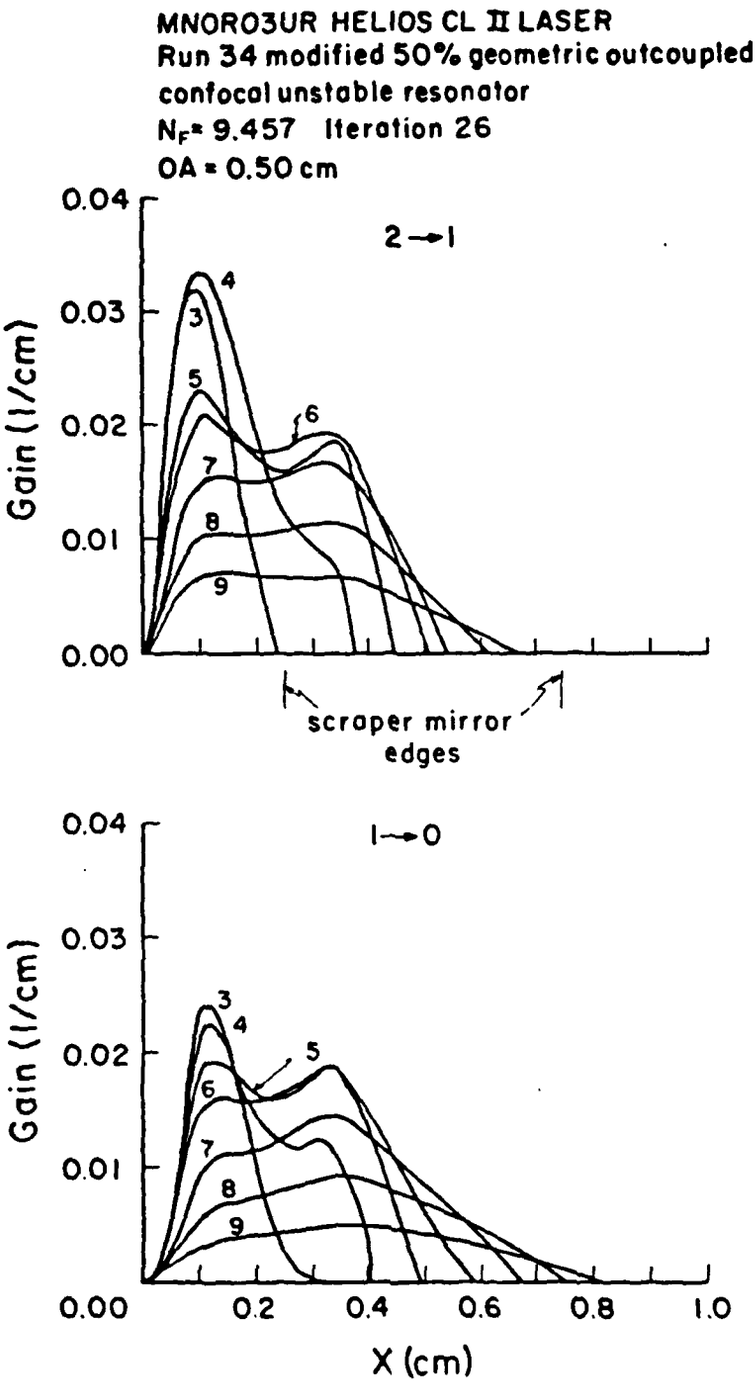

Figure 5 MNORO3UR gains at iteration 26 for a 50% geometric outcoupled, confocal, unstable strip resonator with a large mirror diameter of 1.0 cm for the Helios CL II laser for Run 34 at 5.4 Torr[10,11]. The FPSR baseline parameters were used.

Line	Period	Frequency	Amplitude Modulation	Power
	ns	MHz	% P_V (J)	Watts
Total Power	40	25	36*	11.00
$P_1(4)$	33	30	82	1.70
$P_1(5)$	40	25	100	1.20
$P_1(6)$	40	25	76	1.90
$P_1(7)$	33	30	18	1.00
$P_1(8)$				0.05
$P_2(4)$	40	25	27	0.60
$P_2(5)$	33	30	83	2.70
$P_2(6)$	40-47	21-25	92	1.30
$P_2(7)$	33-40	25-30	40	0.50
$P_2(8)$				0.05

*Amplitude Modulation for Total Power: % P_T

Table 2 MNOR03UR CL II time-dependent oscillation periods, frequencies, and amplitude modulations (% P_V(J)) for a 50% geometric outcoupled, confocal unstable resonator with a 5 mm slit for the Run 34 flow rates at 5.4 Torr[10,11]. The FPSR baseline parameters were used.

Figure 6 shows the layout of the 50% geometric outcoupled, confocal, unstable resonator used on both the Helios CL II and CL I lasers. The resonator consists of a convex and a concave mirror separated by 100 cm, with a flat scraper mirror placed at an angle of 45° to the optical axis near the convex mirror. The radius of curvature of the mirrors is -200 cm for the convex mirror and 400 cm for the concave mirror which result in a resonator magnification of 2. The scraper mirror consists of two flat mirrors which slide apart to form a slit whose width could be varied from 0.0 to 1.0 cm. Since the resonator was a confocal unstable resonator with a magnification of 2, the effective diameter of the convex mirror is equal to the scraper mirror slit width, and the effective diameter of the concave mirror is equal to twice the scraper mirror slit width. The resonator Fresnel number is given by

$$N_F = \frac{D^2}{4\lambda L} \qquad (2.3\text{-}1)$$

where D is the effective diameter of the large mirror, λ is the optical wavelength and L is the mirror spacing. Since the effective diameter of the large mirror is determined by the scraper mirror slit width, the Fresnel number is controlled by the scraper mirror slit width.

2.3.1 RUN 34, LOW PRESSURE DATA

Total power, oscillation frequency and amplitude measurements for the low SF_6 and low H_2 flow rates, Run 34, were taken with a laser cavity pressure of 5.3 Torr in the CL II and 5.4 Torr in the

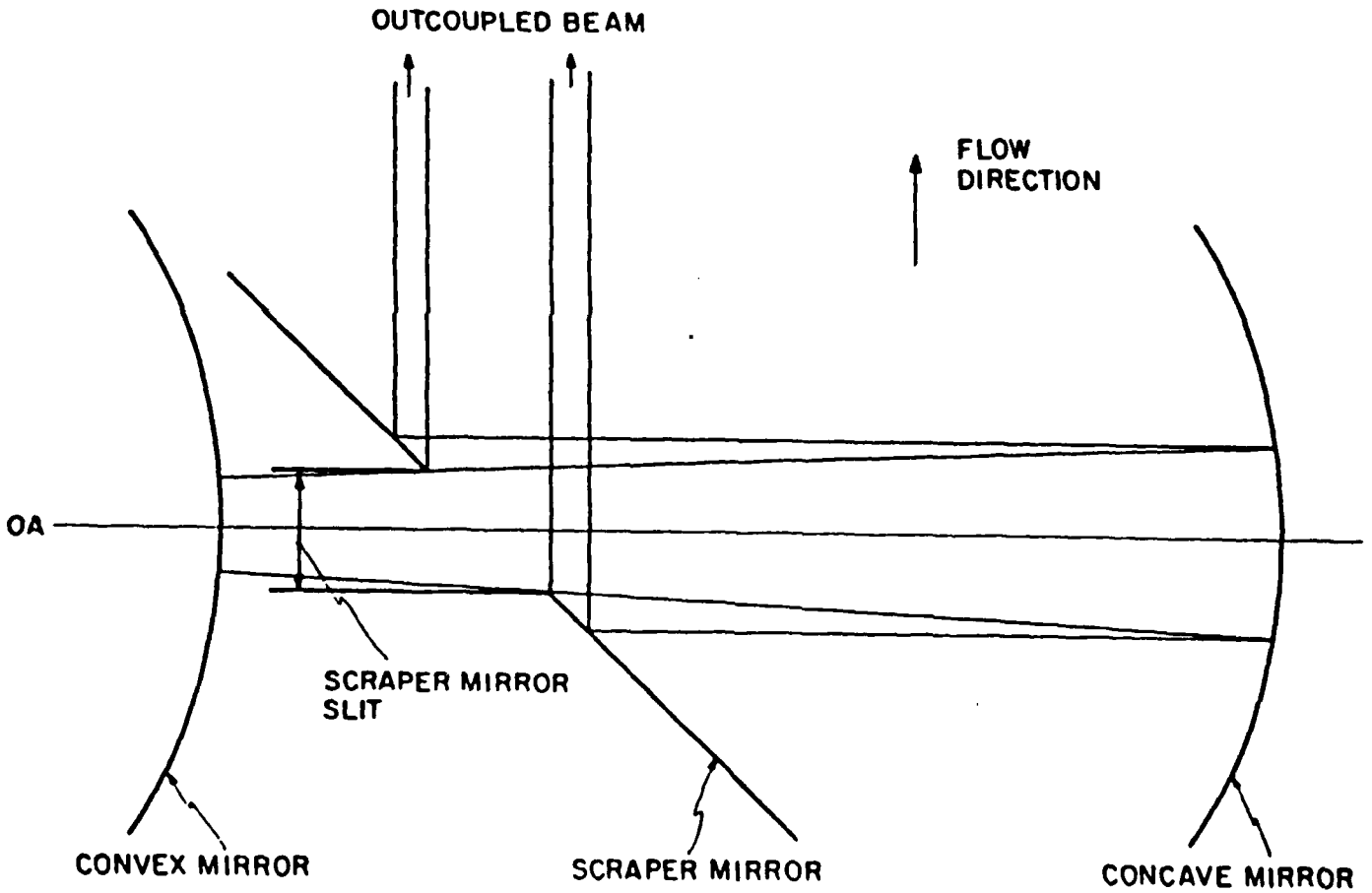

Figure 6 Layout of the unstable resonator used in the measurement of the time-dependent oscillations on lines whose saturated gain does not fill the resonator. The resonator was always aligned with the upstream edge at the hydrogen injectors.

CL I[10,11,13]. Because the resonator was symmetric and was always aligned with the upsteam edge at the H_2 injectors, the distance between the optical axis and the H_2 injectors was always equal to the scraper mirror slit width. The oscillation and total power data are summarized as a function of Fresnel number for the CL II laser in Table 3 and for the CL I laser in Table 4. From Tables 3 and 4 it is seen that, in addition to a 40 nsec oscillation, there was a 7 nsec oscillation superimposed on it. Since the mirror spacing of the resonator was 100 cm and the round trip transit time for a photon is 6.67 nsec, the 7 nsec oscillation corresponds to a mode beat of the laser. The time-dependent oscillations did not occur for Fresnel numbers below a demarcation Fresnel number of 1.5 in the CL II and 3.2 in the CL I. Since calculations had shown that the length of the saturated gain region was independent of the size of the resonator[3], Tables 3 and 4 show that the amplitude of the oscillations increased as the fraction of the resonator filled by the oscillating lines decreased.

The oscillation data for individual lines as a function of Fresnel number are given for the CL II and CL I in Tables 5 and 6, respectively. These data show that the 40 nsec oscillation on lines whose saturated gain did not fill the resonator did not occur for Fresnel numbers below the demarcation Fresnel number of 1.5 for the CL II and 3.2 for the CL I.

2.3.2 RUN 36, LOW PRESSURE DATA

Oscillation frequency and amplitude measurements for Run 36, the middle SF_6 and high H_2 flow rate, were taken at laser cavity pressures

CL II, Run 34, 5.30 Torr, 50% Geometric Outcoupled,
Symmetric, Confocal, Unstable Resonator

Scraper Mirror Slit, mm	N_F	P_{cav} (Torr)	P_T (Watts)	OSC. Period (nsec)	Amplitude Modulation (% P_T)
1.0	0.357	5.31	7.25	7	--
2.0	1.428	5.30	11.7	7	--
3.0	3.214	5.29	9.5	40/7	3.0
4.0	5.714	5.31	7.0	40/7	22.0
5.0	8.929	5.34	2.25	40/7	25.0
6.0	12.857	5.31	0.98	40	50.0

Table 3 Measured[10,11] frequency and amplitude of the time-dependent oscillation of total power as a function of Fresnel number for the Run 34 flow rates at 5.3 Torr.

CL I, Run 34, 5.40 Torr, 50% Geometric Outcoupled,
Symmetric, Confocal, Unstable Resonator

Scraper Mirror Slit, mm	N_F	P_T (Watts)	OSC. Period (nsec)	Amplitude Modulation (% P_T)
1.0	0.357	0.39	--	--
2.0	1.428	1.97	7	5.3
3.0	3.214	1.03	7	4.7
4.0	5.714	0.10	47/7	50.1
5.0	8.929	0.01	--	--

Table 4 Measured[13] frequency and amplitude of the time-dependent oscillation of total power as a function of Fresnel number for the Run 34 flow rates at 5.4 Torr.

CL II, Run 34 50% Geometric Outcoupled, Symmetric, Confocal, Unstable Resonator
Cavity Pressure 5.30 Torr

Scraper Mirror Slit, mm	N_f	Lasing Line	$P_1(4)$	$P_1(5)$	$P_1(6)$	$P_1(7)$	$P_1(8)$	$P_1(9)$	$P_2(5)$	$P_2(6)$	$P_2(7)$	$P_2(8)$	P_T Watts
1.0	0.357	OSC Period, ns	-	-	-				7	7			7.25
1.5	0 804	OSC Period, ns	-	-	7	-			7	7	-	-	12.8
2.0	1.428	OSC Period, ns (Strength of 7 ns OSC)	-	-	7	7	-		7 (weak)	7	7 (weak)	-	11.9
		Amplitude Modulation % $P_v(J)$			9	11				13			
3.0	3.214	OSC Period, ns (Strength of 40 ns OSC)			40/7 (weak)	40/7	40/7 (weak)	7		40/7	40/7 (weak)	7	9.9
		OSC Freq., MHz			23-26	23-34	23-30			18-29	25-31		
		Amplitude Modulation % $P_v(J)$				12.5				20-50	12	12.5	
4.0	5.714	OSC Period, ns (Strength of 40 ns OSC)			-	40/7	40/7	40 (weak)		40	40/7	40/7	7.1
		OSC Freq., MHz				20-30	20-30	20-30		20-28	18-30	22-30	
		Amplitude Modulation % $P_v(J)$				38	80			20-30	66	55	

- means the line lased but was too weak to operate the fast detector.

Table 5 Measured[10,11] frequency and amplitude of the time-dependent oscillations on individual lines for the Run 34 flow rates at 5.3 Torr as a function of Fresnel number. Individual line data were not obtained for the 5 mm and 6 mm slit widths because the individual lines in these cases were too weak to operate the fast detector. A PbSe detector was used to measure time averaged power spectral distributions. Lines too weak to operate the fast InAs detector would operate the PbSe detector.

CL I, Run 34, 5.40 Torr, 50% Geometric Outcoupled,
Symmetric, Confocal, Unstable Resonator

Scraper Mirror Slit (mm)	N_F	Lasing Line	$P_1(6)$	$P_1(7)$	$P_1(8)$	$P_2(5)$	$P_2(6)$	$P_2(7)$	$P_2(8)$	P_T (Watts)
2.0	1.428	OSC Period (ns)	7	7		--	7	7		1.97
		Amplitude Modulation % $P_v(J)$	24.1	17.6			25.0	28.5		
3.0	3.214	OSC Period (ns)	--	--	--		7	7		1.03
		Amplitude Modulation % $P_v(J)$					22.5	13.9		
4.0	5.714	OSC Period (ns)		47/7				--		0.10
		OSC Freq. (MHz)		21.1						
		Amplitude Modulation % $P_v(J)$		34.6						

-- Means that the line lased but was too weak to operate the fast detector.

Table 6 Measured[13] frequency and amplitude of the time-dependent oscillations on individual lines for the Run 34 flow rates at 5.4 Torr as a function of Fresnel number. Individual line data were not taken for the 5 mm slit because the individual lines in this case were too weak to operate the fast detector.

of 6.30 Torr in the CL II and 6.50 Torr in the CL I[10,11,13]. Since a symmetric resonator that was aligned with the upstream edge at the H_2 injectors was used in both cases, the distance between the optical axis and the H_2 injectors was always equal to the scraper mirror slit width. These data are summarized in Tables 7 through 10. Again, both the 7 nsec and the 40 nsec oscillations appear in both lasers on lines whose saturated gain does not fill the resonator. These oscillations did not occur for Fresnel numbers below the demarcation Fresnel numbers of 1.5 for the CL II and 3.2 for the CL I.

2.3.3 COMPARISON OF CL II AND CL I UNSTABLE RESONATOR DATA

It should be noted that a comparison of the CL II and CL I unstable resonator data showed that fewer lines were observed with the CL I and the total powers of the two devices are very different. In Ref. 13, this is shown to be a consequence of the fact that the saturated gain in the CL I is twice as large as the saturated gain in the CL II. Overall, as shown in Ref. 13, the CL I unstable resonator data are consistent with the CL II unstable resonator data.

2.4 COMPARISON OF THE A PRIORI UNSTABLE RESONATOR CALCULATIONS TO THE CL II DATA

Tables 2, 3 and 5 show that when compared to the data, the 5 mm slit MNORO3UR calculation in Section 2.2 accurately predicted both the period and amplitude modulation of the 40 nsec time-dependent oscillations. However, the total power was overpredicted beyond what was expected from the lack of Brewster window losses in the calculation. This indicated that the FPSR baseline parameters used in the calculation were not correct.

CL II, Run 36, 6.30 Torr, 50% Geometric Outcoupled,
Symmetric, Confocal, Unstable Resonator

Scraper Mirror Slit, mm	N_F	P_{cav} (Torr)	P_T (Watts)	OSC. Period (nsec)	Amplitude Modulation (% P_T)
1.0	0.357	6.5	10.5	--	--
2.0	1.428	6.5	17.2	7	--
3.0	3.214	6.5	12.2	40/7	3.7
4.0	5.714	6.5	6.55	40/7	33.0
5.0	8.929	6.5	1.55	40/7	37.5

Table 7 Measured[10,11] frequency and amplitude of the time-dependent oscillation of total power as a function of Fresnel number for the Run 36 flow rates at 6.3 Torr.

CL I, Run 36, 6.50 Torr, 50% Geometric Outcoupled,
Symmetric, Confocal, Unstable Resonator

Scraper Mirror Slit, mm	N_F	P_T (Watts)	OSC. Period (nsec)	Amplitude Modulation (% P_T)
1.0	0.357	1.08	--	--
2.0	1.428	2.59	7	3.7
3.0	3.214	1.22	7	2.9
4.0	5.714	0.11	47/7	15.5
5.0	8.929	0.01	40	80.8

Table 8 Measured[13] frequency and amplitude of the time-dependent oscillation of total power as a function of Fresnel number for the Run 36 flow rates at 6.5 Torr.

CL II, Run 36 50% Geometric Outcoupled, Symmetric, Confocal, Unstable Resonator

Cavity Pressure 6.30 Torr

Scraper Mirror Slit, mm	N_F	Lasing Line	$P_1(4)$	$P_1(5)$	$P_1(6)$	$P_1(7)$	$P_1(8)$	$P_1(9)$	$P_2(5)$	$P_2(6)$	$P_2(7)$	$P_2(8)$	$P_2(9)$	P_T Watts
2.0	1.428	OSC Period, ns			7	7	-		-	7	7 (weak)	-		12.6
		(Strength of 7ns OSC)												
3.0	3.214	OSC Period, ns			7	40/7 (weak)	40/7 (weak)	-		40/7 (weak)	40/7 (weak)	7	-	9.8
		(Strength of 40ns OSC)												
		OSC Freq., MHz				16-28	25-30			18-28	24-30			
4.0	5.714	OSC Period, ns			-	40/7	40/7	40 (weak)			40/7	40	-	3.8
		(Strength of 40ns OSC)												
		OSC Freq., MHz				22-28	23-28	24-28			22-30	22-30		
		Amplitude Modulation % $P_v(J)$				30	50				66	50		
5.0	8.929	OSC Period, ns				40 (weak)	40/7 (weak)	40/7 (weak)				-	-	0.78
		(Strength of 40ns OSC)												
		OSC Freq., MHz				24-26	24-27	25-27						

- Means the line lased but was too weak to operate the fast detector

Table 9 Measured[10,11] frequency and amplitude of the time-dependent oscillations on individual lines for the Run 36 flow rates at 6.3 Torr as a function of Fresnel number. A PbSe detector was used to measure time averaged power spectral distributions. Lines too weak to operate the fast InAs detector would operate the PbSe detector.

CL I, Run 36, 6.50 Torr, 50% Geometric Outcoupled,
Symmetric, Confocal, Unstable Resonator

Scraper Mirror Slit (mm)	N_F	Lasing Line	$P_1(6)$	$P_1(7)$	$P_1(8)$	$P_2(5)$	$P_2(6)$	$P_2(7)$	$P_2(8)$	P_T (Watts)
2.0	1.428	OSC Period (ns)	--	7	7		--	--	--	2.59
		Amplitude Modulation % $P_v(J)$		30.9	20.1					
3.0	3.214	OSC Period (ns)	--	--	7			--	--	1.22
		Amplitude Modulation % $P_v(J)$			20.9					
4.0	5.714	OSC Period (ns)		--	47/7	—				0.11
		OSC Freq. (MHz)			21.1					
		Amplitude Modulation % $P_v(J)$			57.0					

-- Means that the line lased but was too weak to operate the fast detector.

Table 10 Measured[13] frequency and amplitude of the time-dependent oscillation of total power as a function of Fresnel number for the Run 36 flow rates at 6.5 Torr. Individual line data were not taken for the 5 mm slit because the individual lines in this case were too weak to operate the fast detector.

In addition to the 40 nsec oscillation, the data showed a 7 nsec oscillation superimposed on it. Since the mirror spacing of the resonator was 100 cm and the round trip transit time for a photon is 6.67 nsec, the 7 nsec oscillation corresponds to a longitudinal mode beat of the laser. The MNOR03UR calculation did not predict a 7 nsec oscillation because the model does not include the longitudinal modes of the lasing lines.

2.5 UNSTABLE RESONATOR BASELINING CALCULATIONS

The first step required to determine if it was necessary to baseline the unstable resonator model to unstable resonator data was to use the Fabry-Perot and stable resonator parameters in the unstable resonator model. If calculations with these parameters did not correctly model the measured unstable resonator performance, the unstable resonator model would need to be baselined to unstable resonator data. Unstable resonator calculations with the Fabry-Perot and stable resonator parameters were performed for two 50% geometric outcoupled, confocal unstable resonators, one with a 4 mm slit and one with a 5 mm slit. The resonator with the 4 mm slit was the resonator for which the best CL II time-dependent oscillation data were available[10,11]. The resonator with the 5 mm slit was the one for which the a priori calculation was performed that predicted the existance of time-dependent oscillations on lines whose saturated gain does not fill the resonator.

The results of these calculations are summarized in Table 11. Results from calculations with the FPSR parameters are also included in

Baseline Parameters	Slit Width (mm)	Total Power (Watts)	Oscillation Period (nsec)	Oscillation Amplitude (% total power)
EMM Data[10,11]	4	7.0	40	22.0
Fabry-Perot	4	19.9	20	2.5
Stable Resonator	4	30.4	20	1.6
FPSR	4	11.6	20	1.7
EMM Data[10,11]	5	2.25	40	25.0
Stable Resonator	5	29.0	20	1.7
FPSR	5	11.0	40	36.0

Table 11 Summary of the 4 mm and 5 mm slit unstable resonator data and MNORO3UR calculations for the Helios CL II for the low pressure Run 34 flow rates. All calculations used $t_w = 1.0$.

Table 11 since these parameters were used in previous unstable resonator modeling. All of the calculations summarized in Table 11 had no Brewster window losses included and thus were expected to overpredict the total power. Table 11 shows that the FPSR parameters allow the unstable resonator model to more accurately predict the data than either the Fabry-Perot or stable resonator parameters. However, with the FPSR parameters, the model overpredicted the total power in both resonators beyond what was expected from the lack of Brewster window losses in the calculation. Also, the period and amplitude modulation of the time-dependent oscillations were not correct in the 4 mm slit case. Based upon the fact that neither the Fabry-Perot, nor the stable resonator, nor the FPSR parameters allowed the unstable resonator model to accurately predict unstable resonator performance as the size of the resonator was varied, the unstable resonator model was baselined to the unstable resonator data.

To baseline the unstable resonator model, four baseline parameters had to be determined so that the unstable resonator model tracked the unstable resonator data as resonator size, flow rates and size of the laser were varied. The data to be tracked were the total power and the period and amplitude modulation of the time-dependent oscillations that occur on lines whose saturated gain does not fill the resonator. The four baseline parameters are the static temperature of the flow at the H_2 injectors, the percent dissociation of the SF_6 in the arc, the primary mixing length, and the secondary mixing length. Of these four parameters, two had been fixed with confidence in previous studies[1,3]. A primary mixing length of 0.001 cm and a temperature of the flow at the

H_2 injectors of 450 K were found to be appropriate. Thus, only two of the four parameters, the percent dissociation of the SF_6 in the arc and the secondary mixing length, were varied in baselining the unstable resonator model.

In an earlier investigation[1], three of the four baseline parameters were varied and the effect on the total power, power split between vibrational bands and beam diameter was calculated using the rotational equilibrium, Fabry-Perot BLAZE II model. The one baseline parameter that was not varied in this parametric study was the primary mixing length which was set at 0.001 cm. The results of these calculations, which served as a guide in choosing parameter combinations for the unstable resonator, are presented in Figs. 7 through 12.

The low pressure Run 34 flow rates were chosen as the baseline flow rates since the best unstable resonator data were taken at these flow rates[10,11]. The 2 mm slit resonator was chosen as the first baseline case because experimentally it does not display the time-dependent oscillations. Once the data were matched for the 2 mm slit, the data for larger slit sizes would be matched if the parameter set was valid. From Figs. 7 through 12, a set of parameters was chosen to match the 2 mm slit total power data. This parameter set is denoted Set A in Table 12. Two calculations were made with Set A, one with Brewster window losses included and one with no Brewster window losses. This provided a check on the validity of using the stable resonator effective Brewster window transmissivity of $t_w = 0.97$ in the unstable resonator model. Table 13 summarizes the results of the 2 mm slit calculations with Set A. A comparison of the predicted total powers indicated that

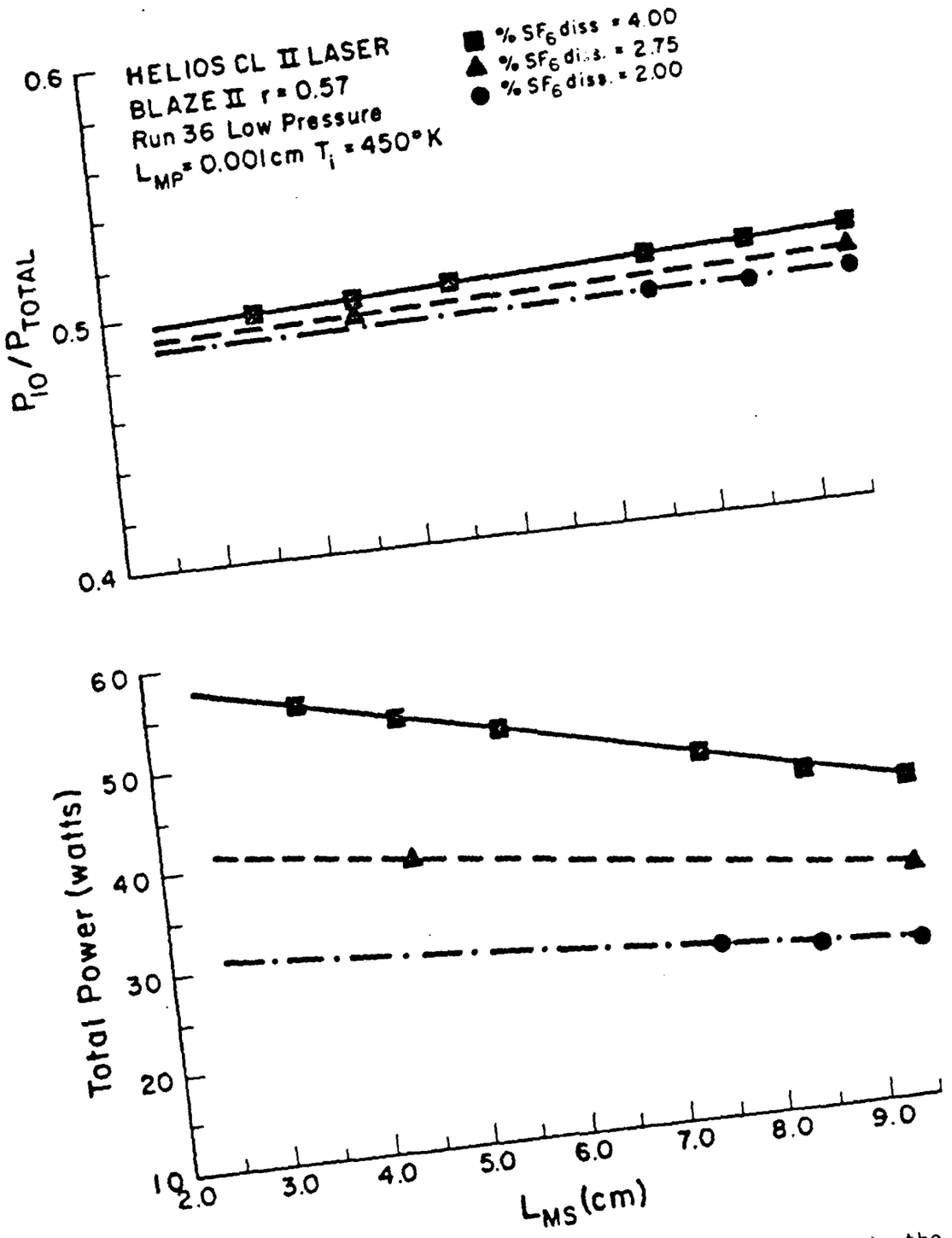

Figure 7 Variation of total power and fraction of power in the 1-0 vibrational band[1] as a function of secondary mixing length from the BLAZE II model of the CL II laser. L_{MP} is the mixing length of the primary stream.

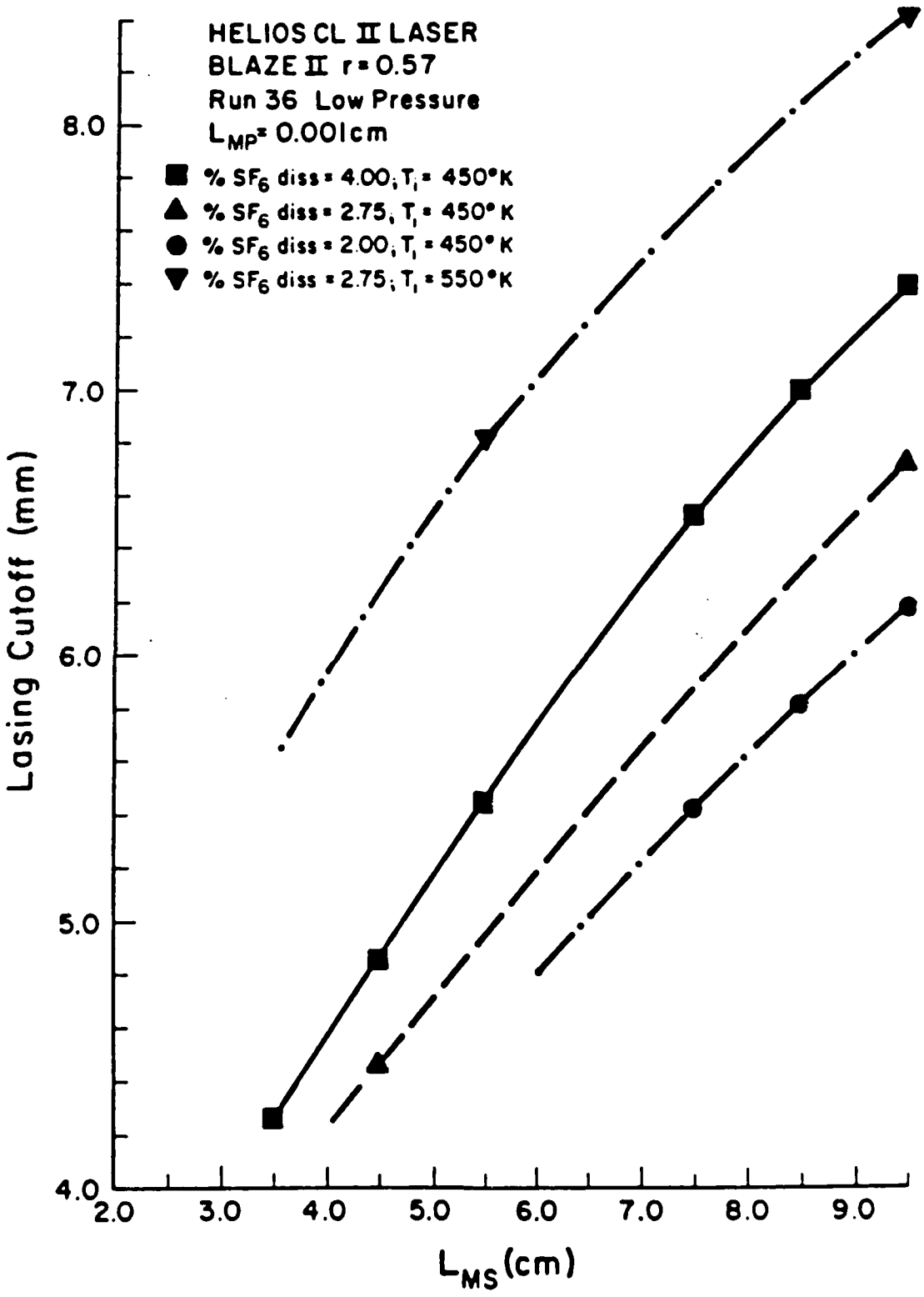

Figure 8 Variation of lasing cutoff[1] as a function of secondary mixing length from the BLAZE II model of the CL II laser. L_{MP} is the mixing length of the primary stream.

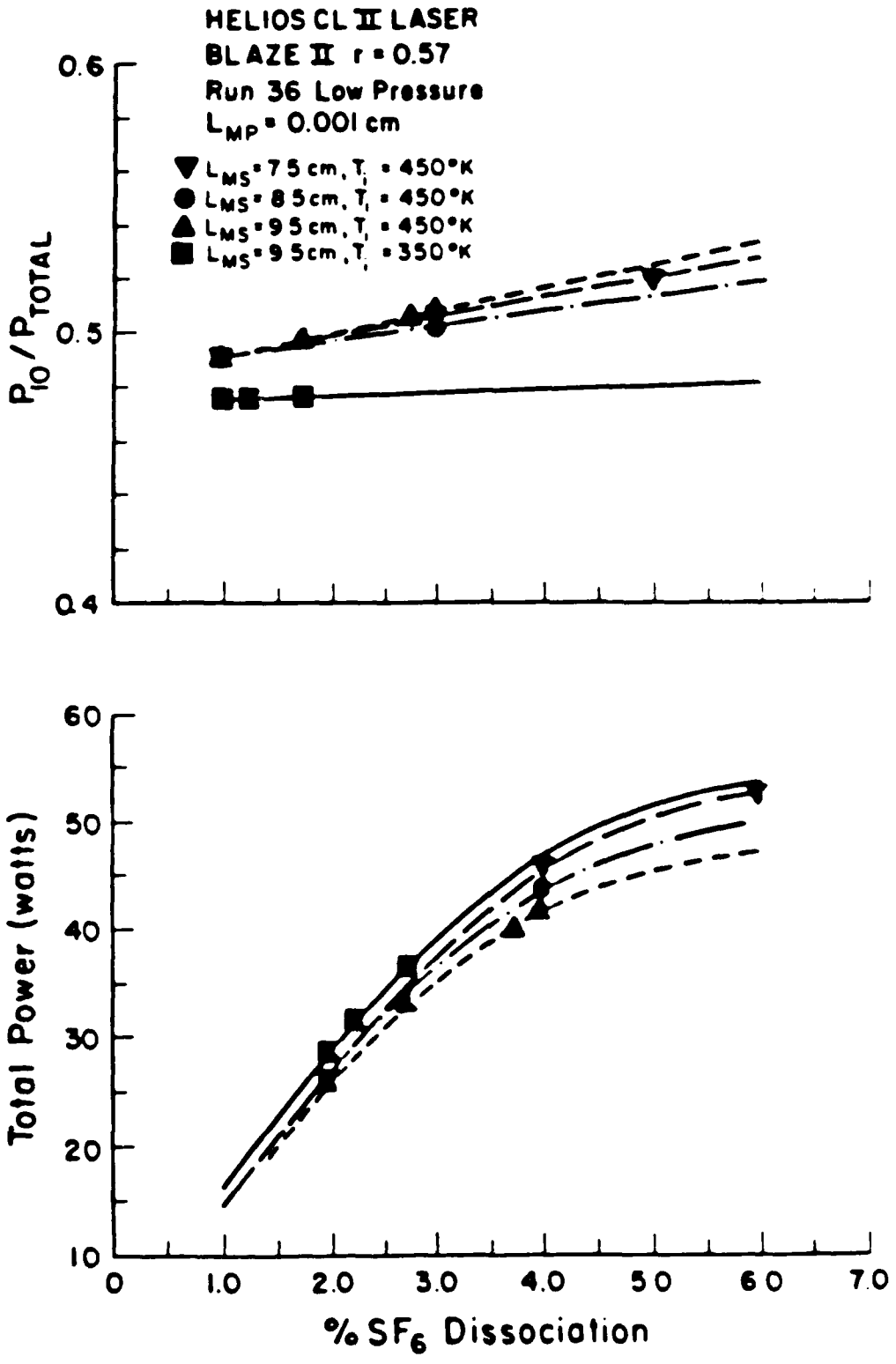

Figure 9 Variation of total power and fraction of power in the 1-0 vibrational band[1] as a function of precent SF_6 dissociation from the BLAZE II model of the CL II laser, L_{MP} is the mixing length of the primary stream, L_{MS} is the mixing length of the secondary stream.

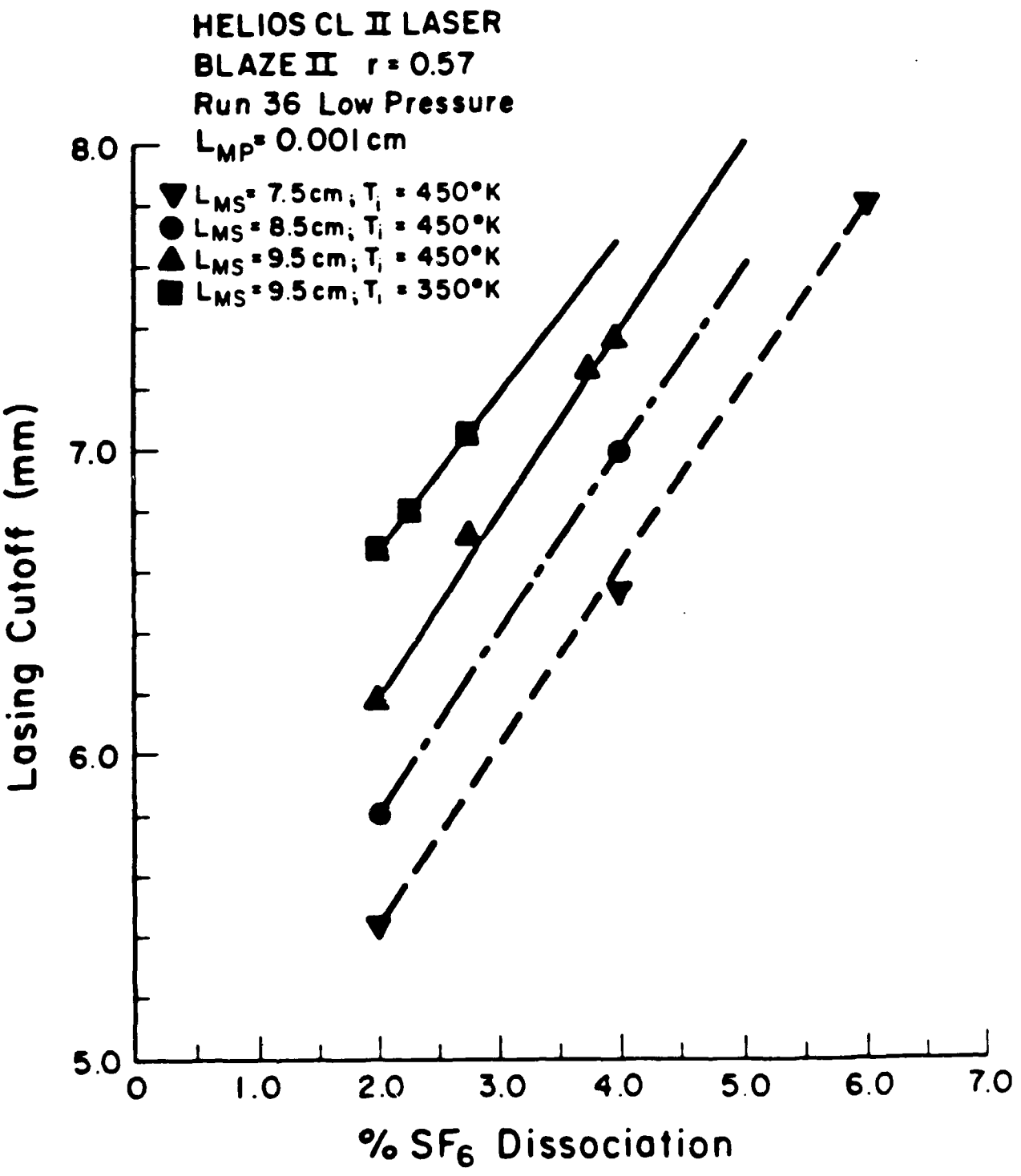

Figure 10 Variation of lasing cutoff[1] as a function of percent SF_6 dissociation from the BLAZE II model of the CL II laser. L_{MP} is the mixing length of the primary stream. L_{MS} is the mixing length of the secondary stream.

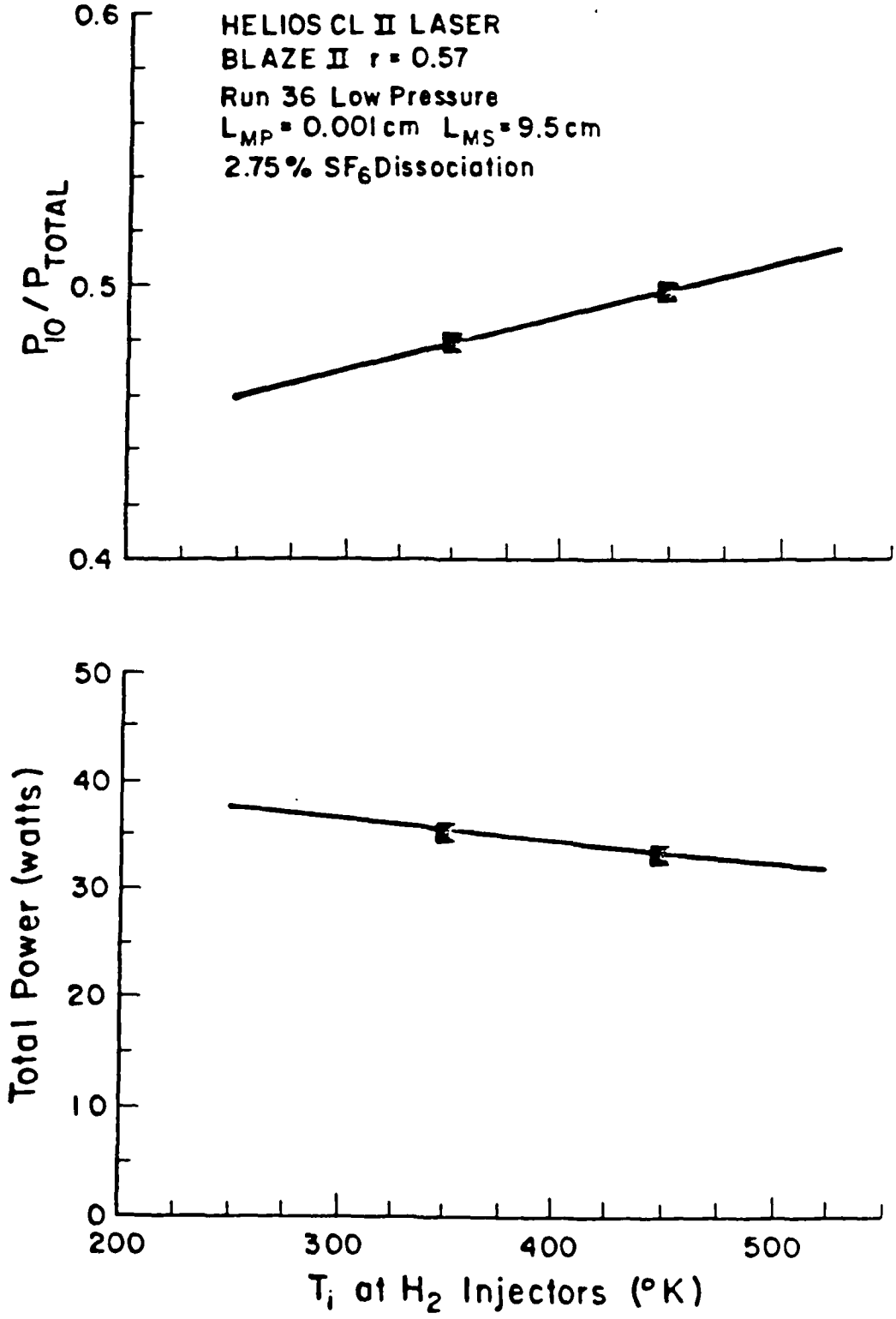

Figure 11 Variation of total power and fraction of power in the 1→0 vibrational band[1] as a function of the initial temperature at the H_2 injectors from the BLAZE II model of the CL II laser. L_{MP} is the mixing length of the primary stream. L_{MS} is the mixing length of the secondary stream.

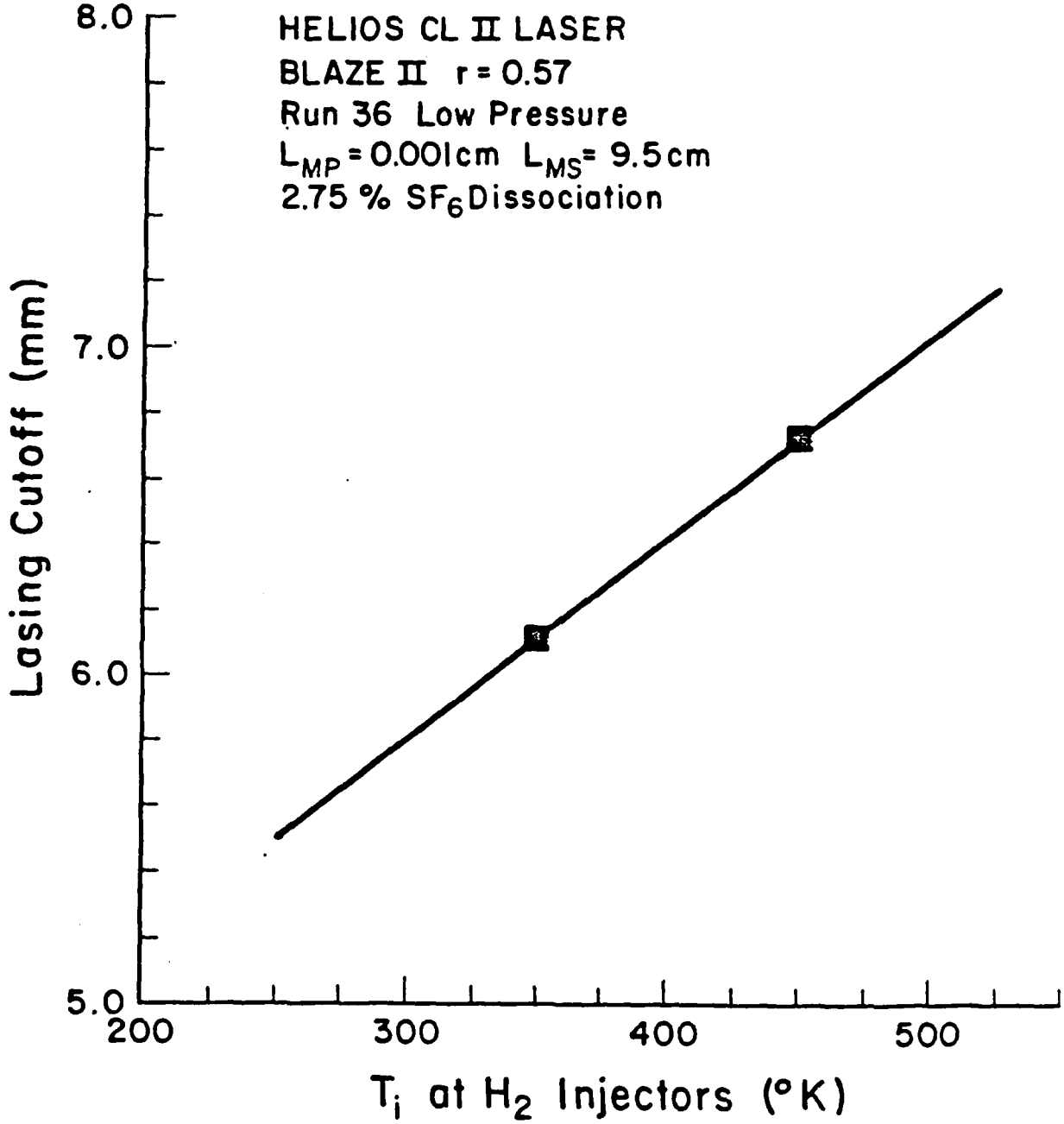

Figure 12 Variation of the lasing cutoff[1] as a function of the initial temperature at the H_2 injectors from the BLAZE II model of the CL II laser. L_{MP} is the mixing length of the primary stream, L_{MS} is the mixing length of the secondary stream.

Parameter Set	Static Temp. at H_2 Injectors (K)	Primary Mixing Length (cm)	Secondary Mixing Length (cm)	% SF_6 Dissociation
Fabry-Perot	450	0.001	8.50	3.25
Stable resonator	450	0.001	2.50	4.73
FPSR	450	0.001	4.00	4.00
Set A	450	0.001	3.10	5.50
Set B	450	0.001	3.10	2.36
Set C	450	0.001	3.10	3.20
Set D	450	0.001	2.50	1.20
Set E	450	0.001	0.95	1.20

Table 12 Summary of parameter sets used in baselining MNOR03UR.

Baseline Parameters	Slit Width (mm)	Total Power (Watts)	Oscillation Period (nsec)	Oscillation Amplitude (% total power)
Data[10,11]	2	11.7	--	--
Data[10,11]	4	7.0	40	22
Set A (t_w = 1.0)	2	26.2	20	7
Set A	2	19.6	20	7
Set B	2	8.8	20	8
Set C	2	12.0	20	8
Set C	4	20.4	40	9
Set D	2	4.7	--	--
Set D	4	7.3	40	9
Set E	2	5.3	40	4
Set E	4	7.5	40	4

Table 13 Summary of 2 mm and 4 mm slit MNOR03UR baselining calculations and data for the Helios CL II for the low pressure Run 34 flow rates. All calculations were with t_w = 0.97 unless otherwise indicated; all calculations were for a 50% geometric outcoupled, confocal, unstable strip resonator.

t_w = 0.97 introduced a 25% loss which compared well with the 27% loss introduced in the stable resonator model, Table 1. The comparable reduction in total power in both stable and unstable resonator models reinforced the conclusion that the value of the effective transmissivity of the Brewster windows determined for the stable resonator model is appropriate for the unstable resonator model.

Table 13 shows that the calculation with Set A that included Brewster window losses overpredicted the total power. Since Figs. 9 and 10 indicated that total power is a strong function of the percent dissociation of SF_6 in the arc, to reduce the predicted total power, the SF_6 dissociation was reduced to 2.36%. This new parameter set is denoted Set B in Table 12. The results of a 2 mm slit calculation performed with Set B are shown in Table 13. The total power calculated with Set B was too low.

A value of the percent SF_6 dissociation that would give the observed 2 mm slit total power was determined through linear interpolation from the calculation with Set A and the calculation with Set B. This percent SF_6 dissociation, 3.2%, along with the other parameters from Set B, comprise parameter Set C, Table 12. A 2 mm unstable resonator calculation with parameter Set C, Table 13, gave good agreement with the measured total power. There was, however, a 20 nsec small amplitude oscillation predicted that was not seen in the data.

Since 2 mm slit calculations with parameter Set C matched the total power data, a calculation with the same parameter set was made for a 4 mm slit resonator, Table 13. Unfortunately, with parameter Set C, the 4 mm slit total power was overpredicted by a factor of three. The

oscillation period, however, was correct at 40 nsec. The inability of Set C to allow the model to predict the data as the resonator size changed indicated that Set C was not correct.

The gains and the intensity distributions from the preceding two calculations with Set C, Figs. 13 through 16, were compared. These figures suggested that the gain zones should be shortened. With the gain zones shortened, the intensity peak would move out from behind the small mirror, making it less symmetric in the 2 mm slit case. Laboratory burn blocks show an unsymmetric intensity distribution in the 2 mm slit case. Since moving the intensity peak into the outcoupling portion of the cavity would increase the total power, the percent SF_6 dissociation should be reduced to compensate.

To choose a parameter set that would shorten the gain zones, a set of BLAZE II zero power gain calculations were performed to determine the variation of the gain distribution as a function of the secondary mixing length and the percent SF_6 dissociation. The resulting zero power gain curves are presented in Figs. 17 through 30. The BLAZE II zero power gain curves indicated that the magnitude of the peak zero power gain was a strong function of the percent SF_6 dissociation and a very weak function of the secondary mixing length and that the axial location of the peak zero power gain is a strong function of the secondary mixing length. Figures 29 and 30 indicated that a secondary mixing length of 2.5 cm would move the gains upstream and a 1.2% SF_6 dissociation would give peak zero power gains of about 0.08 cm^{-1}. This peak zero power gain and position were reasonable and thus another set of baseline parameters was chosen. These parameters are denoted Set D in Table 12.

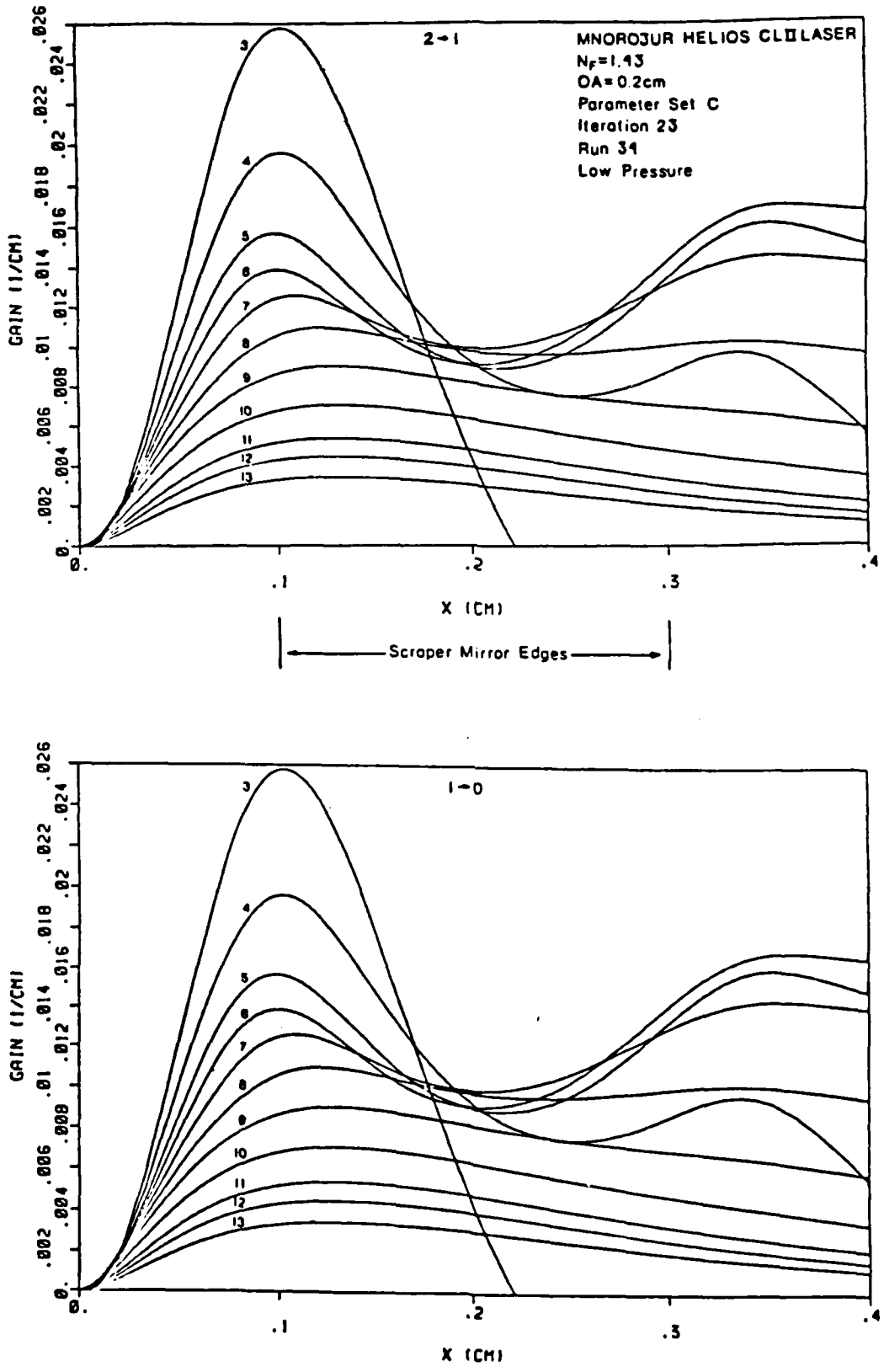

Figure 13 MNORO3UR gains at iteration 23 for a 50% geometric out-coupled, confocal unstable strip resonator with a large mirror diameter of 4 mm for the Helios CL II for the low pressure Run 34 flow rates.

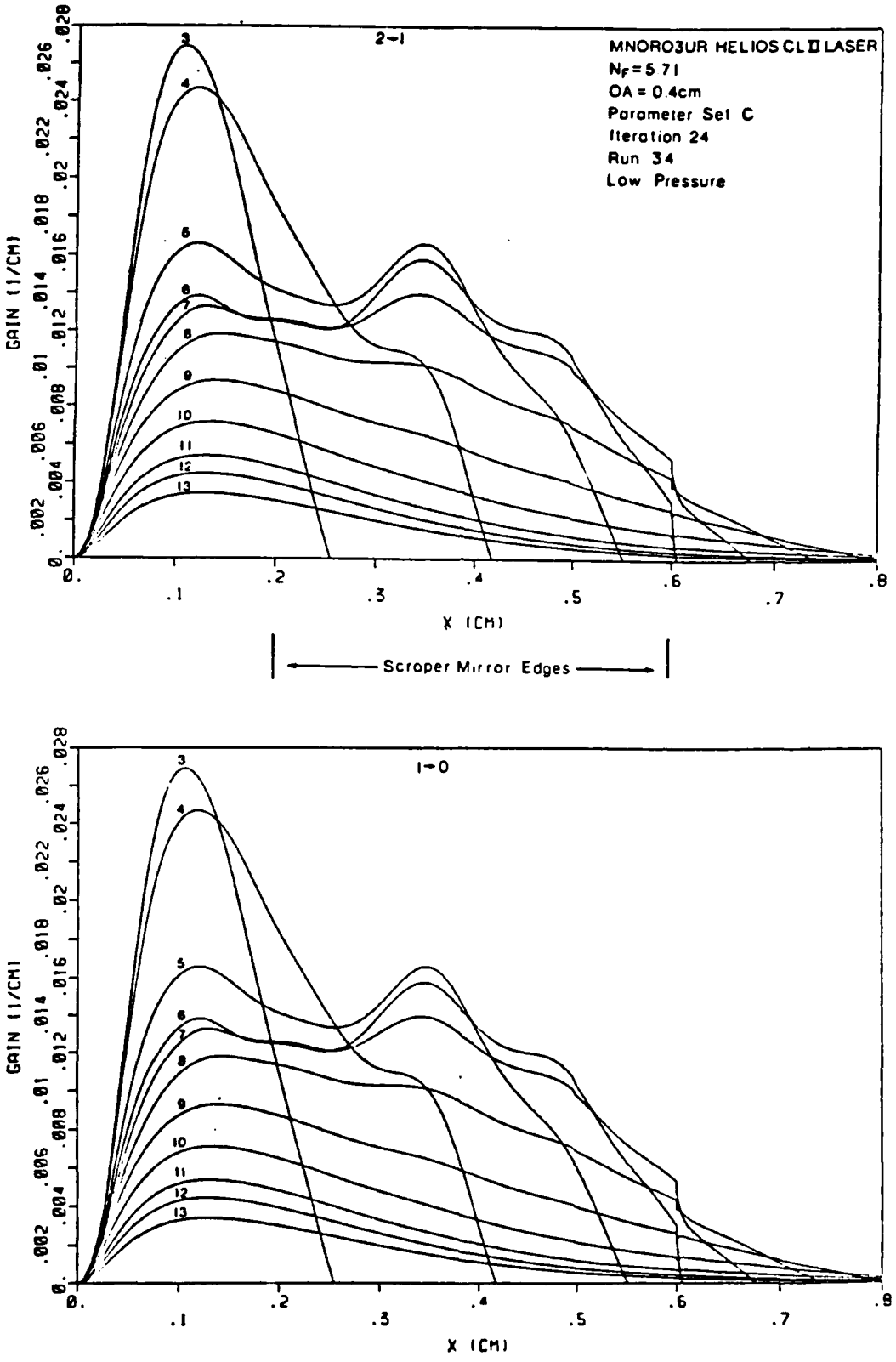

Figure 14 MNORO3UR gains at iteration 24 for a 50% geometric out-coupled, confocal unstable strip resonator with a large mirror diameter of 8 mm for the Helios CL II for the low pressure Run 34 flow rates.

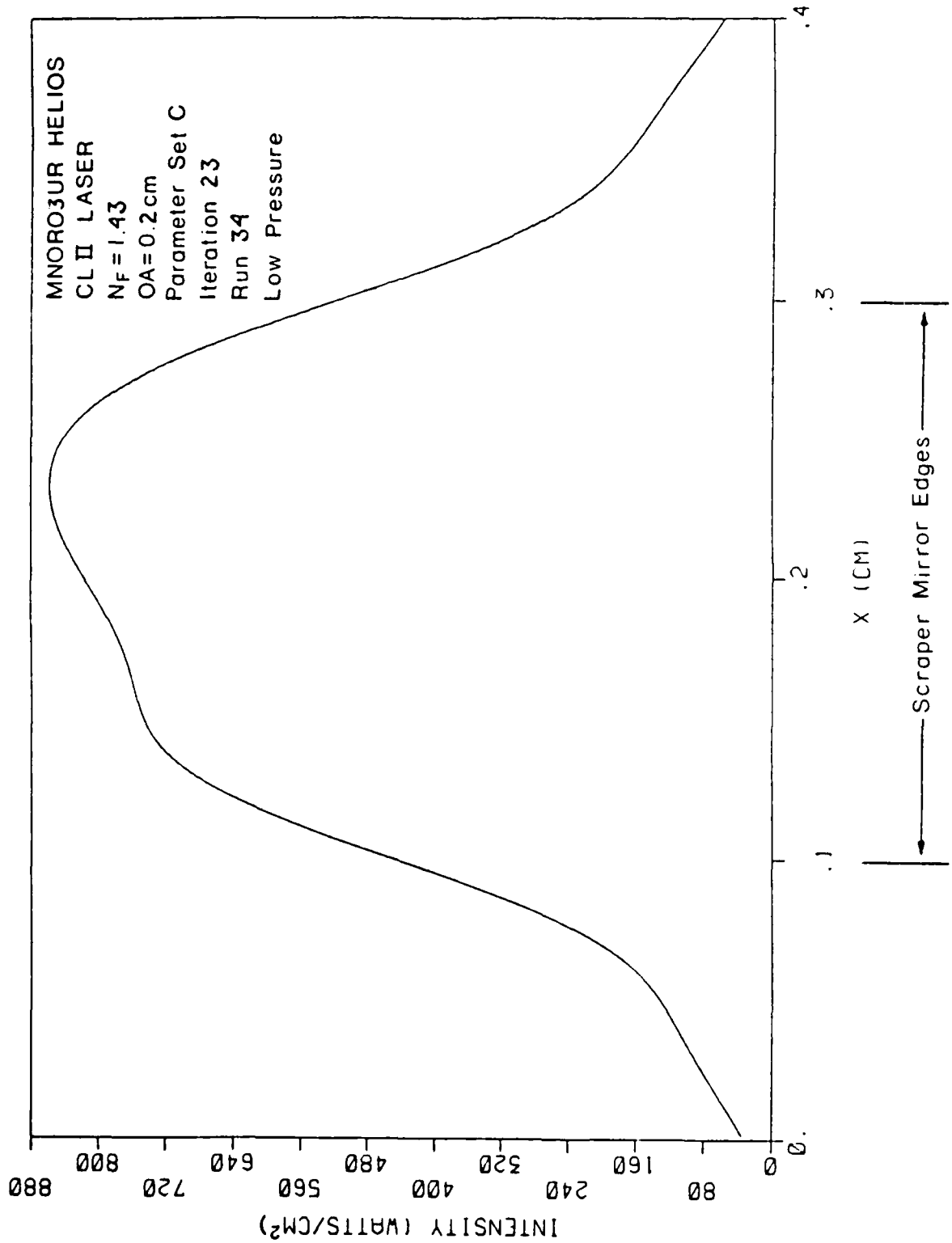

Figure 15 MNORO3UR total intensity distribution at iteration 23 for a 50% geometric outcoupled, confocal strip unstable resonator with a large mirror diameter of 4 mm for the Helios CL II for the low pressure Run 34 flow rates.

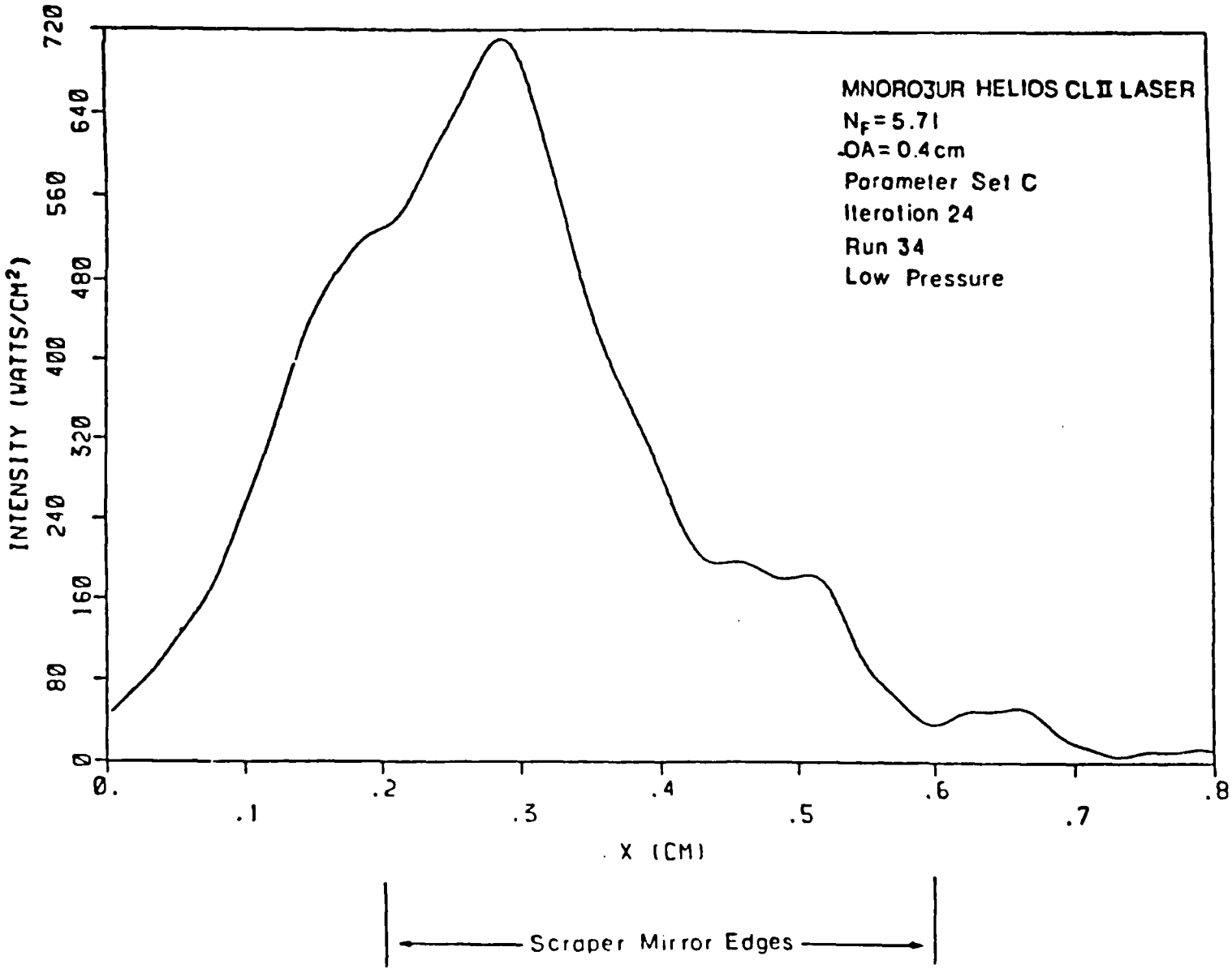

Figure 16 MNORO3UR total intensity distribution at iteration 24 for a 50% geometric outcoupled, confocal strip unstable resonator with a large mirror diameter of 8 mm for the Helios CL II for the low pressure Run 34 flow rates.

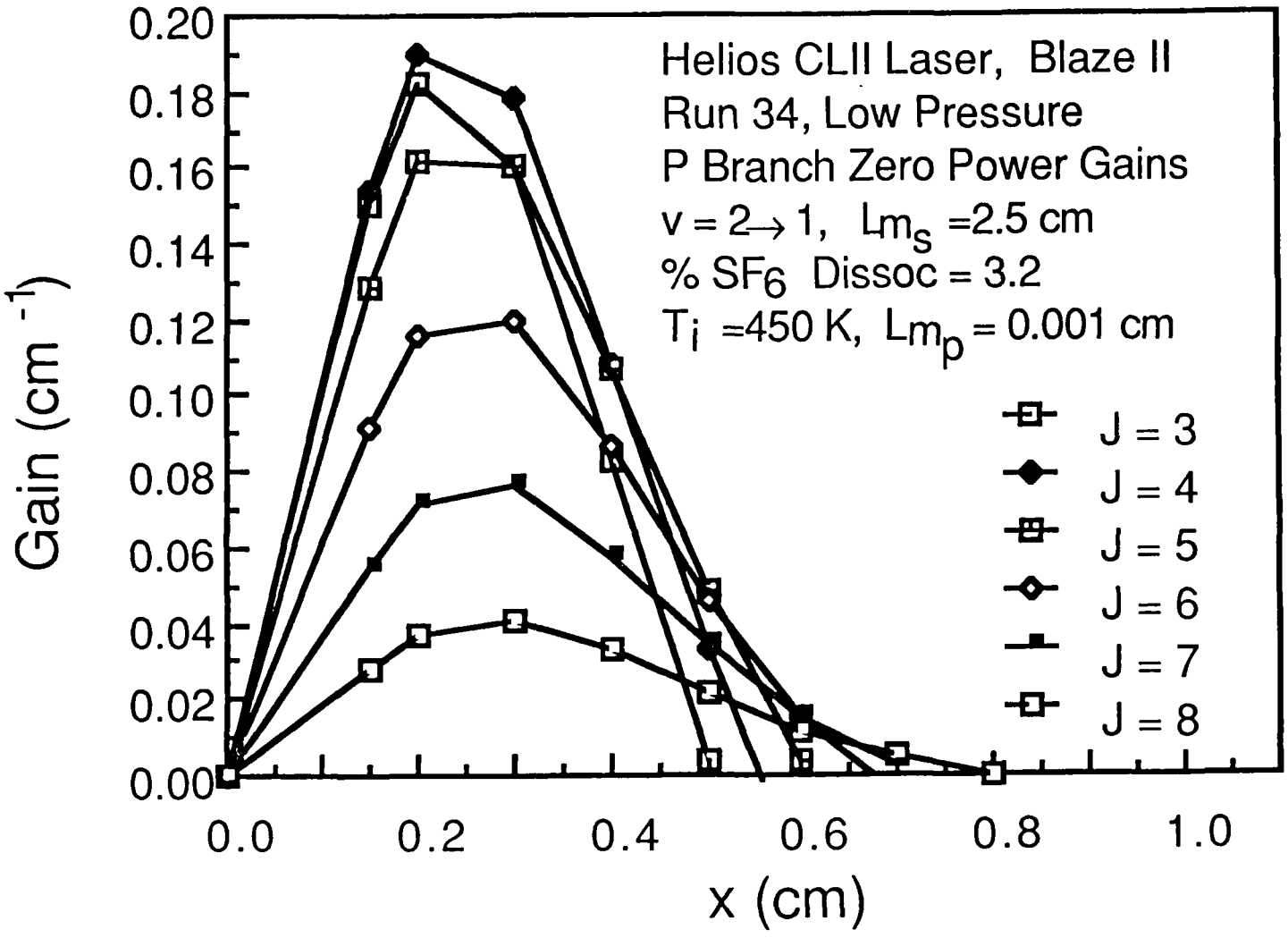

Figure 17 Variation of the zero power gain as a function of distance downstream from the H_2 injectors from the BLAZE II model of the CL II laser. L_{mp} is the mixing length of the primary stream, L_{ms} is the mixing length of the secondary stream, T_i is the static temperature of the flow at the H_2 injectors.

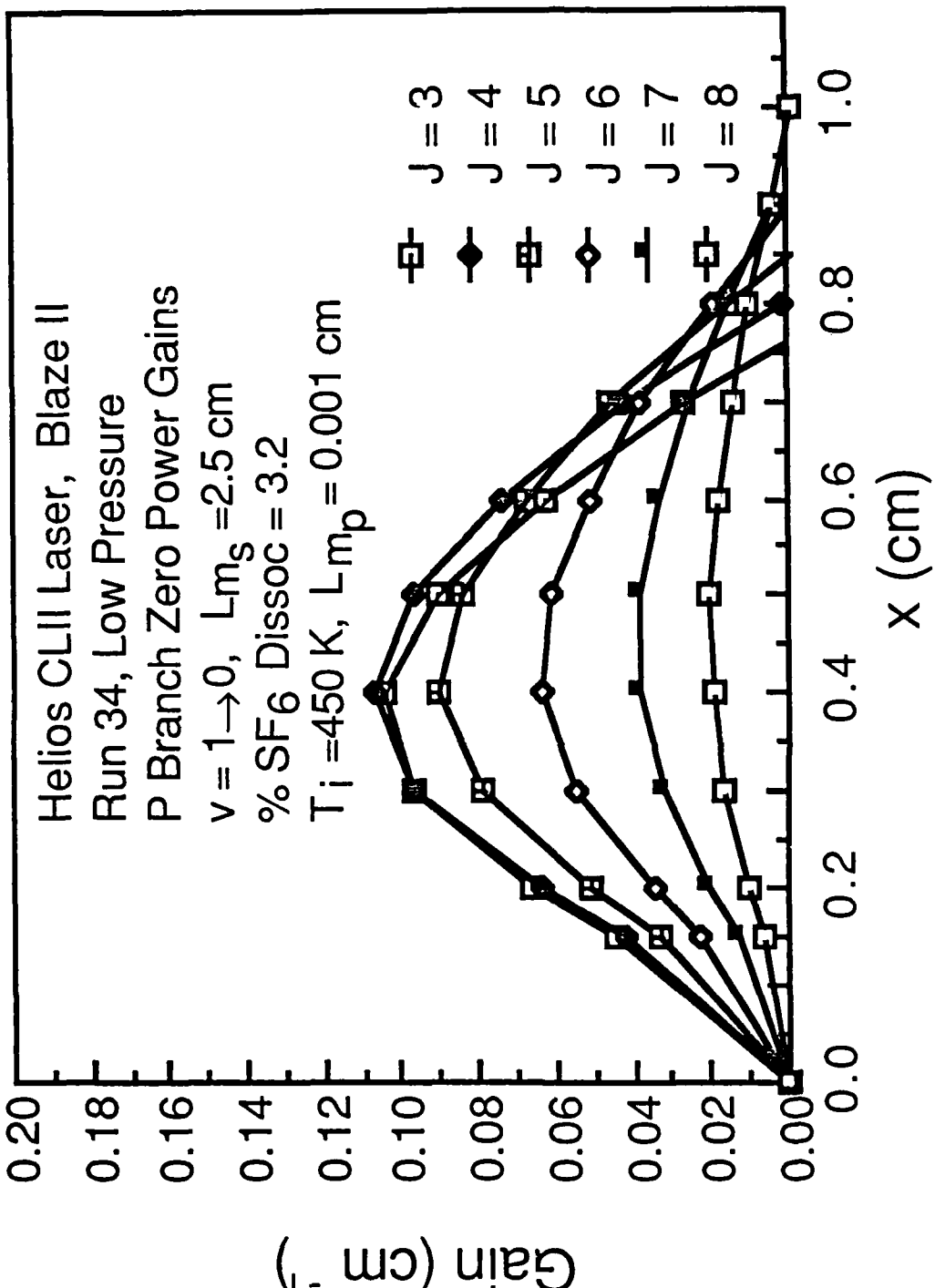

Figure 18 Variation of the zero power gain as a function of distance downstream from the H_2 injectors from the BLAZE II model of the CL II laser. L_{mp} is the mixing length of the primary stream, L_{ms} is the mixing length of the secondary stream, T_i is the static temperature of the flow at the H_2 injectors.

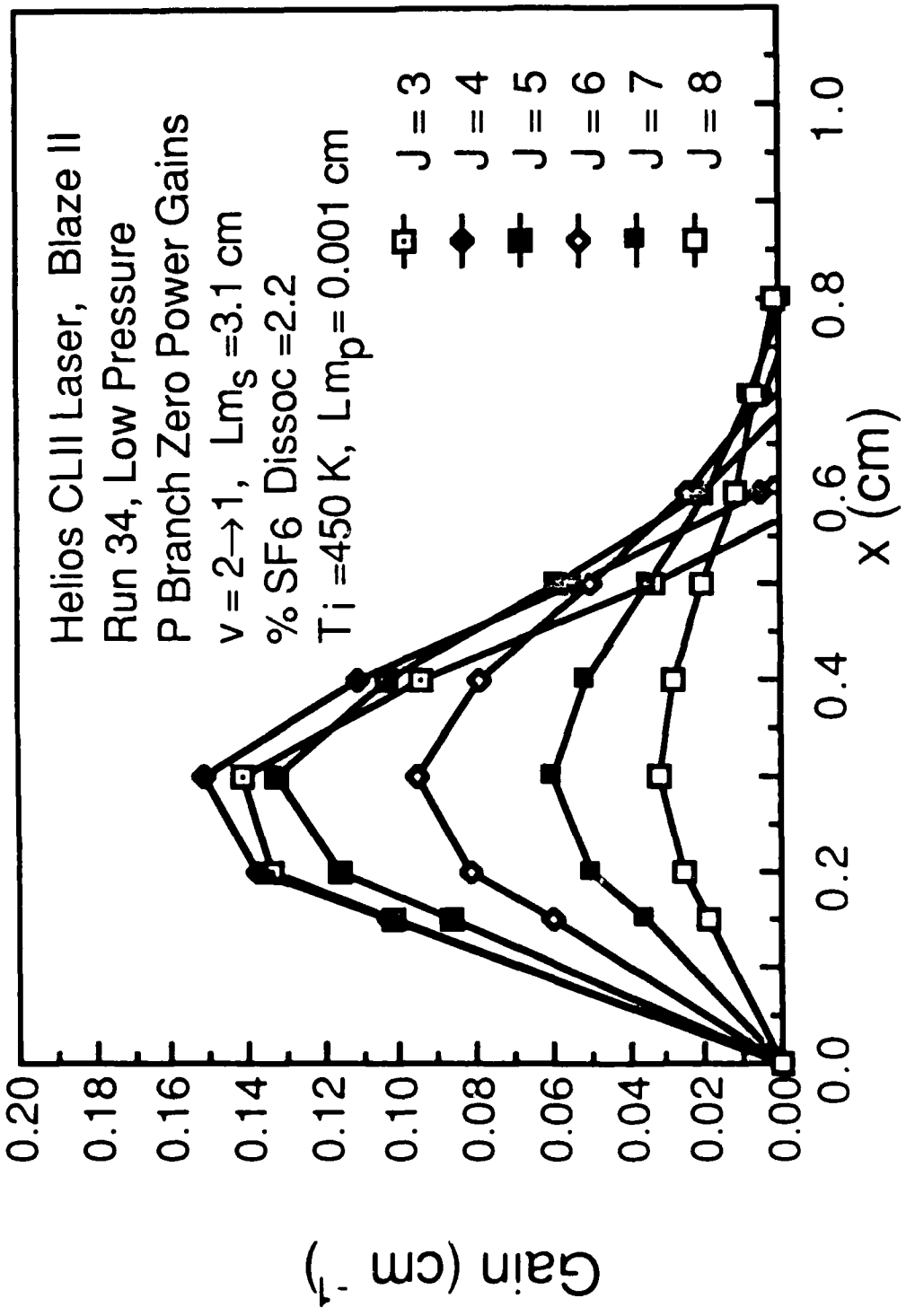

Figure 19 Variation of the zero power gain as a function of distance downstream from the H_2 injectors from the BLAZE II model of the CL II laser. L_{mp} is the mixing length of the primary stream, L_{ms} is the mixing length of the secondary stream, T_i is the static temperature of the flow at the H_2 injectors.

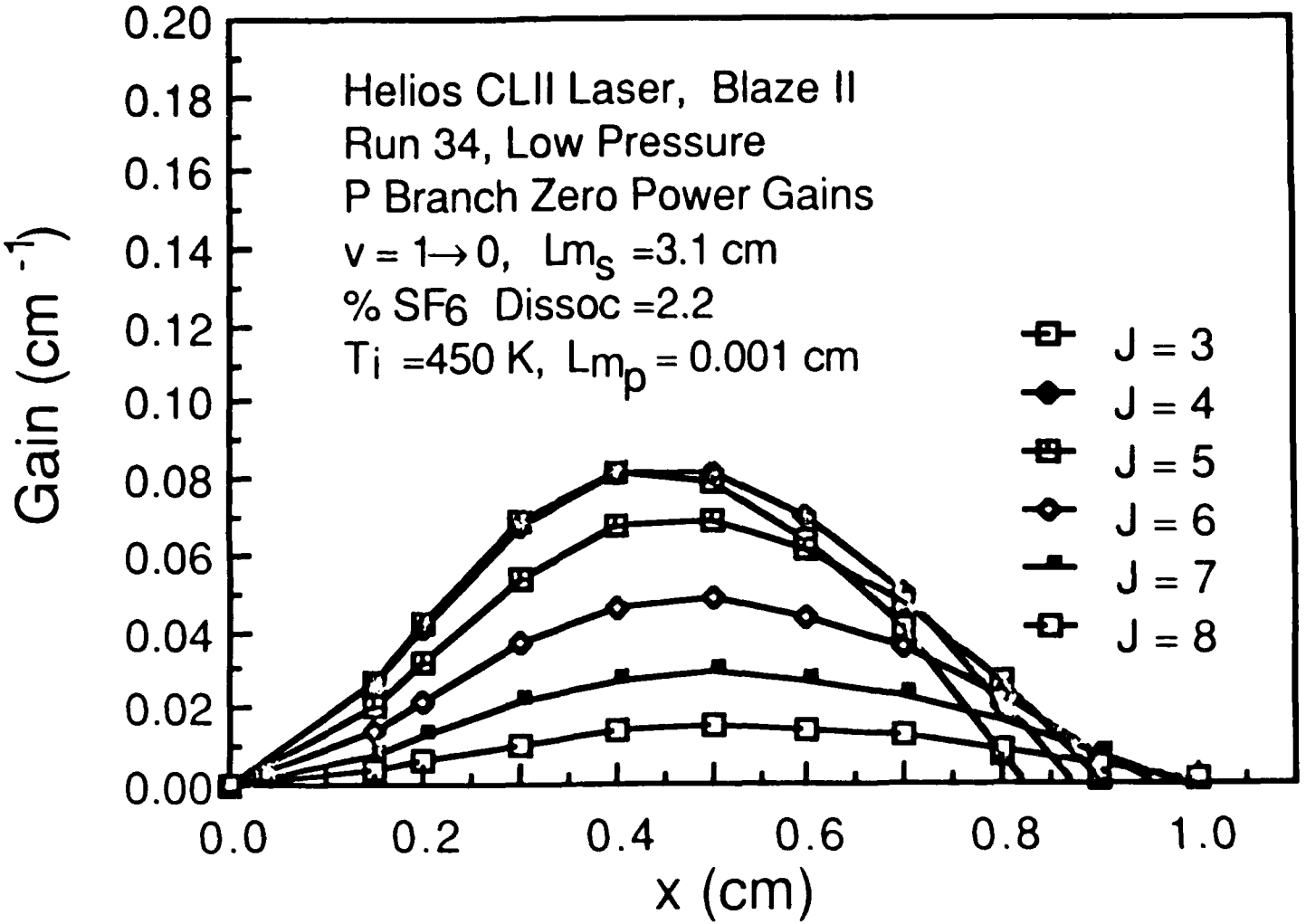

Figure 20 Variation of the zero power gain as a function of distance downstream from the H_2 injectors from the BLAZE II model of the CL II laser. L_{mp} is the mixing length of the primary stream, L_{ms} is the mixing length of the secondary stream, T_i is the static temperature of the flow at the H_2 injectors.

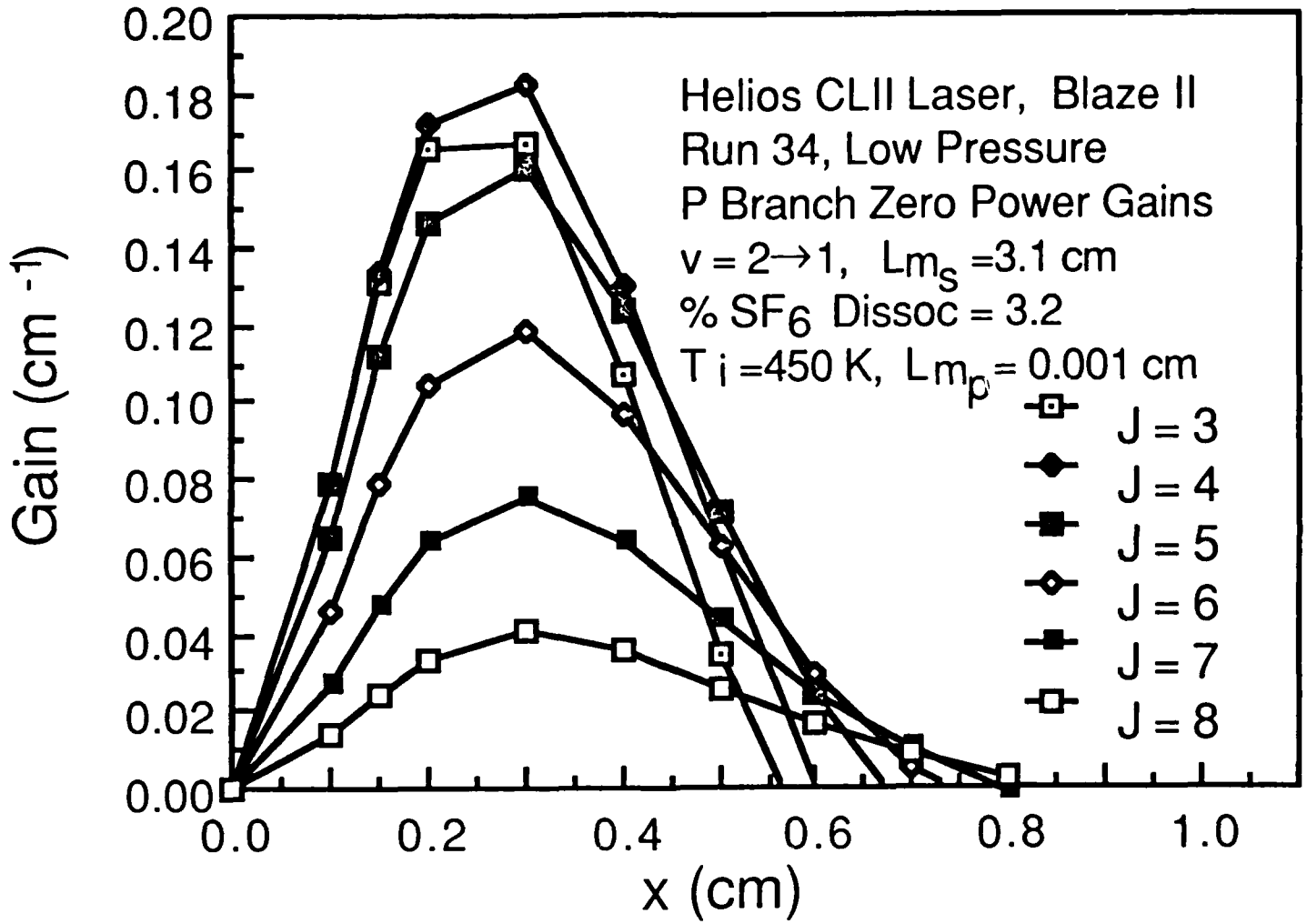

Figure 21 Variation of the zero power gain as a function of distance downstream from the H_2 injectors from the BLAZE II model of the CL II laser. L_{mp} is the mixing length of the primary stream, L_{ms} is the mixing length of the secondary stream, T_i is the static temperature of the flow at the H_2 injectors.

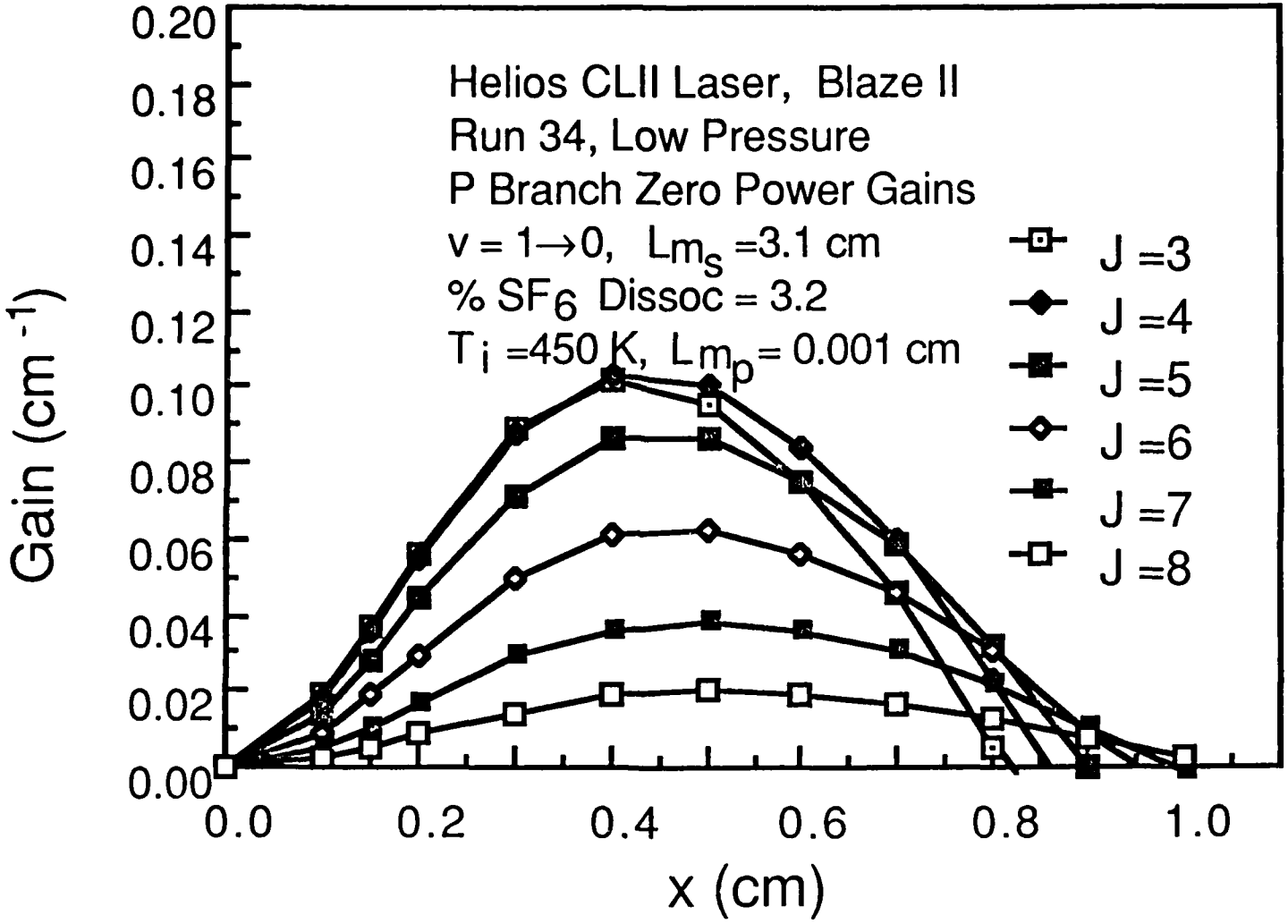

Figure 22 Variation of the zero power gain as a function of distance downstream from the H_2 injectors from the BLAZE II model of the CL II laser. L_{mp} is the mixing length of the primary stream, L_{ms} is the mixing length of the secondary stream, T_i is the static temperature of the flow at the H_2 injectors.

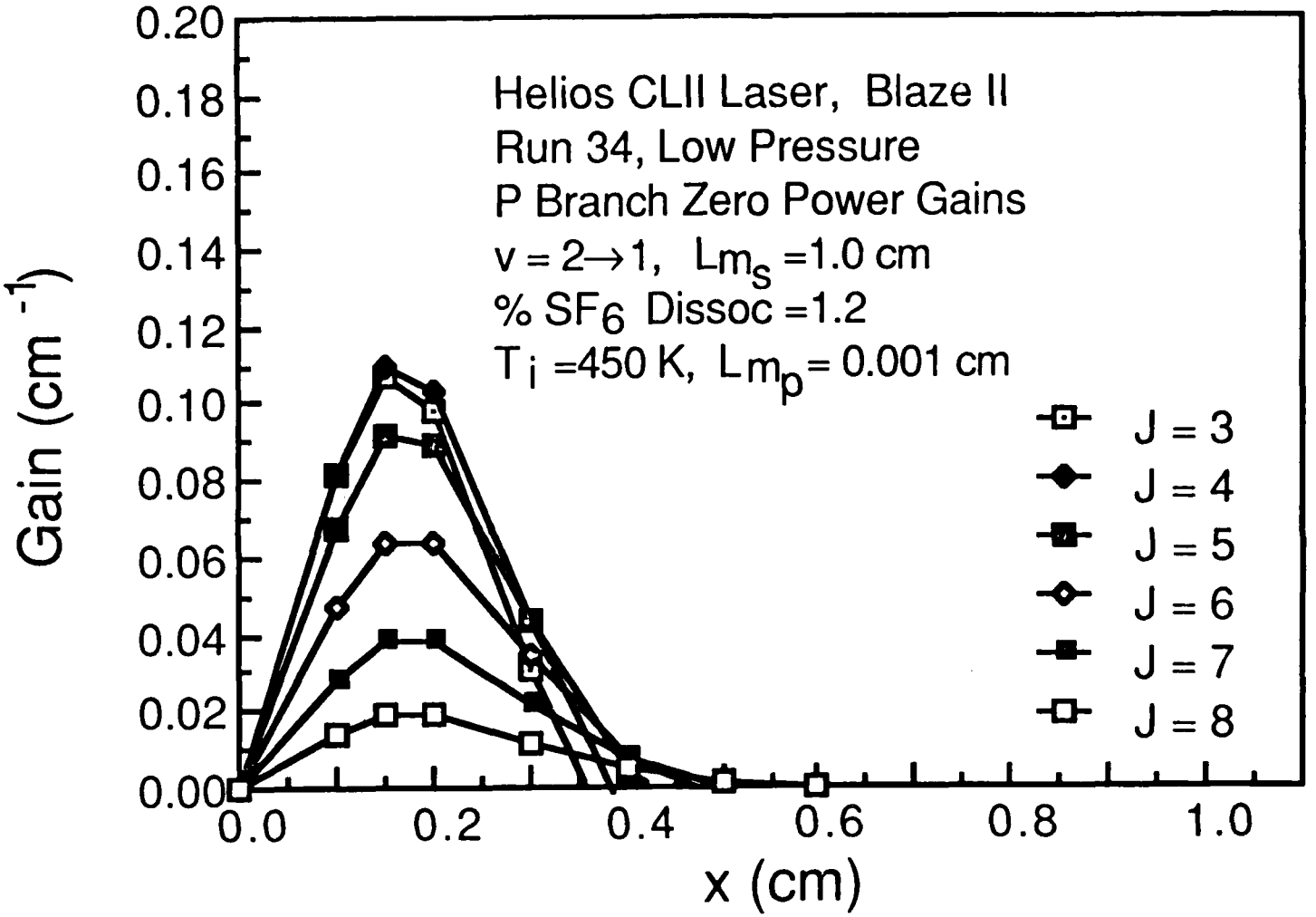

Figure 23 Variation of the zero power gain as a function of distance downstream from the H_2 injectors from the BLAZE II model of the CL II laser. L_{mp} is the mixing length of the primary stream, L_{ms} is the mixing length of the secondary stre ı, T_i is the static temperature of the flow at the H_2 injectors.

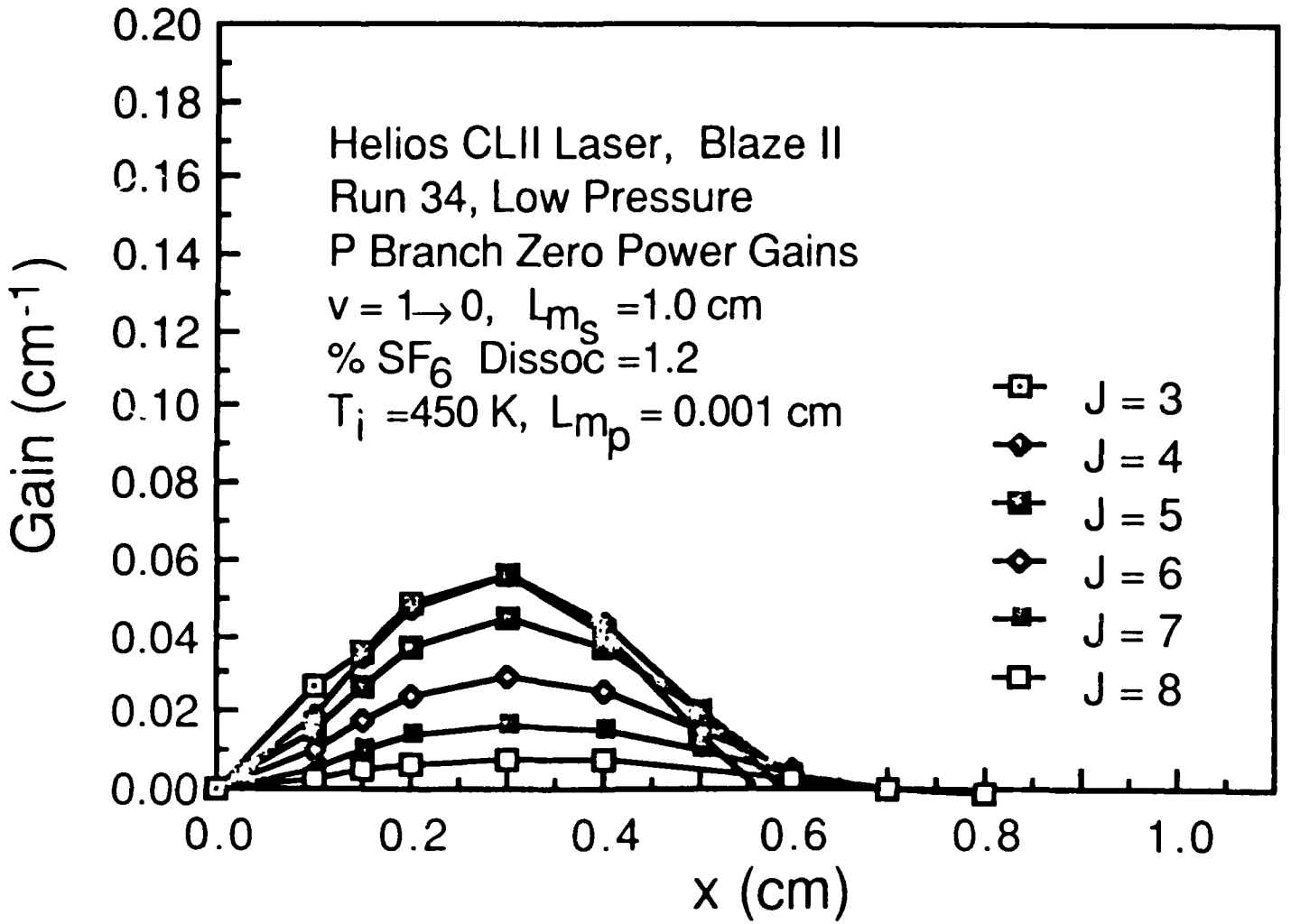

Figure 24 Variation of the zero power gain as a function of distance downstream from the H_2 injectors from the BLAZE II model of the CL II laser. L_{m_p} is the mixing length of the primary stream, L_{m_s} is the mixing length of the secondary stream, T_i is the static temperature of the flow at the H_2 injectors.

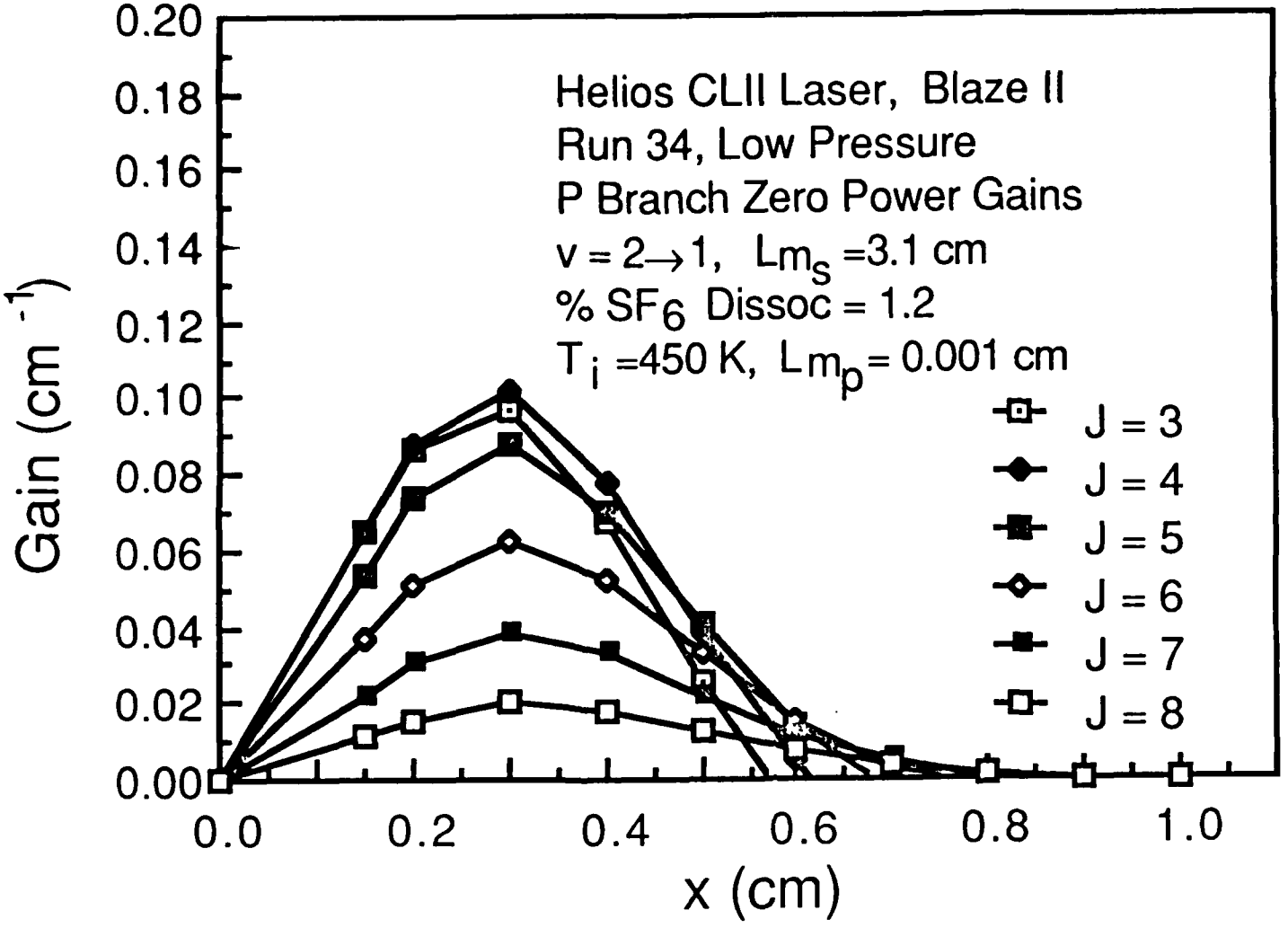

Figure 25 Variation of the zero power gain as a function of distance downstream from the H_2 injectors from the BLAZE II model of the CL II laser. L_{mp} is the mixing length of the primary stream, L_{ms} is the mixing length of the secondary stream, T_i is the static temperature of the flow at the H_2 injectors.

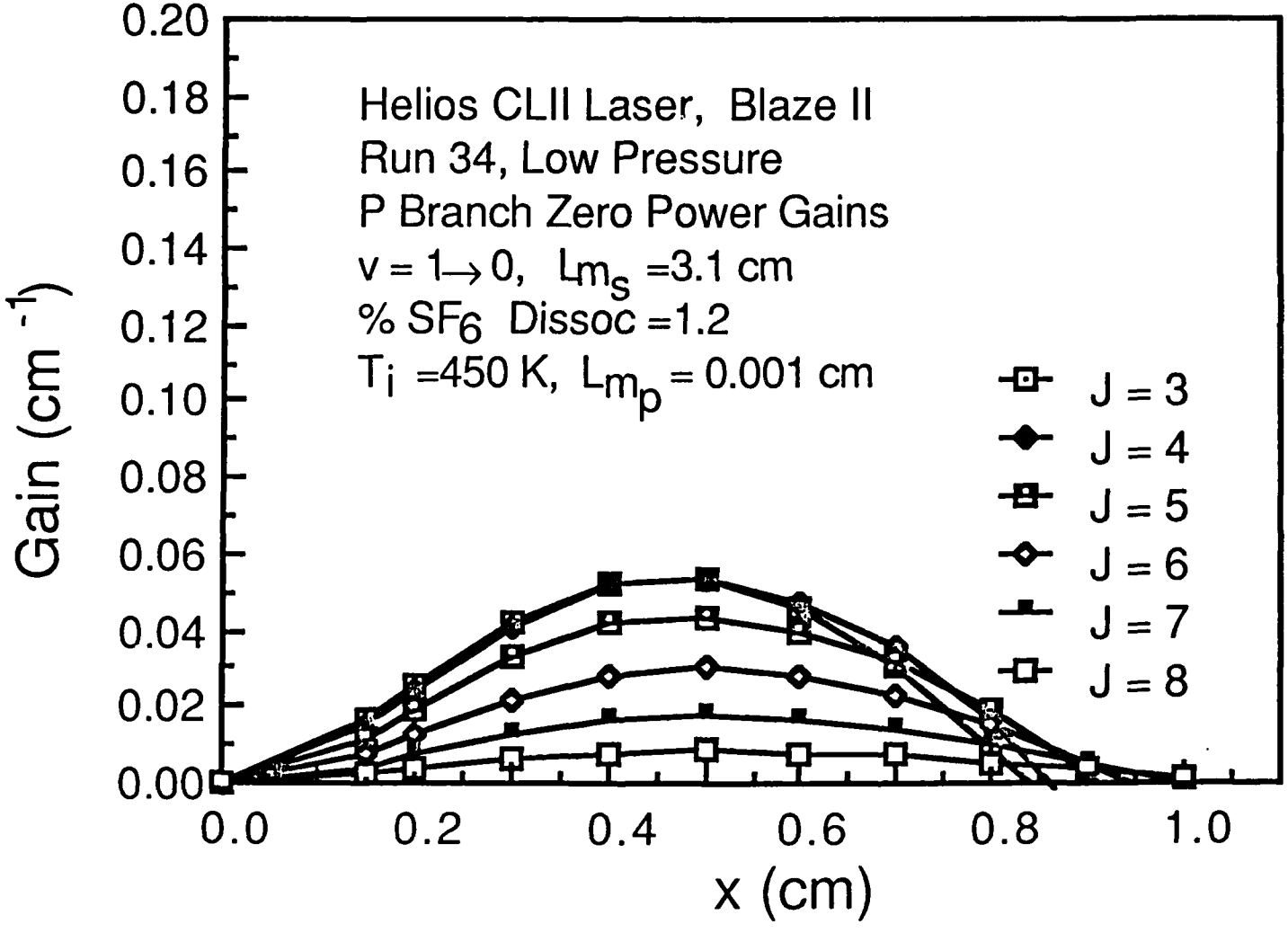

Figure 26 Variation of the zero power gain as a function of distance downstream from the H_2 injectors from the BLAZE II model of the CL II laser. L_{mp} is the mixing length of the primary stream, L_{ms} is the mixing length of the secondary stream, T_i is the static temperature of the flow at the H_2 injectors.

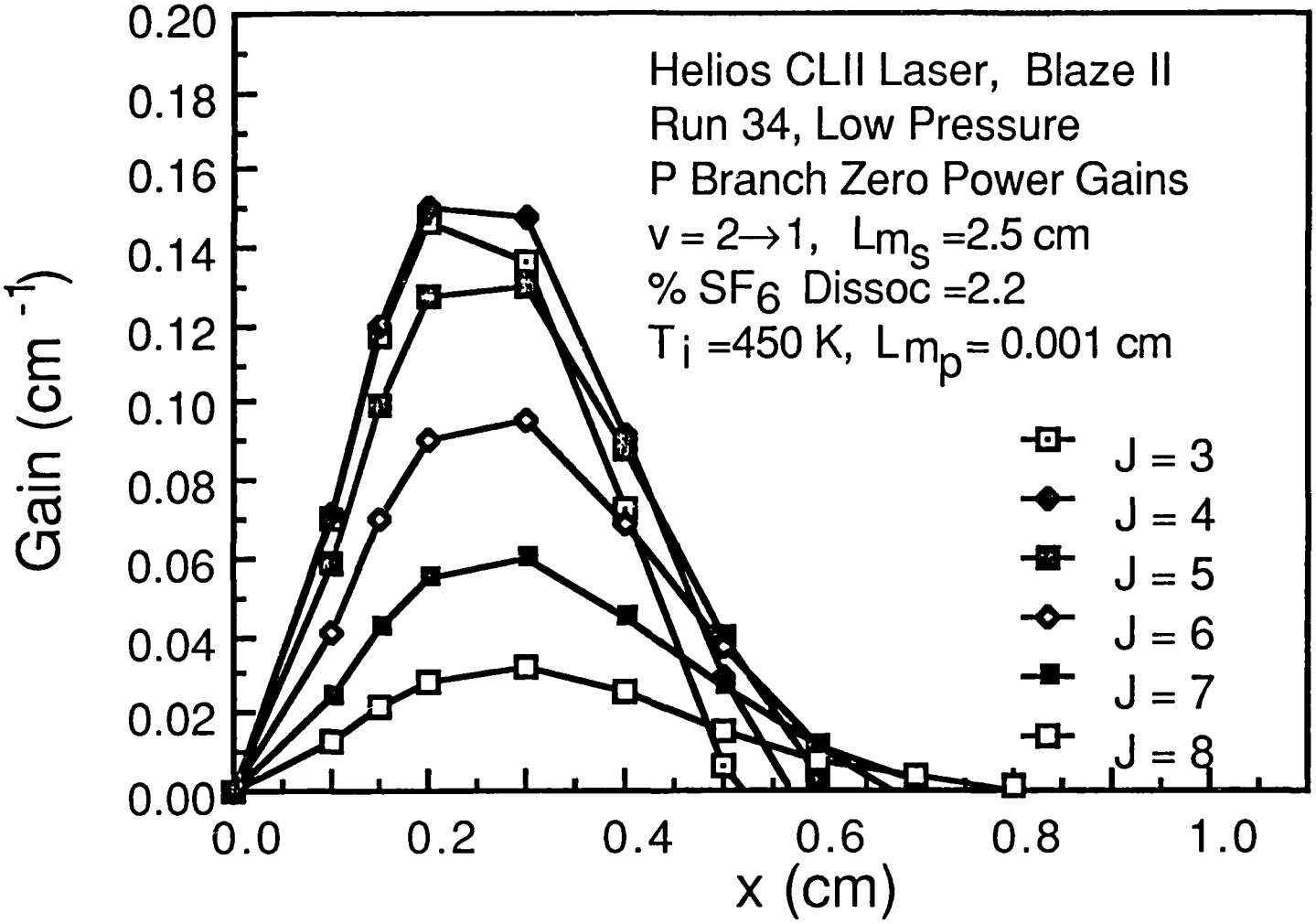

Figure 27 Variation of the zero power gain as a function of distance downstream from the H_2 injectors from the BLAZE II model of the CL II laser. L_{mp} is the mixing length of the primary stream, L_{ms} is the mixing length of the secondary stream, T_i is the static temperature of the flow at the H_2 injectors.

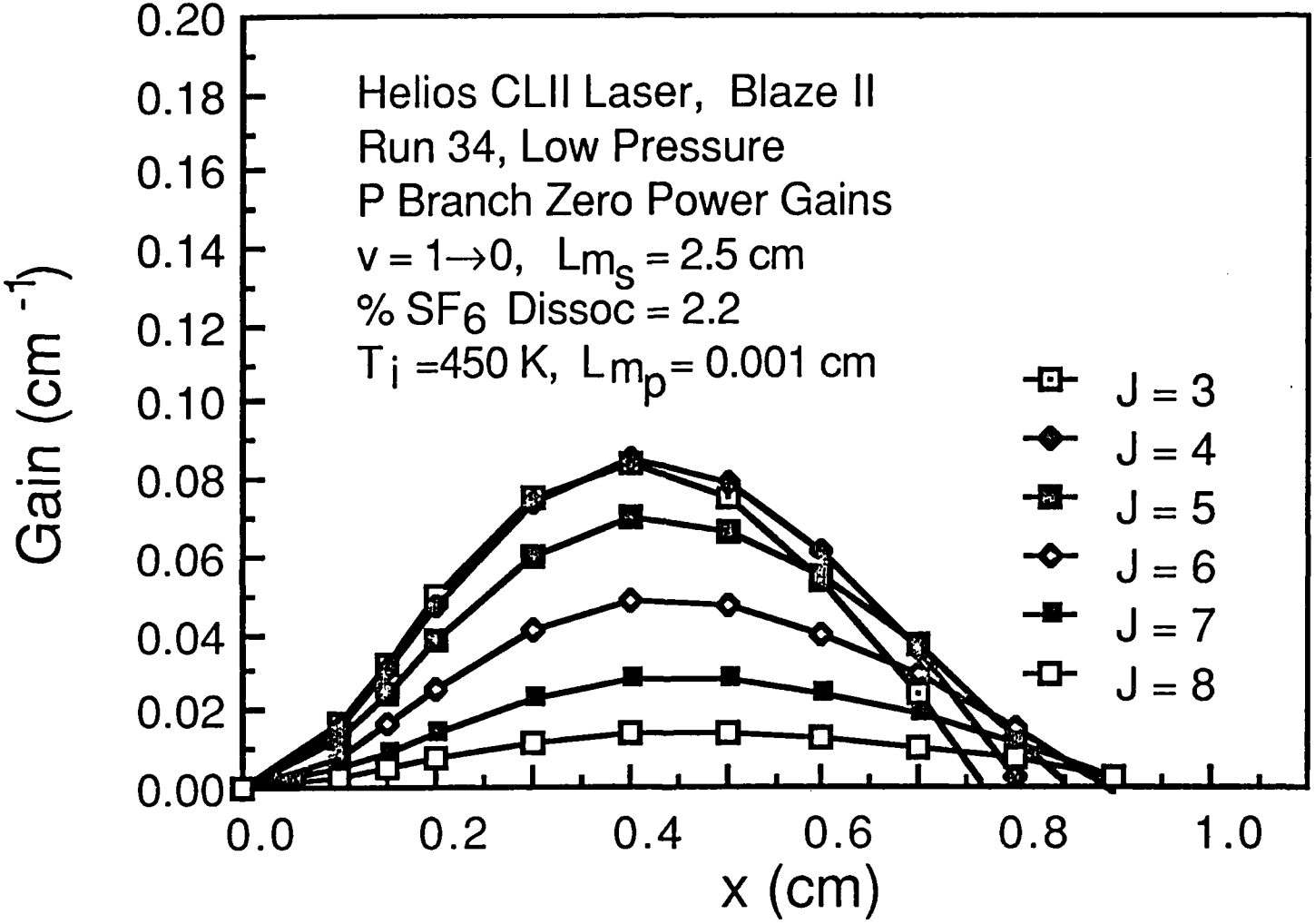

Figure 28 Variation of the zero power gain as a function of distance downstream from the H_2 injectors from the BLAZE II model of the CL II laser. L_{mp} is the mixing length of the primary stream, L_{ms} is the mixing length of the secondary stream, T_i is the static temperature of the flow at the H_2 injectors.

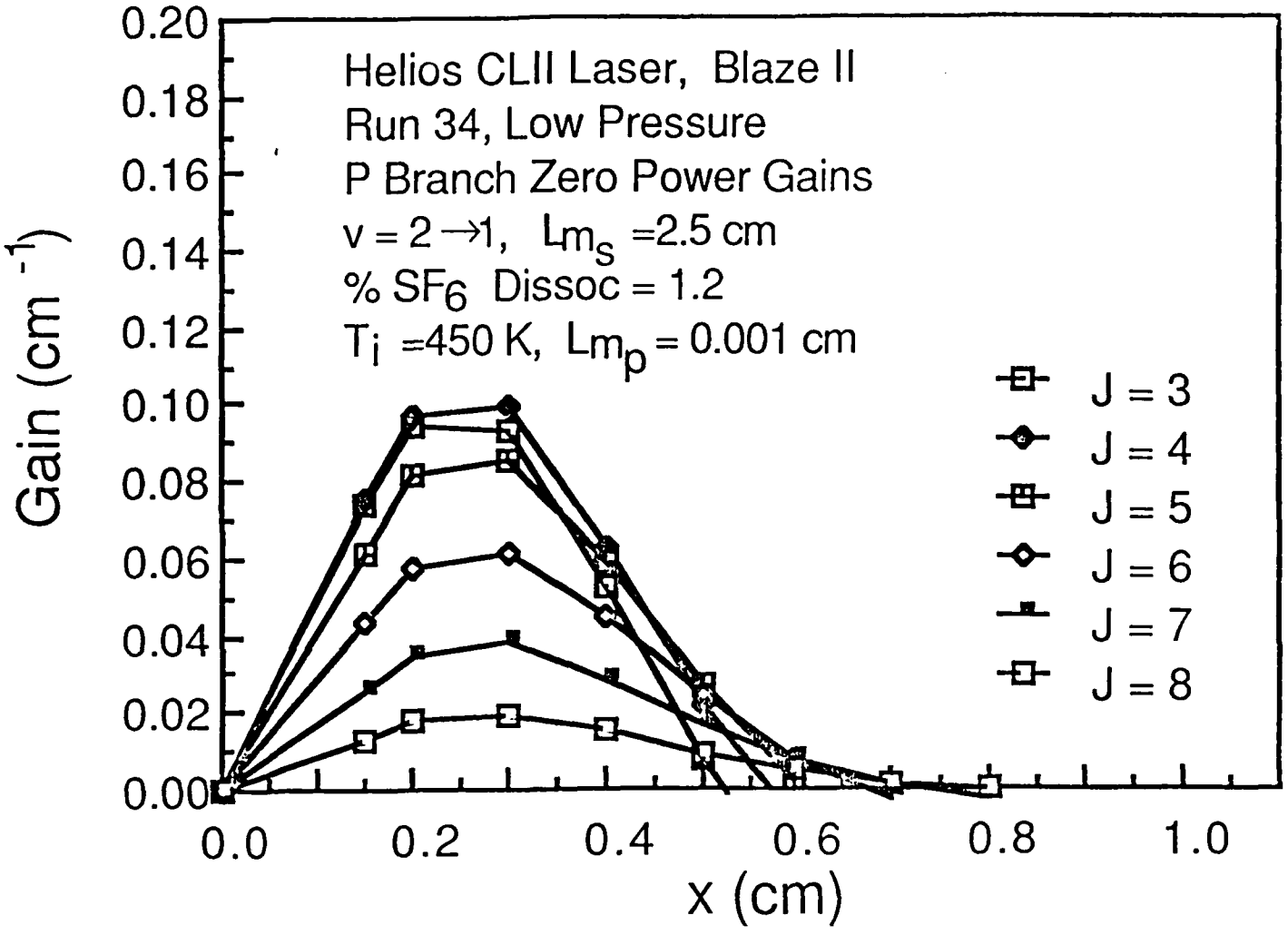

Figure 29 Variation of the zero power gain as a function of distance downstream from the H_2 injectors from the BLAZE II model of the CL II laser. L_{mp} is the mixing length of the primary stream, L_{ms} is the mixing length of the secondary stream, T_i is the static temperature of the flow at the H_2 injectors.

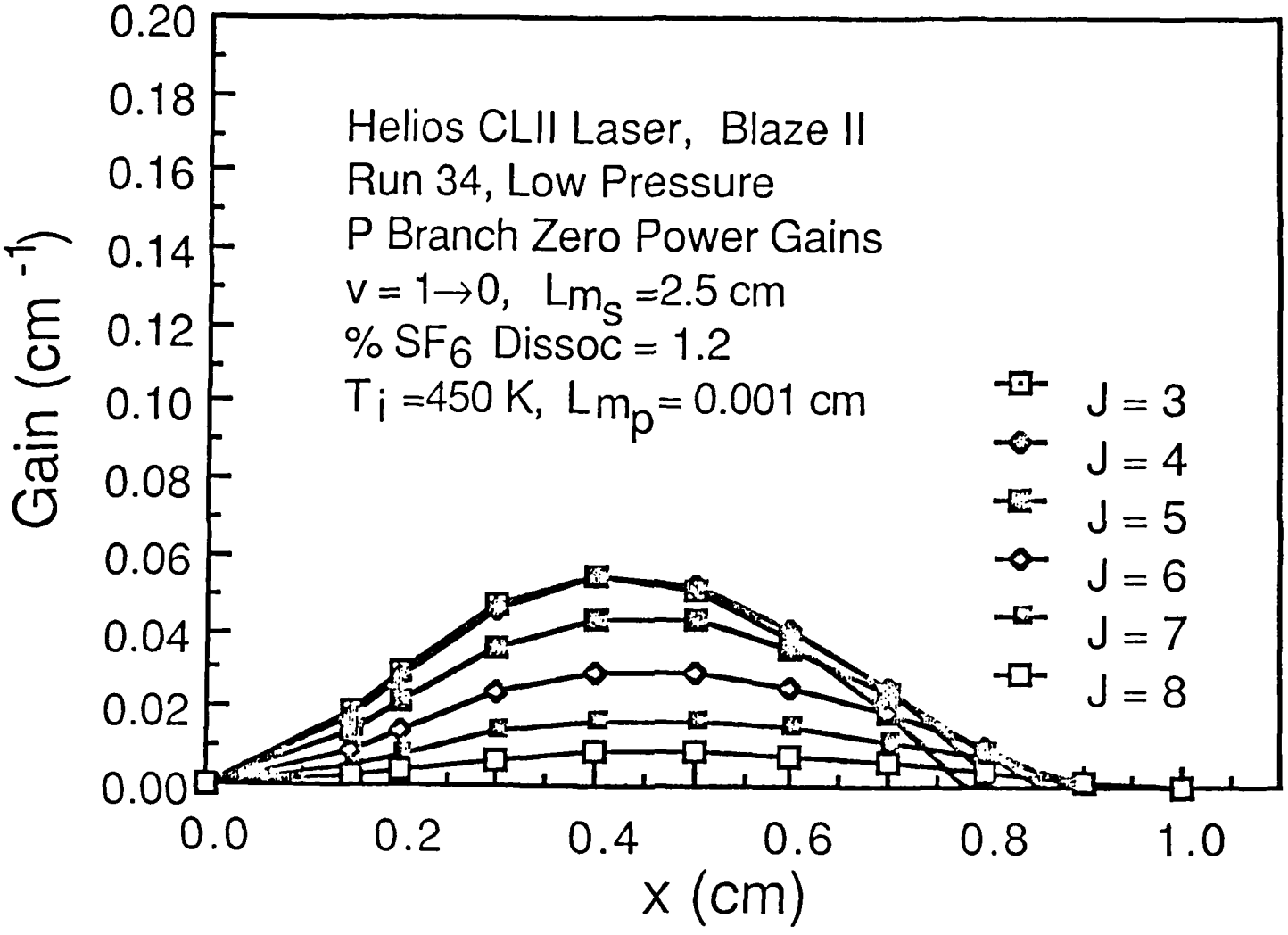

Figure 30 Variation of the zero power gain as a function of distance downstream from the H_2 injectors from the BLAZE II model of the CL II laser. L_{mp} is the mixing length of the primary stream, L_{ms} is the mixing length of the secondary stream, T_i is the static temperature of the flow at the H_2 injectors.

A 2 mm slit unstable resonator calculation with parameter Set D was performed. As shown in Table 13, the total power predicted by this calculation was too low by a factor of two. Figure 31 shows that the intensity peak did not move as desired. A comparison of the 2 mm slit calculations with Sets C and D showed that Set D had cut the total power by approximately 60%. A 60% decrease in the total power calculated with Set B in the 4 mm slit case would result in a total power of about 8 Watts, which would agree with the data. Thus a 4 mm slit calculation with Set D was performed. The results of this calculation, Table 13, show that the 4 mm slit data was matched well in both total power and the period of the time-dependent oscillations. The calculated amplitude modulation, however, was low compared to the data.

A plot of total power vs. percent SF_6 dissociation was constructed from the existing calculations. Figure 32 indicated that a near linear relationship existed between total power and percent SF_6 dissociation, independent of the secondary mixing length. This relationship held for both the 2 mm and 4 mm slit cases. Figure 32 also suggested that if the slope of the 2 mm slit line could be made larger than that of the 4 mm slit line, a set of parameters that would accurately predict both 2 mm and 4 mm slit performance could be determined. Thus, in an attempt to increase the slope of the 2 mm slit line, the secondary mixing length was drastically cut to 0.95 cm. The resulting parameter set, denoted Set E, is presented in Table 12. The results of a 2 mm slit calculation with parameter Set E are summarized in Table 13 and Fig. 32. This calculation indicated that the slope of the 2 mm slit line did not become greater than that of the 4 mm slit line.

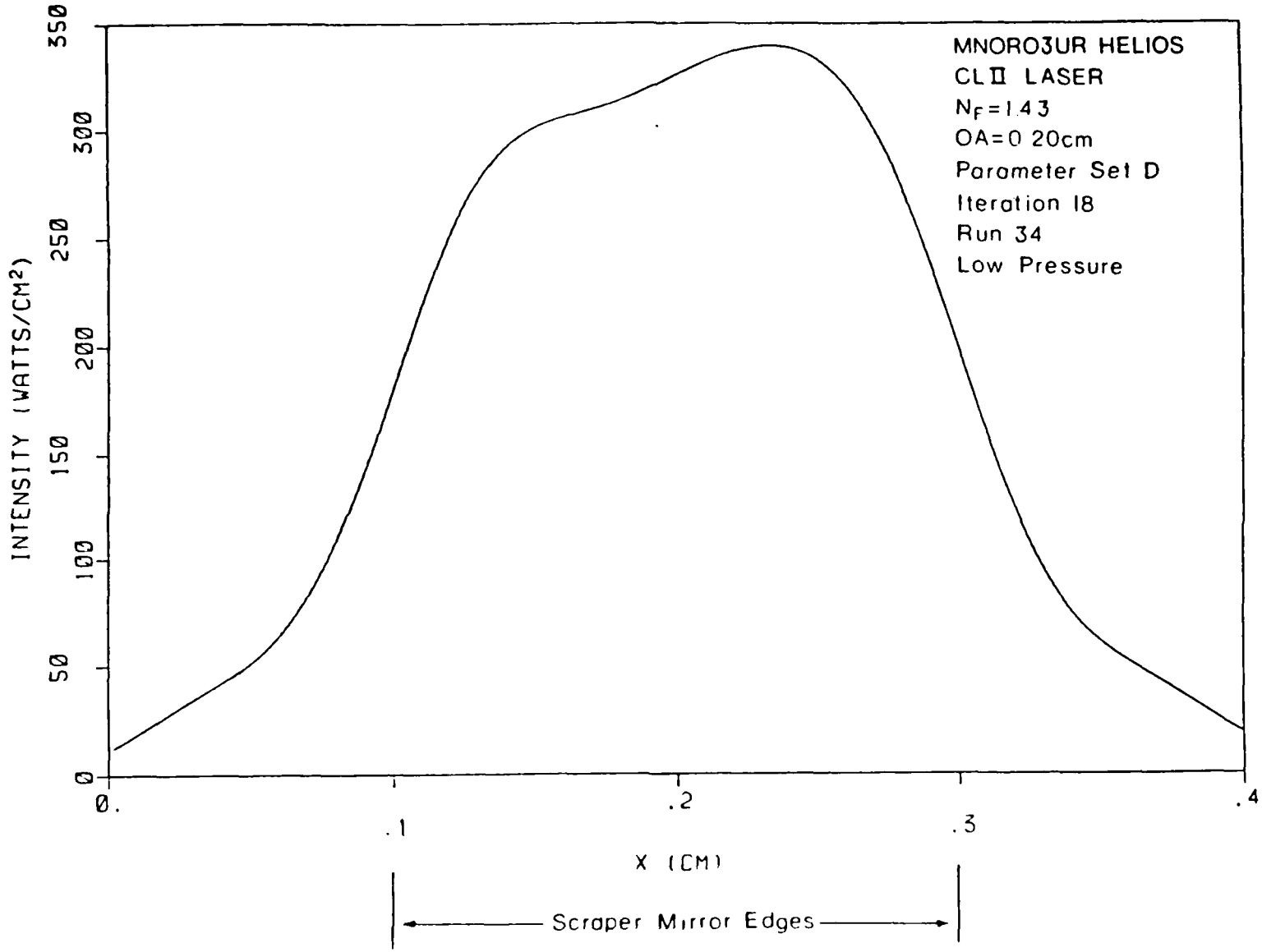

Figure 31 MNORO3UR total intensity at iteration 18 for a 50% geometric outcoupled confocal unstable strip resonator with a large mirror diameter of 4 mm for the Helios CL II for the low pressure Run 34 flow rates.

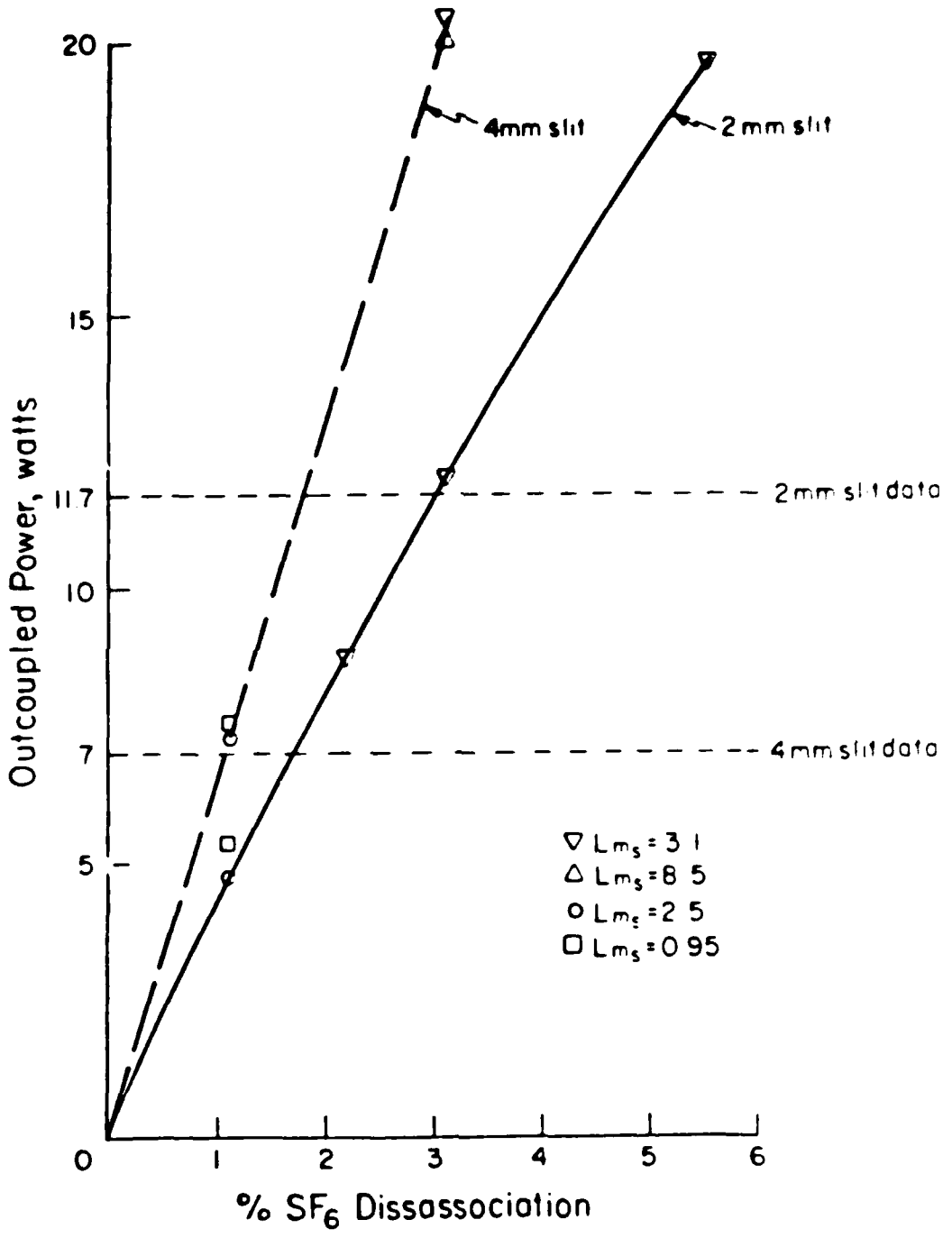

Figure 32 Variation of the total power as a function of the percent SF_6 dissociation from the MNORO3UR CL II low pressure Run 34 baselining calculations.

A final 4 mm slit calculation was made to investigate whether a drastic cut in secondary mixing length would make the slope of the 4 mm slit line less than that of the 2 mm slit line. If a drastic cut in secondary mixing length could make the slope of the 4 mm slit line in Fig. 32 less than the slope of the 2 mm slit line, a set of parameters that accurately predict both 2 and 4 mm slit total power data could be determined. The results of the 4 mm slit calculation with parameter Set D, shown in Table 13 and Fig. 32, indicated no departure from the behavior of the previous 4 mm slit calculations.

The results of the unstable resonator calculations for the 2 mm and 4 mm slit widths indicated that one set of baseline parameters that would allow the model to predict performance as the size of the resonator changed could not be found. However, a set of parameters was obtained for both the 2 mm and 4 mm slit cases that allowed the unstable resonator model to accurately predict the total power and oscillation period. The amplitude modulation was underpredicted in the 4 mm slit case. For the 2 mm slit width, the best fit parameter set was Set C, Table 12. For the 4 mm slit width, the best fit parameter set was Set D, Table 12.

2.5.1 CL I CALCULATIONS

A previous study demonstrated that an appropriate set of stable resonator baseline parameters is able to accurately predict laser performance as the scale of the laser device changes[13]. Thus unstable resonator calculations were performed to determine if parameter sets C and D could predict scale effects. The calculations were conducted for

the Helios CL I laser for the low pressure, Run 34 flow rates. The Helios CL I laser is identical to the Helios CL II laser except that the flow rates and gain length are reduced by a factor of two. A 2 mm slit calculation was performed with Set C and a 4 mm slit calculation was performed with Set D. The results of these calculations are shown in Table 14. Neither the 2 mm nor the 4 mm slit calculation predicted the data. From this it was evident that parameter Sets C and D cannot predict scale effects.

2.6 SUMMARY OF UNSTABLE RESONATOR MODELING RESULTS

The results of the unstable resonator baselining process indicated that one set of baseline parameters that allow the model to track unstable resonator data as the size of the resonator varied could not be found. It was, however, possible to obtain different sets of baseline parameters for individual resonator sizes. The best fit parameter set for the 2 mm slit case accurately predicted the total power, but also predicted a 20 nsec small amplitude modulation which was not seen experimentally. The best fit parameter set for the 4 mm slit case accurately predicted the total power and the period of the time-dependent oscillations, but underpredicted the amplitude modulation. Neither parameter set predicted scale effects. The best fit parameter set for the 5 mm slit was the FPSR parameters. They predicted the period and amplitude modulation of the oscillations but overpredicted the total power.

The inability to obtain one set of baseline parameters for the unstable resonator model demonstrates that the model is inadequate. The

Baseline Parameters	Slit Width (mm)	Total Power (Watts)	Oscillation Period (nsec)	Oscillation Amplitude (% total power)
EMM Data[13]	2	1.97	--	--
EMM Data[13]	4	0.10	47	50
Set C	2	6.23	27	18
Set D	4	2.48	27	36

Table 14 Summary of 2 mm and 4 mm slit MNOR03UR baselining calculations and data for the Helios CL I for the low pressure Run 34 flow rates. All calculations used t_w = 0.97 and a 50% geometric outcoupled, confocal, unstable strip resonator.

limitations of the model arise mainly from the treatment of the fluid dynamic mixing. Sonic transverse injection into a subsonic multi-component reacting shear flow results in a three-dimensional flow field. The idealization of this as a two-dimensional array of parallel, alternating fuel and oxidizer slit nozzles with subsequent linear mixing is an oversimplification which limits the model.

The limitations imposed by the mixing model did not prevent the Fabry-Perot and stable resonator models from being baselined to the data. This suggested two possible explanations. Since the actual fluid dynamics is independent of the resonator and the unstable resonator model is a more exact treatment of the optics, the wave optics model of the unstable resonator may have brought out inadequacies in the mixing model that were not apparent with geometric optics models. Another possible explanation is that the way in which the optical fields sample the media in an unstable resonator has brought out the inadequacies in the mixing model. Fabry-Perot and stable resonators have no upstream/downstream coupling and full upstream/downstream coupling of the media and optical fields, respectively. The unstable resonator couples upstream of the optical axis and downstream of the optical axis, but not across the optical axis. Both possible explanations demonstrate that unstable resonator data as a function of resonator size and size of the laser provide a severe test of a coupled, wave optics, chemical kinetics, fluid dynamic model of a chemical laser.

III. UNSTABLE RESONATOR TIME-DEPENDENT OSCILLATIONS

3.1 PROPOSED MECHANISM FOR THE TIME-DEPENDENT OSCILLATIONS IN AN UNSTABLE RESONATOR

An objective of this study was to investigate the mechanism responsible for the time-dependent oscillations that occur on lines whose saturated gain does not fill the unstable resonator. These oscillations have been the subject of several earlier studies[3,10,11,13]. In these studies, the oscillations were found to occur in both the CL II and CL I lasers at low cavity pressures for resonator Fresnel numbers above a demarcation Fresnel number of 1.5 in the CL II and 3.2 in the CL I. The period of the oscillations was 40 nsec in both the CL II and CL I and was independent of the flow rates. The period of the oscillation was determined by the resonator magnification, and the amplitude modulation was determined by the fraction of the resonator filled by the saturated gain of the lasing line. In addition to the 40 nsec oscillation, a 7 nsec oscillation was superimposed on it. The 7 nsec oscillation corresponds to a mode beat of the laser.

The data showed that the occurrance of the time-dependent oscillations was Fresnel number dependent and that the period of the oscillation was determined by the resonator magnification. Accordingly, a series of unstable resonator MNORBUR calculations with 4 mm and 5 mm slit resonators were performed to investigate the effect of varying the resonator Fresnel number and the resonator magnification. The resonator magnification was varied through the radii of curvature of the mirrors. The Fresnel number was varied by changing the size of the large mirror,

$$N_F = \frac{D^2}{4\lambda L} \qquad (3.1\text{-}1)$$

where D is the diameter of the large mirror, λ is the optical wavelength, and L is the mirror separation. The calculations were performed for the CL II laser for the low pressure Run 34 flow rates. The baseline parameters used were the best fit parameter sets for the 4 mm and 5 mm slit resonators, Sets D and FPSR, respectively. Selected information from the 4 mm and 5 mm slit calculations is presented in Table 15.

The central Fresnel zone in an unstable resonator is the region about the optical axis whose radius is such that the Fresnel number is unity. In the central Fresnel zone, the media is strongly coupled to the optical fields by diffraction. The size of the central Fresnel zone is determined by setting the Fresnel number to unity,

$$N_F \equiv \frac{D^2}{4\lambda L} = 1 \qquad (3.1\text{-}2)$$

where D is the diamter of the central Fresnel zone, L is the mirror separation, and λ is the optical wavelength. The diameter of the central Fresnel zone is then

$$D_{CF} = 2\sqrt{\lambda L} \qquad (3.1\text{-}3)$$

Thus, the extent of the central Fresnel zone is determined by the optical wavelength and the mirror separation.

Baseline Parameters	D_L (cm)	D_S (cm)	L (cm)	t_w	M	Geometric Outcoupling	D_{CF} (mm)	N_F	n_p	τ	Amp. mod.
EMM data[10,11]	1.0	0.50	100	----	2.00	50%	---	8.93	---	40	25% P_{total}
FPSR	1.0	0.50	100	1.00	2.00	50%	3.3	9.46	1.6	40	18 to 100%
FPSR	1.0	0.80	100	1.00	1.25	20%	3.3	8.93	4.9	∞	--
EMM data[10,11]	0.8	0.40	100	----	2.00	50%	---	5.71	---	40	20 to 80%
Set D	0.8	0.40	100	0.97	2.00	50%	3.3	5.71	1.3	40	10 to 20%
Set D	0.8	0.52	100	0.97	1.54	35%	3.3	5.71	2.0	60	5%
Set D	0.8	0.64	100	0.97	1.25	20%	3.3	5.71	3.9	∞	--

Table 15 Selected information from MNORO3UR calculations for the CL II laser for the low pressure, Run 34 flow rates for various confocal unstable resonators. D_L is the large mirror diameter. D_S is the small mirror diameter. L is the mirror separation. t_w is the effective Brewster window transmissivity. M is the resonator magnification. D_{CF} is the diameter of the central Fresnel zone. N_F is the resonator Fresnel number. n_p is the number of passes for a wave to exit the resonator after leaving the central Fresnel zone. τ is the calculated period of the time-dependent oscillations. Amp. mod. is the calculated single line amplitude modulation of the time-dependent oscillations.

The number of passes required for a wave to exit the resonator after leaving the central Fresnel zone is given through a geometric optics approximation to the unstable resonator as[14]

$$n_p = \frac{\ell n\left[\frac{M(D_s)}{2\sqrt{\lambda L}}\right]}{\ell n(M)} \qquad (3.1\text{-}4)$$

where D_s is the diameter of the small mirror, M is the resonator magnification, λ is the optical wavelength and L is the mirror separation. Equation (3.1-4) shows that the number of passes for a wave to exit the resonator is determined by the resonator magnification for a fixed resonator size. It should be noted that one round trip through the resonator corresponds to two passes. The number of passes requried for a wave to exit the resonator after leaving the central Fresnel zone was calculated for the cases shown in Table 15.

The calculations presented in Table 15 showed a correlation between the period of the time-dependent oscillations and the number of passes, n_p, for a wave to exit the resonator after leaving the central Fresnel zone. As n_p increased, the period of the time-dependent oscillations increased. The trend was evident in both the 4 mm and 5 mm slit calculations. his correlation between the number of passes for a wave to exit the re·onator after leaving the central Fresnel zone and the period of the time-dependent oscillations led to the following hypothesis concerning the mechanism responsible for the time-dependent oscillations.

The time-dependent oscillations of the laser power are the result of a competition between chemical pumping and radiative deactivation due to lasing. If, in a given time, radiative deactivation removes more HF molecules from an upper laser level than the chemistry can repopulate, the gain on that line is reduced. The reduced gain results in reduced intensities. Since the stimulated radiative processes are proportional to the intensity, reduced intensities reduce the radiative deactivation rate. The chemical processes, which are independent of the intensity, then catch up and reestablish the population inversion. Once the population inversion is reestablished, the entire cycle repeats itself.

The data and the MNORO3UR calculations in Table 15 indicated that strong coupling, either diffractive or geometric, prevented the oscillations by locking the media and the optical fields together. Strong diffractive coupling occurs when the Fresnel number is small. Strong geometric coupling occurs when the photons require several passes to exit the resonator. Thus, for the oscillations to occur, the rate of chemical pumping must be less than the rate of radiative deactivation, and the media must not be strongly coupled to the optical fields either diffractively or geometrically.

3.2 NUMERICAL INVESTIGATIONS OF THE PROPOSED MECHANISM

To investigate the validity of the proposed mechanism for the time-dependent oscillations, several sets of calculations were performed. A Fabry-Perot calculation was conducted with the rotational nonequilibrium MNORO3 model to compare the relative magnitudes of the pumping terms and

the radiative deactivation terms in the species equation for v = 2. These terms represent the rate of HF production by the pumping reactions and the rate of HF depletion due to lasing, respectively. The calculation was carried out for the low pressure Run 34 flow rates with the FPSR baseline parameters. The pumping and radiative deactivation terms from the species equations for the upper laser levels for two lasing lines as calculated by MNOR03 are presented in Table 16. These results indicated that the rate of radiative deactivation was two to four times faster than the chemical pumping rate.

To study the effect on the time-dependent oscillations of altering the relative rate of chemical pumping versus radiative deactivation, 5 mm slit MNOR03UR calculations using the FPSR parameters were performed with the pumping reaction rate constants increased. When the pumping reaction rate constants were multiplied by a factor of two, making them gas kinetic, the time-dependent oscillations were slightly damped. When the pumping reaction rate constants were multipled by a factor of ten, the time-dependent oscillations were damped as shown in Figs. 33 and 34.

A previous study[12] had shown that the time-dependent oscillations occurred only when there was rotational nonequilibrium present in the system. Since the concentration of HF increased by a factor of ten when the pumping rate was increased by a factor of ten and the rotational relaxation rate increases as the square of the HF concentration (a factor of one-hundred in this case), an MNOR03UR calculation was performed to investigate whether the damping that occurred when the pumping rate constants were multiplied by ten was due to an increased rotational relaxation rate. The pumping rate constants were set at

Lasing Line	$\lvert x_{chem,pumping} \rvert$ $(\frac{molecules}{cc\ sec.})$	$\lvert x_{rad} \rvert$ $(\frac{molecules}{cc\ sec.})$
$P_2(4)$	0.11383E-4	0.41061E-4
$P_2(5)$	0.15302E-4	0.24229E-4

Table 16 Comparison of the magnitudes of the pumping and radiative deactivation terms in the species equation for v = 2 as calculated by MNORC3. All values are from the lasing zone at a point 0.2 cm downstream of the H_2 injectors.

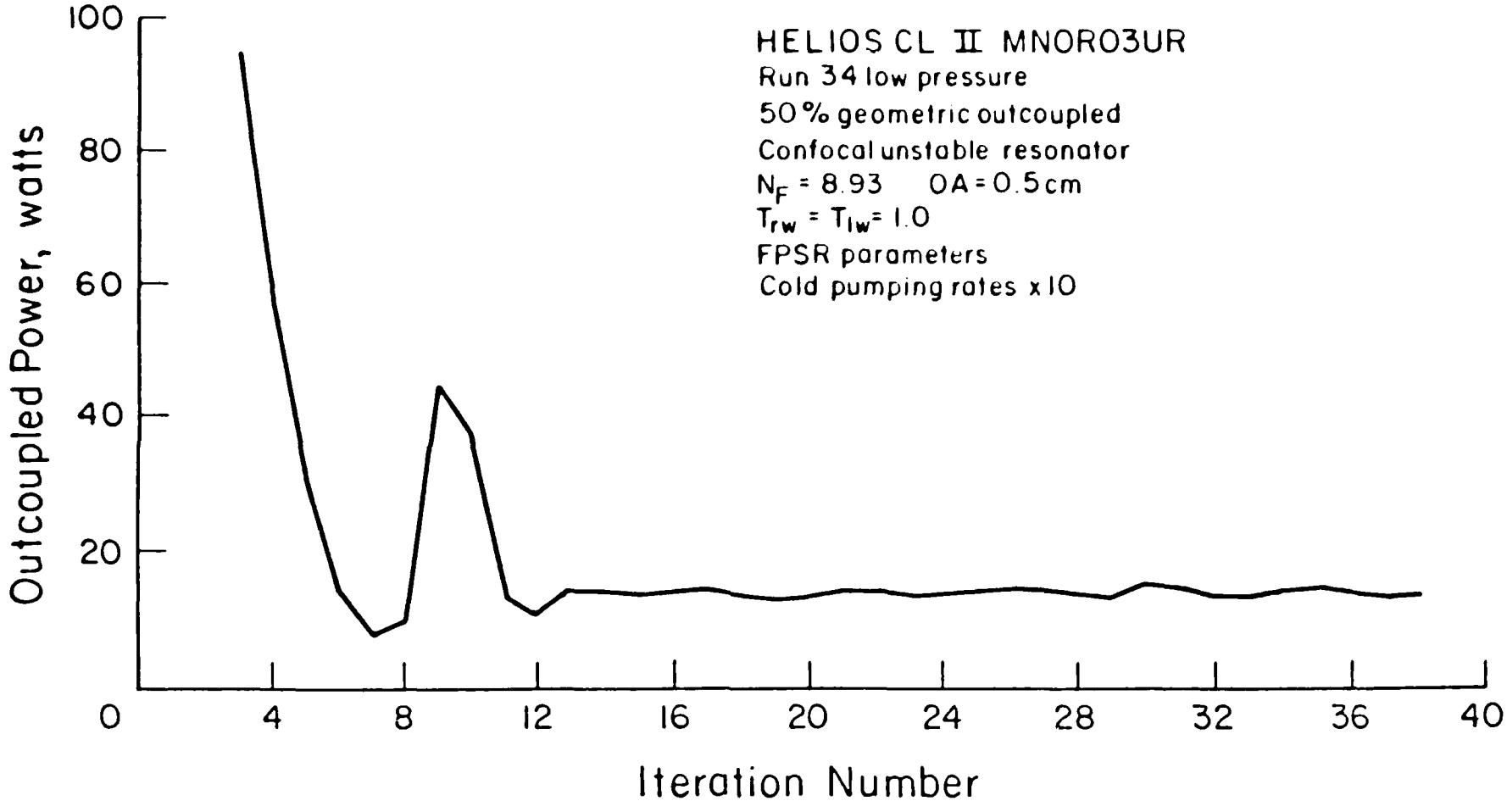

Figure 33 MNORO3UR multiline outcoupled power calculated in the optics[8], P_{out}, vs. iteration number for rotational nonequilibrium for a 50% geometric outcoupled, confocal unstable strip resonator with a large mirror diameter of 1.0 cm for the Helios CL II laser for Run 34 at 5.4 Torr.

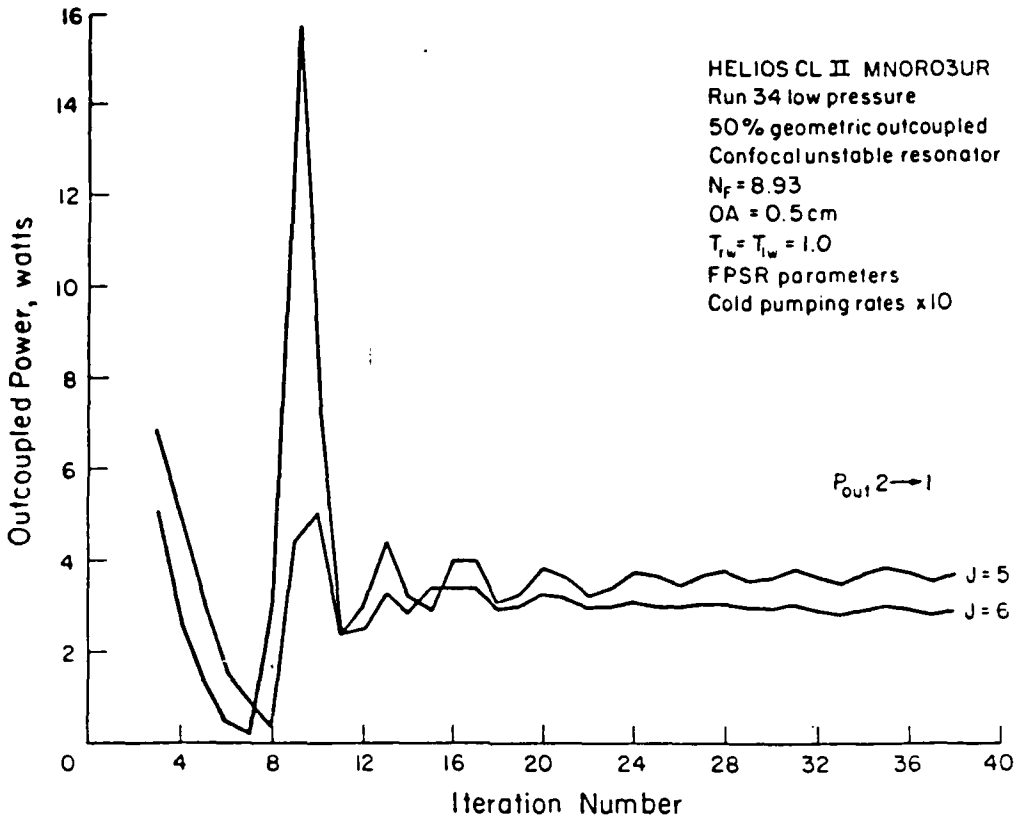

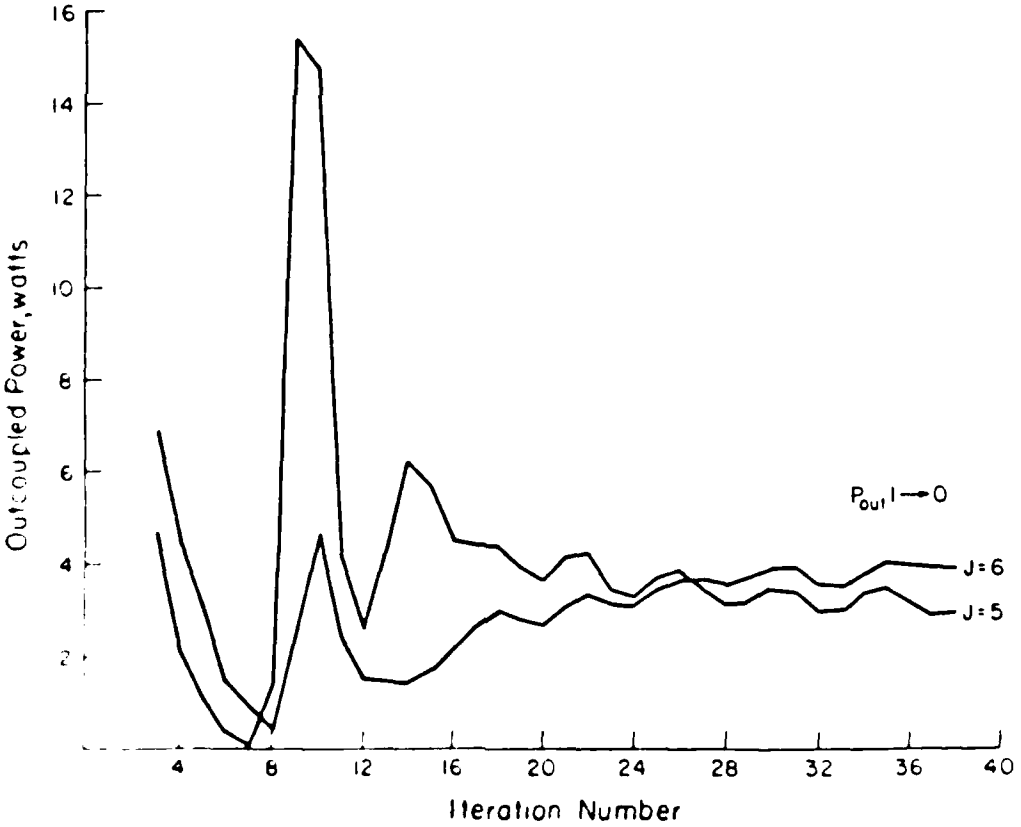

Figure 34 MNORO3UR outcoupled power[8], P_{out}, for individual lines vs. iteration number for a 50% geometric outcoupled, confocal, unstable strip resonator with a large mirror diameter of 1.0 cm for the Helios CL II laser for Run 34 at 5.4 Torr.

their experimental values and the rotational relaxation rate was increased by a factor of one hundred. Figures 35 and 36 show that, with the rotational relaxation rate increased by factor of one hundred, the amplitude modulation of the time-dependent oscillations decreased and the period was unchanged compared to the a priori calculation (Figs. 3 and 4). The damping, however, was not as great as when the pumping rate constants were increased by a factor of ten, Figs. 33 and 34. This indicated that the increased rotational relaxation rate was not responsible for the heavy damping seen in the calculation with the pumping rate constants multiplied by a factor of ten.

The preceding two MNORO3UR calculations showed that increasing the chemical pumping rate damped the time-dependent oscillations, and this damping was due to the increased rate of production of HF molecules by the pumping reactions, not the increased rotational relaxation rate. These results supported the hypothesis that the mechanism responsible for the time-dependent oscillations is a competition between chemical pumping and radiative deactivation of the upper laser levels of HF.

According to the proposed mechanism, if the media is strongly coupled to the optical fields, the oscillations are damped out since the media and the optical fields are locked together. Previous MNORO3UR calculations, Table 15, illustrated the effect on the time-dependent oscillations of geometric coupling of the media and optical fields. For a fixed resonator Fresnel number, as n_p increased, the period of the time-dependent oscillations increased.

Diffractive coupling of the media and the radiation field was investigated with MNORO3UR calculations that varied the resonator

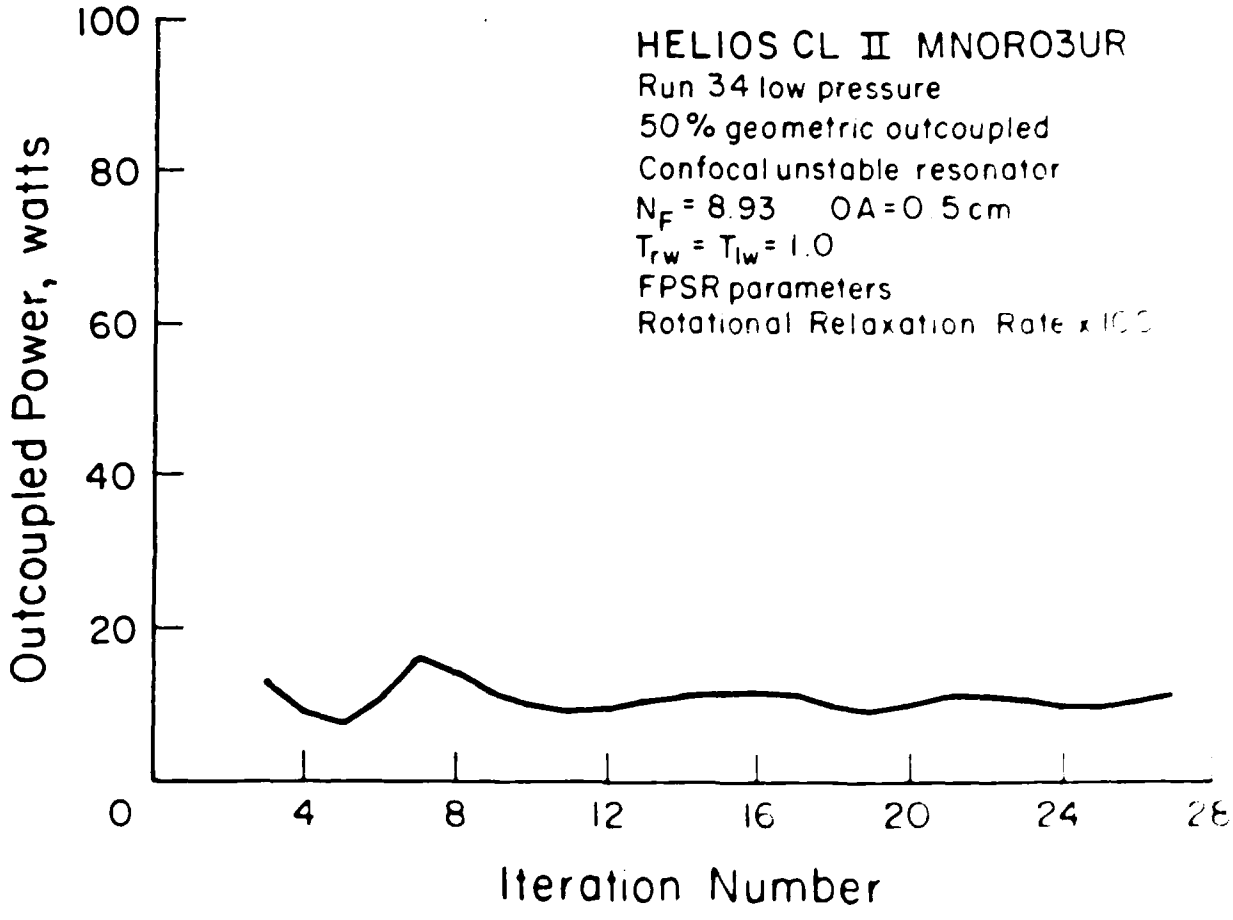

Figure 35 MNORO3UR multiline outcoupled power calculated in the optics[8], P_{out}, vs. iteration number for rotational nonequilibrium for a 50% geometric outcoupled, confocal unstable strip resonator with a large mirror diameter of 1.0 cm for the Helios CL II laser for Run 34 at 5.4 Torr.

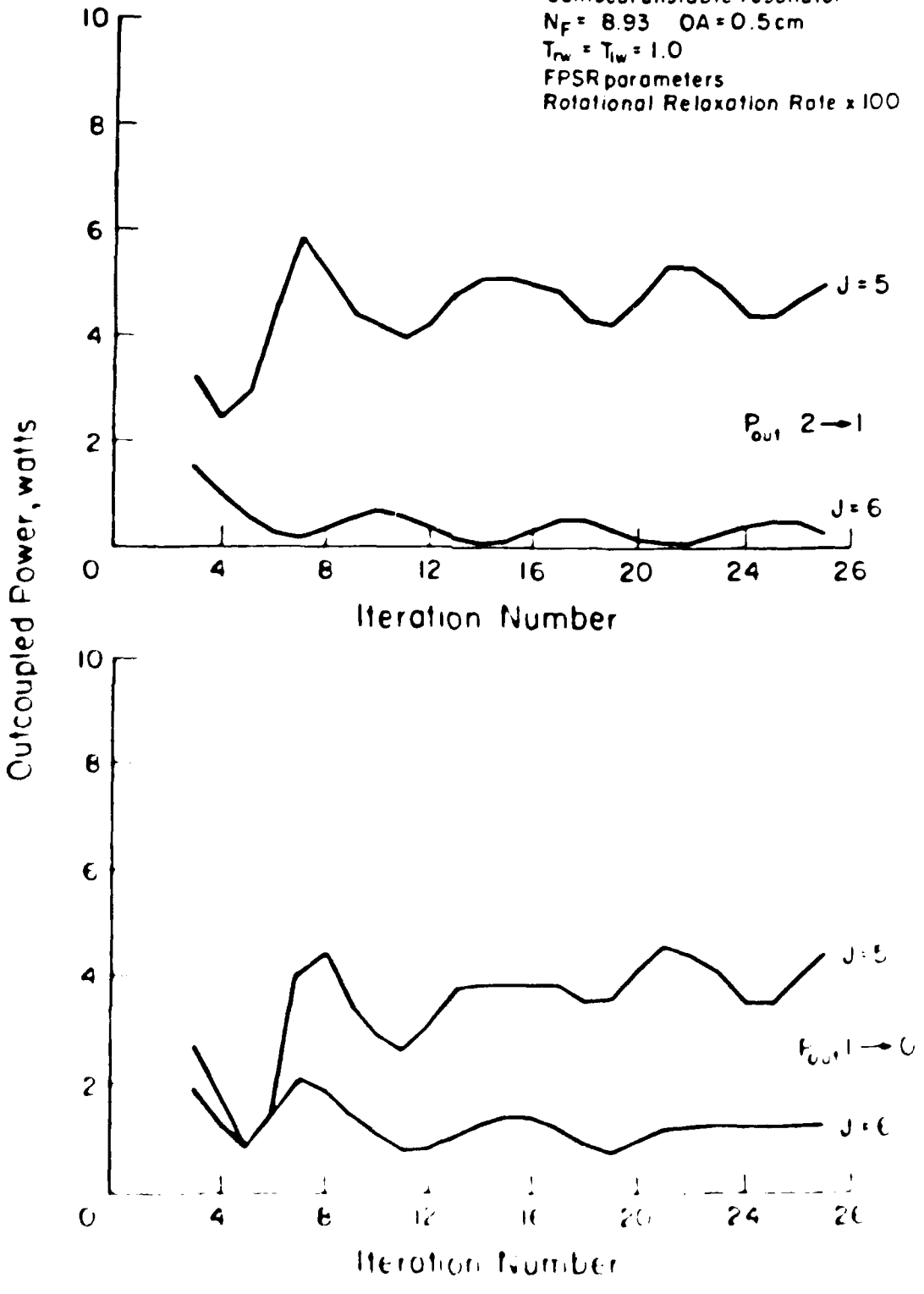

Figure 36 MNORO3UR outcoupled power, P_{out}, for individual lines vs. iteration number for a 50% geometric outcoupled, confocal, unstable strip resonator with a large mirror diameter of 1.0 cm for the Helios CL II laser for Run 34 at 5.4 torr.

Fresnel number by changing the mirror spacing. The calculations were performed for the CL II laser with a 4 mm slit resonator for the low pressure, Run 34 flow rates. Baseline parameter Set D, Table 12, was used. Table 17 shows three MNOR03UR calculations. In calculation A, the nominal calculation, the mirror spacing was 100 cm and the resonator Fresnel number was 5.71. In calculation B, the mirror spacing was 200 cm, double the nominal value, and the resonator Fresnel number was 2.85. In calculation C, the mirror spacing was 50 cm, half the nominal value, and the resonator Fresnel number was 11.42. Calculation A, with a Fresnel number of 5.71, exhibited 40 nsec time-dependent oscillations as seen in Figs. 37 and 38. Calculation B, with a Fresnel number of 2.85, had a central Fresnel zone that was larger than the small mirror. Thus, a large portion of the active media was in a region of high diffractive coupling. Calculation B showed no time-dependent oscillations. The results of calculation C, with a Fresnel number of 11.42 are presented in Figs. 39 and 40. A comparison of the results of calculations A and C shows that as the Fresnel number was increased, the amplitude of the time-dependent oscillations increased. This was in accordance with the proposed mechanism, which indicates that as the degree of diffractive coupling between the media and the optical fields decreases, the oscillations become stronger. In this case, the diffractive coupling decreased (larger Fresnel number) while the geometric coupling stayed the same (n_p approximately the same as for case A). In addition, the results of calculation C showed that the period of the oscillations decreased. This was a result of the reduction in round trip transit time due to the decreased mirror spacing.

Calculation	D_L (cm)	D_S (cm)	L (cm)	t_w	M	D_{CF} (cm)	N_F	n_p	τ (nsec)	Amp.mod.
A	0.8	0.4	100	0.97	2.0	0.33	5.71	1.3	40	10 to 20%
B	0.8	0.4	200	0.97	2.0	0.47	2.85	---	∞	--
C	0.8	0.4	50	0.97	2.0	0.24	11.42	1.8	17	30 to 70%

Table 17 Selected information from MNOR03UR calculations for a 50% geometric outcoupled, confocal, unstable 4 mm slit resonator for the CL II laser for the low pressure Run 34 flow rates and baseline parameter Set D for three different mirror separations. D_L is the large mirror diameter. D_S is the small mirror diameter. t_w is the effective Brewster window transmissivity. L is the mirror spacing. M is the resonator magnification. D_{CF} is the diameter of the central Fresnel zone. N_F is the resonator Fresnel number. n_p is the number of passes for a wave to exit the resonator after leaving the central Fresnel zone. τ is the calculated period of the time-dependent oscillations. Amp. mod. is the calculated single line amplitude modulation of the time-dependent oscillations.

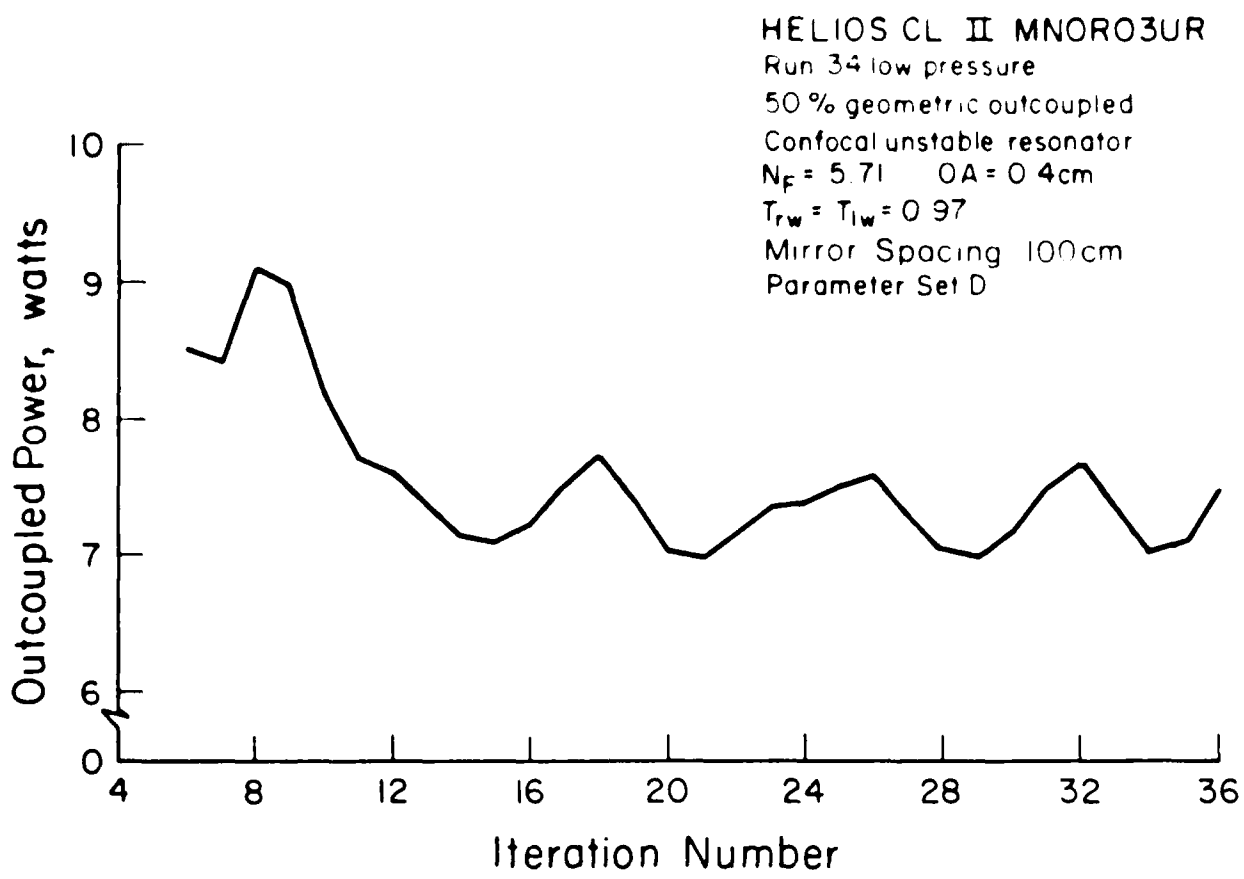

Figure 37 MNORO3UR multiline outcoupled power calculated in the optics[8], P_{out}, vs. iteration number for rotational nonequilibrium for a 50% geometric outcoupled, confocal unstable strip resonator with a large mirror diameter of 0.8 cm for the Helios CL II laser for Run 34 at 5.4 Torr.

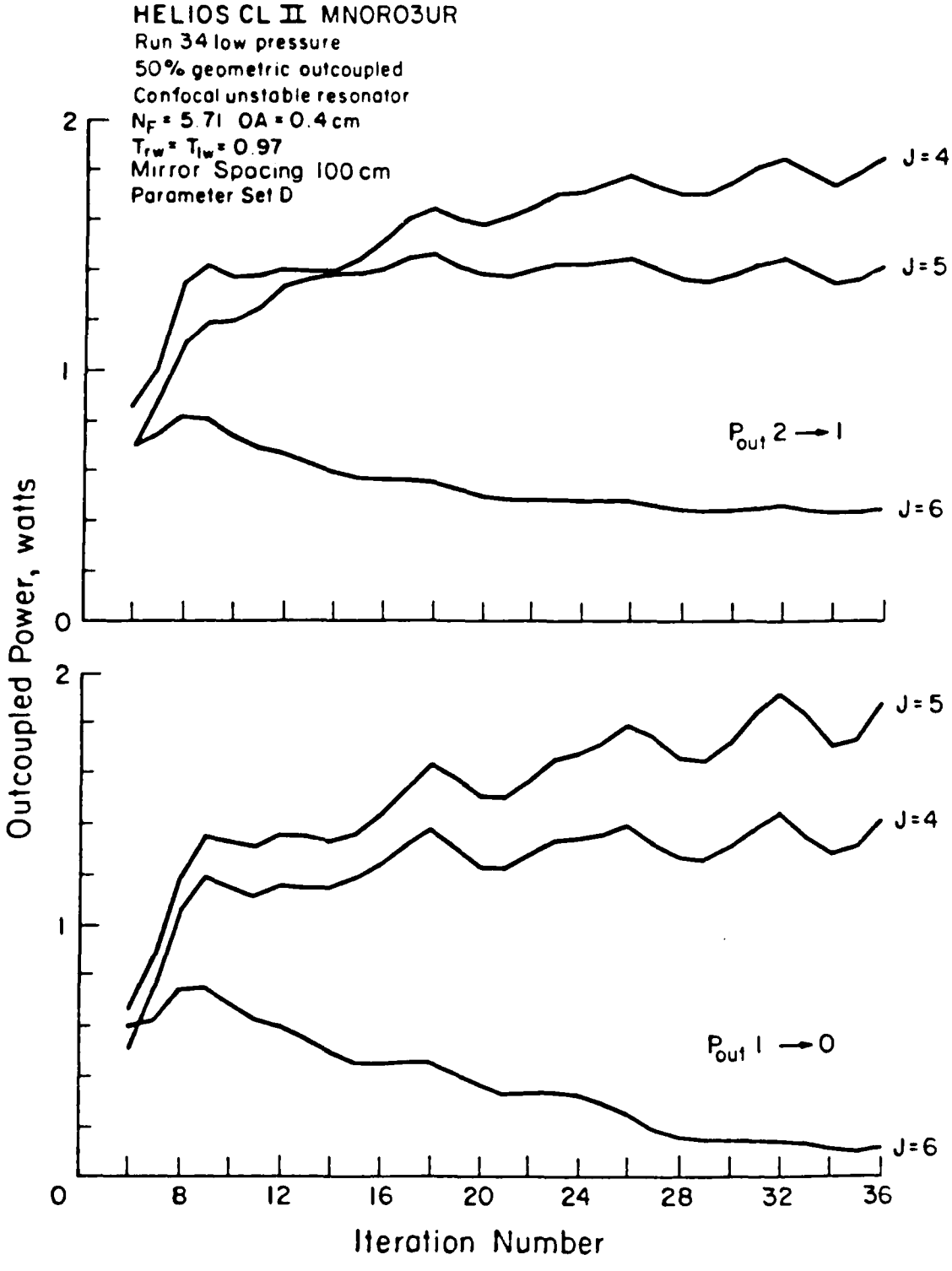

Figure 38 MNORO3UR outcoupled power[8], P_{out}, for individual lines vs. iteration number for a 50% geometric outcoupled, confocal, unstable strip resonator with a large mirror diameter of 0.8 cm for the Helios CL II laser for Run 34 at 5.4 Torr.

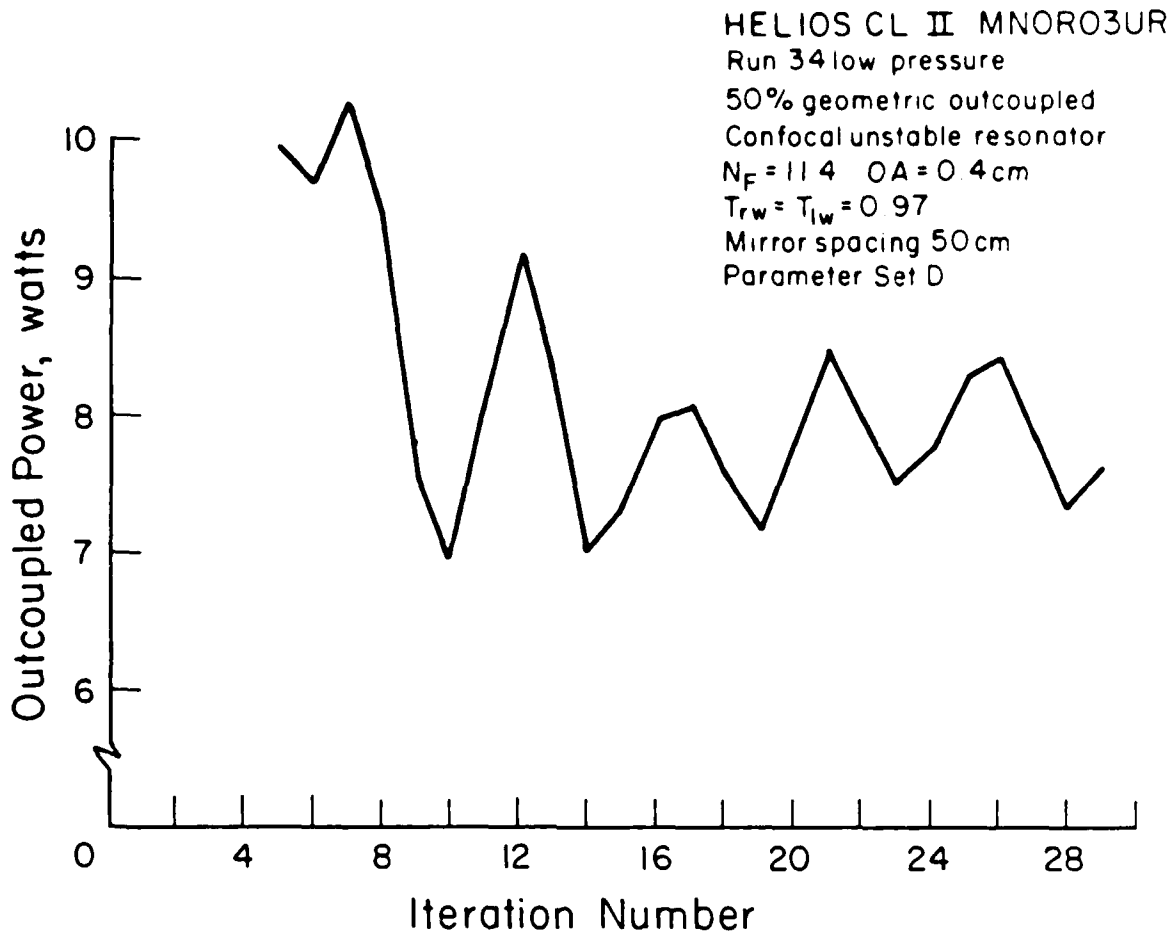

Figure 39 MNORO3UR outcoupled power[8], P_{out}, for individual lines vs. iteration number for a 50% geometric outcoupled, confocal, unstable strip resonator with a large mirror diameter of 0.8 cm for the Helios CL II laser for Run 34 at 5.4 Torr.

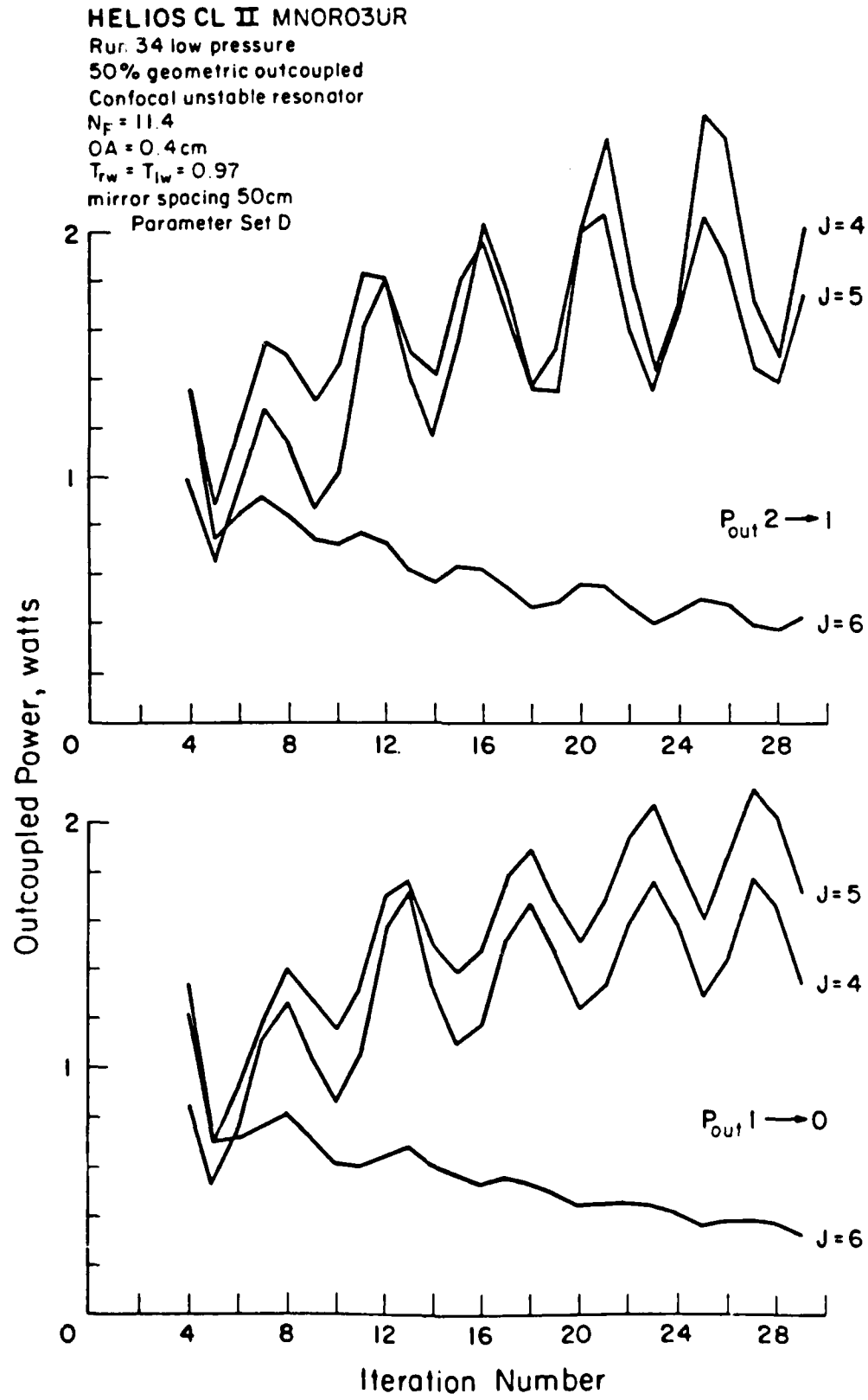

Figure 40 MNORO3UR multiline outcoupled power calculated in the optics[8], P_{out}, vs. iteration number for rotational nonequilibrium for a 50% geometric outcoupled, confocal unstable strip resonator with a large mirror diameter of 0.8 cm for the Helios CL II laser for Run 34 at 5.4 Torr.

The data showed that the oscillations occurred for Fresnel numbers above 1.5 in the CL II and 3.2 in the CL I. This difference in the demarcation Fresnel numbers is due to the gain length in the CL I being half that in the CL II. Because the gain length in the CL I is shorter and the diffractive losses are higher, for the same resonator Fresnel number (Eq. (3.1-1)), the CL I operates at an effective Fresnel number that is lower. Thus for the oscillations to appear, the resonator Fresnel number must be higher in the CL I than in the CL II.

3.3 RELATIONSHIP OF THE PROPOSED MECHANISM TO OTHER MODELS

Other models of the temporal stability of unstable resonators have been proposed by Dreizin and Dykhne[15] and Mirels[16]. The present hypothesis considers the time-dependent oscillations as the result of a competition between chemical pumping and radiative deactivation of the upper laser levels of HF. The models of Dreizin and Dykhne and Mirels consider the time-dependent oscillations as the result of a chemical kinetic-fluid dynamic phenomena, in which fluid elements flow into the upstream portion of the resontor, lase, and are subsequently replaced by fresh media in the upstream portion of the resonator. Accordingly, the oscillation period is on the order of the fluid transit time through the resonator. The experimental evidence[10,11,13], however, indicates that time-dependent oscillations occur even when the velocity of the media is so low that the media is essentially frozen for times on the order of the period of the oscillations. Therefore, it is clear that these time-dependent oscillations are not the result of chemical kinetic-fluid dynamic coupling. The mechanism responsible for these time-dependent

oscillations is a competition between chemical pumping and radiative deactivation.

3.4 SUGGESTED EXPERIMENTS

The proposed mechanism for the time-dependent oscillations in unstable resonators on lines whose saturated gain does not fill the resonator was supported by the calculations in Section 3.2. To verify the proposed mechanism, new unstable resonator experiments should be conducted. Based on the proposed mechanism, for a fixed resonator Fresnel number, the period of the time-dependent oscillations should increase as the geometric coupling increases, since the media is more coupled to the optical fields. Thus an experiment with a 4 mm slit resonator with a magnification of 1.25 (20% outcoupled) should be performed to determine whether the period increases as predicted. The proposed mechanism also predicts that the oscillation amplitude modulation should increase as Fresnel number increases since the media is less coupled to the optical fields. If the geometric coupling is held constant as the Fresnel number is increased, the period should decrease as shown by the MNORO3UR calculations in Tables 15 and 17. Thus experiments with mirror spacings of 200 cm and 50 cm should be performed for a 50% geometric outcoupled 4 mm slit resonator. There should be no oscillations observed with the 200 cm mirror spacing since the diffractively coupled central Fresnel zone will be larger than the small mirror and contain most of the media. The oscillations observed with the 50 cm mirror spacing should have a larger amplitude and a shorter period than those for a 100 cm mirror spacing since the media

and the optical fields are coupled less by diffraction. Changing the mirror spacing should also change the period of the mode beat. For a 200 cm mirror spacing, the mode beat should have a period of 13 to 14 nsec. For a 50 cm mirror spacing, the mode beat should not appear since the longitudinal mode frequency of approximately 300 MHz and the line width of approximately 400 MHz indicate that only one longitudinal mode would lase.

3.5 SUMMARY

A mechanism to explain the time-dependent oscillations that occur on lines whose saturated gain does not fill the unstable resonator was proposed. It was suggested that the time-dependent oscillations are the result of a competition between chemical pumping and radiative depopulation of the upper laser levels of HF. The oscillations occur only if the media is not strongly coupled to the optical fields diffractively or geometrically.

Computer calculations with the full, nonlinear, coupled, chemical kinetic, fluid dynamic, wave optics unstable resonator model supported the proposed mechanism. The calculations showed that the oscillations were damped out by either increasing the rate of the chemical pumping reactions or by increasing the degree of coupling between the media and the optical fields.

Three experiments with a 4 mm slit resonator were suggested to test the validity of the proposed mechanism. For a fixed resonator Fresnel number, decreasing the magnification of the resonator to 1.25 should increase the period of the time-dependent oscillations since the media

will be more geometrically coupled to the optical fields. Changing the mirror spacing to 50 cm should increase the amplitude modulation and decrease the period since the media will be less diffractively coupled to the optical fields. Changing the mirror spacing to 200 cm should prevent the oscillations since the central Fresnel zone will be larger than the small mirror diameter, thereby increasing the diffractive coupling of the media to the optical fields.

AD-A185 059 COMPUTER SIMULATION OF CW HF CHEMICAL LASER UNSTABLE RESONATOR PERFORMANCE(U) ILLINOIS UNIV AT URBANA DEPT OF AERONAUTICAL AND ASTRONAUTICA.. L H SENTMAN ET AL. 2/2

UNCLASSIFIED AUG 87 AAE-87-5 N00014-85-K-0326 F/G 9/3 NL

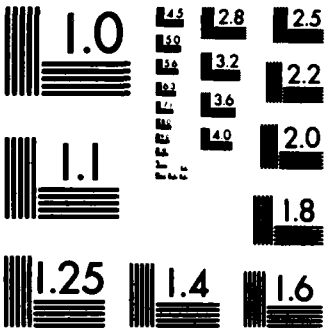

MICROCOPY RESOLUTION TEST CHART
NATIONAL BUREAU OF STANDARDS-1963-A

IV. CONCLUDING REMARKS

The objective of this study was to simulate cw HF chemical laser unstable resonator performance. To accomplish this the unstable resonator data were modeled with a fluid dynamic, chemical kinetic, rotational nonequilibrium, wave optics model, MNORO3UR. The calculations showed that one set of baseline parameters that allow the model to predict the data as the size of the resonator and size of the laser varied could not be found. This inability to obtain one set of baseline parameters revealed limitations in the unstable resonator model. The limitations are due primarily to the treatment of the fluid dynamic mixing. Since these limitations were not apparent in Fabry-Perot and stable resonator models with the same mixing model, the unstable resonator data as a function of resonator size and size of the laser was shown to be a severe test of a coupled, wave optics, chemical kinetic, fluid dynamic model of a chemical laser.

To improve the MNORO3UR model, the treatment of the fluid dynamic mixing should be improved. Sonic transverse injection into a subsonic multicomponent reacting shear flow results in a three-dimensional flow field. The idealization of this as a two-dimensional array of parallel, alternating fuel and oxidizer slit nozzles with subsequent linear mixing is an oversimplification. A full, three-dimensional mixing model is needed.

A mechanism that explains the time-dependent oscillations that occur on lines whose saturated gain does not fill the unstable resonator

was proposed. According to the proposed mechanism, the time-dependent oscillations are the result of a competition between chemical pumping and radiative deactivation of the upper laser levels of HF. The oscillations occur only if the media is not strongly coupled to the optical fields diffractively or geometrically. Computer calculations supported the proposed mechanism. To verify the proposed mechanism, new unstable resonator experiments should be conducted. Based on the proposed mechanism, for a fixed resonator Fresnel number, the period of the time-dependent oscillations should increase as the magnification of the resonator decreases. Thus an experiment with a 4 mm slit resonator with a magnification of 1.25 (20% outcoupled) should be conducted. For this resonator, the period of the oscillations should be greater than for a 4 mm slit resonator with a magnification of 2. The proposed mechanism also predicts that the oscillation amplitude modulation should increase and the period decrease as the Fresnel number of the resonator increases with the geometric coupling held constant. Thus experiments with mirror spacings of 200 cm and 50 cm should be performed for a 50% geometric outcoupled 4 mm slit resonator. There should be no oscillations with the 200 cm mirror spacing, except for the mode beat of the laser which should have a period of 13 to 14 nsec. With the 50 cm mirror spacing, there should be oscillations that have a larger amplitude and a shorter period than the oscillations seen with a mirror separation of 100 cm. A mode beat with the 50 cm mirror spacing should not be observed.

REFERENCES

1. L. H. Sentman, J. D. Bichanich, D. Carroll, V. Coverstone, and P. Theodoropoulos, "Simulation of Fabry-Perot and Stable Resonator cw HF Chemical Laser Performance," AAE TR 85-6, UILU Eng. 85-0506, Aeronautical and Astronautical Engineering Department, University of Illinois, Urbana, IL, September 1985.

2. L. H. Sentman, G. Tsioulos, J. Bichanich, D. Carroll, P. Theodoropoulos, J. Gilmore, and A. Gumus, "A Comparative Study of cw HF Chemical Laser Fabry-Perot and Stable Resonator Performance," Proceedings, International Conference on Lasers '85, Las Vegas, Nevada, 2-6 December 1985 (STS Press, McLean, VA, 1986).

3. L. H. Sentman, W. O. Mosebach and P. Renzoni, "Theoretical and Experimental Study of cw Chemical Laser Performance," AAE TR 81-8, UILU Eng. 81-0508, Aeronautical and Astronautical Engineering Department, University of Illinois, Urbana, IL, December 1981.

4. L. H. Sentman, M. H. Nayfeh, W. O. Mosebach, P. Renzoni, K. Herrick, K. King, P. Schmidt, and S. Townsend, "Theoretical and Experimental Study of cw HF Chemical Laser Performance," Proceedings, Fourth International Symposium on Gas Flow and Chemical Lasers, Stresa, Italy, 13-17 September 1982 (Plenum, New York, 1985).

5. L. H. Sentman, M. Subbiah, and S. W. Zelazny, "BLAZE II, a Chemical Laser Simulation Program," TR H-CR-77-8, Bell Aerospace Textron, Buffalo, NY, 1977.

6. J. W. Raymonda, M. Subbiah, J. T. Schimke, S. W. Zelazny and L. H. Sentman, "Advanced HF and DF Chemical Laser Performance Modeling, Vol. 1, the CNCDE/BLAZE Rotational Equilibrium Code," TR DRCPM-HEL-CR-79-7, Bell Aerospace Textron, Buffalo, NY, 1979.

7. L. H. Sentman, and P. Schmidt, "MNOR03: An Efficient Rotational Nonequilibrium cw HF Chemical Laser Model," AAE TR 83-1, UILU Eng. 83-0501, Aeronautical and Astronautical Engineering Department, University of Illinois, Urbana, IL, June 1983.

8. L. H. Sentman, P. F. Schmidt and G. M. Marinos, "Effects of the HF Rate Package and the Optical Resonator on cw HF Chemical Laser Performance," AAE TR 83-6, UILU, Eng. 83-0506, Aeronautical and Astronautical Engineering Department, University of Illinois, Urbana, IL, June 1983.

9. L. H. Sentman, and W. Brandkamp, "An Efficient Rotational Nonequilibrium Model of a cw Chemical Laser," AAE TR 79-5, UILU Eng. 79-0505, Aeronautical and Astronautical Engineering Department, University of Illinois, Urbana, IL, July 1979.

10. L. H. Sentman, M. Nayfeh, S. W. Townsend, K. King, G. Tsioulos, and J. Bichanich, "Time-Dependent Oscillations in a cw Chemical Laser Unstable Resonator," Applied Optics, Vol. 24, No. 21, November 1985.

11. L. H. Sentman, S. Townsend, G. Tsioulos, J. Bichanich, M. Nayfeh, and K. King, "Time-Dependent Oscillations in a cw HF Chemical Laser Unstable Resonator," AAE TR 84-2, UILU Eng. 84-0502, Aeronautical and Astronautical Engineering Department, University of Illinois, Urbana, IL, May 1984.

12. L. H. Sentman, "Chemical Laser Power Spectral Performance: A Coupled Fluid Dynamic, Kinetic, and Physical Optics Model," Applied Optics, Vol. 17, No. 14, July 1978.

13. L. H. Sentman, D. L. Carroll, P. Theodoropoulos, and A. Gumus, "Scale Effects in a cw HF Chemical Laser," AAE TR 86-5, UILU Eng. 86-0505, Aeronautical and Astronautical Engineering Department, University of Illinois, Urbana, IL, September 1986.

14. R. Gross and J. Bott, Handbook of Chemical Lasers, Ch. 2, pp. 118-119, John Wiley, New York, 1976.

15. Y. A. Dreizin and A. M. Dykhne, "Self Oscillating Instability of Fast Flow Lasers Using Unstable Resonators," JETP Lett., Vol. 19, No. 12, June 1974.

16. H. Mirels, "Temporal Stability of Unstable Resonator With Crossflow," Applied Physics Letters," Vol. 28, No. 10, May 1976.

END

11-87

DTIC